ISSN 0915-6364

NATIONAL INSTITUTE FOR FUSION SCIENCE

Computer Simulation and Data Compilation of Sputtering Yield by Hydrogen Isotopes ($^1H^+$, $^2D^+$, $^3T^+$) and Helium ($^4He^+$) Ion Impact from Monatomic Solids at Normal Incidence

Y. Yamamura, K. Sakaoka and H. Tawara

(Received - Oct. 3, 1995)

NIFS-DATA-31 Oct. 1995

RESEARCH REPORT
NIFS-DATA Series

NAGOYA, JAPAN

COMPUTER SIMULATION AND DATA COMPILATION OF SPUTTERING YIELD BY HYDROGEN ISOTOPES ($^1H^+$, $^2D^+$, $^3T^+$) AND HELIUM ($^4He^+$) ION IMPACT FROM MONATOMIC SOLIDS AT NORMAL INCIDENCE

Yasunori Yamamura[a)], Kazuho Sakaoka[a)] and Hiro Tawara

National Institute for Fusion Science, Chigusa-ku, Nagoya 464-01, Japan

Abstract

The ion-induced sputtering yields from monatomic solids at normal incidence are presented graphically for light-ion ($^1H^+$, $^2D^+$, $^3T^+$, $^4He^+$) bombardment on various target materials as a function of the incident ion energy. To supplement the experimental data, the sputtering yields are calculated by the Monte Carlo simulation code ACAT for all possible light ion-target combinations. Each graph shows the available experimental and ACAT data points, together with the sputtering yield calculated by the Yamamura and Tawara empirical formula.

[Key words : sputtering yields, monatomic solids, normal incidence, light-ion impact, empirical formula, Monte Carlo simulation

Permanent address:

a) Department of Applied Physics, Okayama University of Science, Ridai-cho, Okayama 700, Japan

1. Introduction

Sputtering of surfaces is an important parameter in the understanding of the operation feature in fusion plasma device. Sputtering ejects high atomic number materials into the main plasma, causing significant contamination and increasing the effective charge of the plasma, and thus results in inefficient heating of the fusion plasma. From the point of view of plasma-wall interactions, sputtering is an undesirable process which erodes the surrounding walls and contaminates the plasma. With our particular interest in fusion related applications, we will restrict our discussions to sputtering from monatomic materials by light ions ($^1H^+$, $^2D^+$, $^3T^+$, $^4He^+$) at energies from a few tens of eV to several tens of keV that might be most relevant to tokamak plasmas.

The main concern of this paper is the physical sputtering yields due to light-ion bombardment where the ejection mechanism relates to collisional transfer of kinetic energy and momentum from the projectile to target atoms. This process is in principle independent of the target temperature. We here do not consider chemical sputtering as well as radiation enhanced sublimation. The chemical sputterings are very well known as one of the erosion of graphites by hydrogen isotopes where the volatile species such as hydrocarbons are formed under some environments.

In 1984 the working group at the Institute of Plasma Physics, Nagoya University, published the compiled sputtering yield data available up to early 1983 and proposed an empirical formula which could predict the energy dependence of sputtering yields for any ion-target combination [1]. Since then, a large number of new data have been published. Recently, Yamamura and Tawara [2] collected new experimental sputtering data published during 1983 - 1994, and proposed a new empirical formula.

Two years ago, Eckstein et al. [3] reported their survey of experimental sputtering yields measured at Max-Plank Institut für Plasmaphysik (Garching, Germany) in which the data for normal incidence as a function of ion energy were fitted with a formula derived by Bohdansky [4]. Thomas et al.[5] also presented an evaluated data base for light ion sputtering, again employing the Bohdansky formula [4]. Basically, both groups used the following expression for the sputtering

yield:

$$Y(E) = Q_B\, s_n(\varepsilon)\left[1 - \left(\frac{E_{th}}{E}\right)^{2/3}\right]\left[1 - \left(\frac{E_{th}}{E}\right)\right]^2 \quad , \tag{1}$$

where E is the projectile energy, $s_n(\varepsilon)$ is the reduced nuclear stopping cross section, and ε is the reduced energy

$$\varepsilon = E\frac{M_2}{M_1+M_2}\frac{a_L}{Z_1 Z_2 e^2} \quad . \tag{2}$$

Here, Z_1 and Z_2 are the atomic numbers, M_1 and M_2 are the masses of the projectile and the target atom, respectively. e is the electron charge, and a_L is the Lindhard screening length given as [6]

$$a_L = 0.4685\left\{Z_1^{2/3} + Z_2^{2/3}\right\}^{-1/2} \ \text{Å} \quad . \tag{3}$$

The values Q_B and E_{th} are used as parameters to fit to the data available.

For the reduced nuclear stopping power in eq. (1), Bohdansky originally used the following analytical expression based on the Thomas-Fermi potential [1]:

$$s_n^{TF}(\varepsilon) = \frac{3.441\sqrt{\varepsilon}\ln(\varepsilon + 2.718)}{1 + 6.355\sqrt{\varepsilon} + \varepsilon(6.882\sqrt{\varepsilon} - 1.708)} \quad . \tag{4}$$

In their recent revision of Bohdansky formula, Eckstein et al. [2] used the following reduced nuclear stopping power based on the Kr-C potential:

$$s_n^{KrC}(\varepsilon) = \frac{0.5\ln(1 + 1.2288\varepsilon)}{\varepsilon + 0.1728\sqrt{\varepsilon} + 0.008\varepsilon^{0.1504}} \quad . \tag{5}$$

The best-fit values of Q_B and E_{th} are listed for each ion-target combination in their data book [3].

The purpose of this report is to simulate the light-ion sputtering yields for possible target materials with the Monte Carlo simulation code ACAT to supplement the experimental data. In this report we represents in graphs the aggregate data on the ion-induced sputtering yield as a function of the energy of the incident ion for light-ion sputtering at normal incidence. Every graph also includes

the yield vs energy curves calculated by the Yamamura and Tawara empirical formula [2].

2. Simulations

For light incident ion, sputtering yields have been calculated with the Monte Carlo simulation code ACAT program [7] in order to supplement the limited experimental data. Especially, since there is no experimental sputtering yield data at all under a ^{3}T ion bombardment, it is meaningful to get the sputtering yields for the T ion bombardment on possible target materials. The ACAT program is based on the binary collision approximation, where the target is assumed to be amorphous, and the surface is randomly rough in a depth of half a monolayer. The details about the ACAT code is described in Ref. 7.

As an interatomic potential we used the Kr-C potential [8] with the Firsov screening length a_F for heavy ion ($Z_1 > 3$) sputtering, where a_F is given as

$$a_F = 0.4685 \left\{ Z_1^{1/2} + Z_2^{1/2} \right\}^{-2/3} \ \mathring{A}$$

Some efforts were undertaken to get good agreement with experimental data by adjusting the Firsov screening length by adjusting a_F to $a_F(1+q)$, because in principle the Thomas-Fermi statistical model cannot be applied to light ions. The adjusting parameter q is listed in Table 1 for possible target materials. As it is very difficult to get the adjusting parameters q for ^{3}T ions, we estimated them by interpolating the adjusting parameters for ^{2}D and ^{4}He.

At high collision energies the electronic energy loss is simulated with the path-length-dependent non-local model, where we used the ZBL electronic stopping formula [9] for all the ion-target combinations. The electronic energy loss due to the violent collision between a light ion and a

target atom, however, is estimated by the Oen-Robinson (OR) local model [10]. At low collision energies it is estimated by the OR local model. This is referred to as "the mixed model" in Ref.7. The "mixed model " of the present ACAT code is as follows: We use the OR local model if the apsidal distance at the zero impact parameter is larger than $0.5R_0$. It is well known that the calculated sputtering yields are dependent on which electronic energy loss model is used, the non-local or the OR local model. For several targets, namely C, Cu, Ag Tb, Tm and Au (which are marked as an asterisk in Table 1), we have obtained better results for the energy dependence of the sputtering yield if we employ the OR local model.

3. The empirical formula

Recently Yamamura and Tawara [2] proposed the following empirical formula which can be applied to any ion-target combination:

$$Y(E) = 0.042 \frac{Q(Z_2)\alpha^*(M_2/M_1)}{U_s} \frac{S_n(E)}{1 + \Gamma k_e \varepsilon^{0.3}} \left[1 - \sqrt{\frac{E_{th}}{E}}\right]^s \tag{6}$$

with the numerical factor in units of $Å^{-2}$. The Γ factor has the following form:

$$\Gamma = \frac{W(Z_2)}{1 + (M_1/7)^3} \tag{7}$$

with M_1 in a.m.u. The best-fit values of the dimensionless parameters $W(Z_2)$ and $Q(Z_2)$ are listed in Table 2 with U_s in eV, and the power s of the above empirical formula is slightly dependent on the target material, as is shown in Table 2. The best-fit values of α^* are analytically described as a function of the mass ratio M_2/M_1 in the following manner:

$$\alpha^* = 0.249(M_2/M_1)^{0.56} + 0.0035(M_2/M_1)^{1.5} \qquad M_1 \le M_2$$
$$= 0.0875(M_2/M_1)^{-0.15} + 0.165(M_2/M_1) \qquad M_1 \ge M_2 \quad . \tag{8}$$

Concerning the sputtering threshold in eq. (6), we use the following best-fit functional relation

$$\frac{E_{th}}{U_s} = \frac{6.7}{\gamma} \qquad M_1 \ge M_2$$
$$= \frac{1 + 5.7(M_1/M_2)}{\gamma} \qquad M_1 \le M_2 \tag{9}$$

which is derived based on Yamamura and Bohdansky's theory [11], where γ is the energy transfer factor in an elastic collision given by

$$\gamma = \frac{4M_1M_2}{(M_1+M_2)^2} . \tag{10}$$

The Lindhard electronic stopping coefficient k_e is given as [12]

$$k_e = 0.079 \frac{(M_1+M_2)^{3/2}}{M_1^{3/2}M_2^{1/2}} \frac{Z_1^{2/3}Z_2^{1/2}}{(Z_1^{2/3}+Z_2^{2/3})^{3/4}} \tag{11}$$

with M_i in a.m.u. The nuclear stopping cross section $S_n(E)$ in the present formula is calculated by

$$S_n(E) = \frac{8.478Z_1Z_2}{(Z_1^{2/3}+Z_2^{2/3})^{1/2}} \frac{M_1}{M_1+M_2} s^{TF}(\varepsilon) \tag{12}$$

in units of eVÅ^2/atom, using the analytic expression of $s_n^{TF}(\varepsilon)$ which is given in eq. (4). The explicit expression for the reduced energy ε is

$$\varepsilon = \frac{0.03255}{Z_1Z_2\{Z_1^{2/3} + Z_2^{2/3}\}^{1/2}} \frac{M_2}{M_1+M_2} E \text{ (eV)} \quad . \tag{13}$$

From the theoretical point of view, the sputtering yield for high-energy light ion is not directly proportional to the reduced nuclear stopping cross section $s_n(\varepsilon)$, because it is influenced strongly by the electronic energy loss. In this sense, it is difficult for the Bohdansky formula to predict the sputtering yield by high-energy light ions. The fitting parameter

Q_B of the Bohdansky formula does include the effect of the electronic stopping, but the influence of the electronic stopping on sputtering depends on the incident energy. Still, from the perspective of plasma-wall interactions where one is mainly interested in the low-energy sputtering, it seems that the Bohdansky formula can predict the sputtering yield reasonably well. Until now there is no apparent rule governing the behavior of the Bohdansky's Q_B factor for different ion-target combinations. Therefore, it is very difficult to predict the sputtering yield for the case that there is no experimental data, for example, the sputtering yield due to ^{3}T ions bombardment.

The parameters included in the present Yamamura and Tawara formula are given as a function of the physical quantities of the target material and the mass ratio between the projectile and the target material. Therefore, even if there are no experimental data of the sputtering yield by ^{3}T ions, we can predict reasonably its sputtering yield from any monatomic solid.

4. Presentation of data and discussion

The Graphs show available experimental and ACAT data, and the yield vs energy curve calculated by the Yamamura and Tawara empirical formula for each light ion-target combination. For plots of experimental and the ACAT data, different symbols are used to indicate different references; the complete reference citation is given in the References for Graphs. The calculated yield vs energy curves are shown as solid lines. The light ion-target combinations shown in Graphs are listed in Table 3, where the number in each grid position represents the number of references of experimental works for that particular combination. If one wishes to estimate the sputtering yield for unlisted ion-target combinations with the present formula, one should use $Q = 1.0$, $W = 0.35U_s$, and $s = 2.5$, where U_s is the heat of sublimation in eV.

Agreement between the solid curve and data points is much improved as compared with the early work [1]. Since the sputtering data for the hydrogen isotope on the C target include the chemical sputtering yield, the significant deviation of the empirical curve and the ACAT data from the experimental data is observed. The observed sputtering data for the C target are often scattered, because the sputtering yield data for different kinds of graphite materials are plotted in one figure. For the Al target data we also observe the deviation of the empirical curve and the ACAT data from the experimental data. Since the light-ion sputtering yield is very low (< 0.1 atoms/ion), the speed of the oxide formation at the surface may be larger than that of the sputtering, and the surface is covered with the aluminum oxide whose surface binding energy is much larger than that of the aluminum metal.

5. Conclusion

We have presented the incident energy dependence of the sputtering yields for $^{1}H^{+}$, $^{2}D^{+}$, $^{3}T^{+}$, and $^{4}He^{+}$ ions which are bombarded on possible target materials for plasma device. Concerning the sputtering yield by a T ion, the yields are estimated by the ACAT simulation and the Yamamura and Tawara empirical formula, and so they might be within the accuracies of the present-day experimental data source.

In the Yamamura and Tawara empirical formula, there is no ambiguity about the projectile, because the parameters included in the empirical formula are functions of the physical quantities of the target material and the mass ratio between the projectile and the target material. This means that if the accuracy of the sputtering yield due to $^{1}H^{+}$, $^{2}D^{+}$ and $^{4}He^{+}$ ions is much more improved experimentally, the sputtering yield by ^{3}T ions may be reasonably estimated by the Yamamura and

Tawara empirical formula.

Acknowledgement

The authors would like to express their sincere thanks to a number of students of Okayama University of Science for their continuous efforts of searching out experimental data from many published articles.

References

[1] N. Matsunami,Y. Yamamura,Y. Itikawa,N. Itoh,Y. Kazumata,S. Miyagawa, K.Morita, R. Shimizu and H.Tawara, At. Data and Nucl.Data Tables 31, 1 (1984).

[2] Y. Yamamura and H. Tawara, At. Data and Nucl. Data Tables (accepted)

[3] W. Eckstein, C. Garcia-Rosales, J. Roth and W. Ottenberger, IPP 9/82 (Inst. Plasma Physics, Garching, Germany, 1993).

[4] J. Bohdansky, Nucl. Instr. Meth. B2, 587 (1984)

[5] E.W. Thomas, R.K. Janev, J. Botero, J.J. Smith and Yanghui Qiu, INDC(NDS)-287 (1993).

[6] J.Lindhard, V.Nielson and M.Scharff, Mat. Fys. Medd. Dan. Vid. Selsk., 36 no.10 (1968).

[7] Y.Yamamura and Y. Mizuno, IPPJ-AM-40 (Inst. Plasma Physics. Nagoya University, 1985).

[8] W.D. Wilson, L.G. Haggmark and J. Biersack, Phys. Rev. B15 (1977) 2458.

[9] H.H.Andersen and J.F.Ziegler, Hydrogen Stopping and Ranges in All Elements (Pergamon, New York, 1985).

[10] O.S. Oen and M.T. Robinson, Nucl. Instr. Meth. 132 (1976) 647.

[11] Y.Yamamura and J.Bohdansky, Vacuum 35 561 (1985).

[12} J.Lindhard and M.Scharff, Phys. Rev., 124 128 (1961).

Appendix Sample calculation of the sputtering yield

As an example, we calculate the sputtering yield for D on Ni at the incident energy of 1 keV, using the Yamamura and Tawara empirical formula eq. (6). First calculate ε using eq. (13):

$$\varepsilon = \frac{0.03255}{1\times 28\times\left(1^{2/3}+28^{2/3}\right)^{1/2}}\frac{58.69}{2.014+58.69}\times 1000 = \frac{0.03255\times 58.69}{89.52\times 60.70}\times 1000 = 0.3516$$

Next we obtain $s_n^{TF}(\varepsilon)$ using eq. (4), i.e.,

$$s_n^{TF}(\varepsilon) = \frac{3.441\times\sqrt{0.3516}\ln 3.070}{1+6.355\times\sqrt{0.3516}+0.3516(6.882\times\sqrt{0.3516}-1.708)} = \frac{2.288}{4.768+0.8342} = 0.4084$$

Calculate $k_e(\varepsilon)$ using eq. (11):

$$k_e(\varepsilon) = 0.079\times\frac{(2.014+58.69)^{3/2}}{2.014^{3/2}58.69^{1/2}}\frac{1^{2/3}\times 28^{1/2}}{\left(1^{2/3}+28^{2/3}\right)^{3/4}} = \frac{37.36\times 5.292}{21.83\times 5.716} = 1.584$$

Then calculate the nuclear stopping cross section $S_n(E)$ from eq. (12):

$$S_n(E) = 84.78\frac{1\times 28}{\left(1^{2/3}+28^{2/3}\right)^{1/2}}\times\frac{2.014}{2.014+58.69}\times 0.4084 = \frac{84.78\times 23.03}{3.197\times 60.70} = 10.06 \quad \text{eVÅ}^2/\text{atom}\ .$$

From Table 2, we read off $Q = 0.94$, $U_s = 4.44$ eV, $W = 1.33$, and $s = 2.5$, and we obtain $\Gamma = 1.30$ from eq. (7). Next, calculate α^* using eq. (8), where $M_2/M_1 = 29.14$:

$$\alpha^* = 0.249\times(29.14)^{0.56}+0.0035\times(29.14)^{1.5} = 1.646+0.5506 = 2.197\ .$$

Since the energy transfer factor γ is given by eq. (10) as $\gamma = 4\times 2.014\times 58.69/(2.014+58.69)^2 = 0.1283$, we get $E_{th} = 41.37$ eV from eq. (9). Finally, the sputtering yield of 1 keV D → Ni is, from eq. (6),

$$Y = 0.042\frac{0.94\times 2.197\times 10.06}{4.44\times(1+1.30\times 1.584\times 0.3516^{0.3})}\left[1-\sqrt{\frac{41.37}{1000}}\right]^{2.5} = \frac{0.8726}{11.12}\times 0.5664 = 0.0444\ .$$

Explanation of Graphs

The graphs are ordered by target group in increasing target atomic number and then within each group, by increasing projectile atomic number.

Ordinate	Sputtering yield (atoms/incident ion) at normal incidence.
Abscissa	Kinetic energy of incident ion in eV.
Heading	Ion-target combination He → Cu means He ion on Cu target.
Symbols	Experimental and ACAT simulation data points.
Legend	Reference key for the symbols. The first author and the publication year for each experimental reference are given, the ACAT data are denoted by YAMAMURA, Y.(ACAT). For the complete citation, see References for Graphs.
Solid line	Energy dependence of the sputtering yield calculated using the Yamamura and Tawara empirical formula eq.(6).
Caption	The figure caption lists the mass ratio $A = M_2/M_1$, and the parameters $Q(Z_2)$, $U_s(Z_2)$, $s(Z_2)$, and $W(Z_2)$. The latter is expressed in terms of a factor multiplying U_s.

Table 1 Values of the adjusting parameter q used in the ACAT simulation

target	Z	^{1}H	^{2}D	^{3}T	^{4}He
Be	4	-0.1	-0.1	0.0	0.0
B	5	-0.1	-0.1	0.0	0.0
C*	6	0.0	0.0	0.0	0.1
Al	13	-0.1	-0.1	-0.1	-0.1
Si	14	-0.25	-0.25	-0.3	-0.4
Ti	22	-0.35	-0.35	-0.35	-0.35
V	23	-0.3	-0.3	-0.3	-0.25
Cr	24	-0.1	-0.1	-0.1	-0.1
Mn	25	0.0	0.0	0.0	0.0
Fe	26	-0.25	-0.25	-0.25	-0.2
Co	27	-0.2	-0.2	-0.2	-0.2
Ni	28	-0.2	-0.2	-0.2	-0.15
Cu*	29	0.0	-0.1	-0.1	-0.1
Ge	32	-0.2	-0.2	-0.2	-0.2
Zr	40	-0.25	-0.25	-0.25	-0.25
Nb	41	-0.05	-0.05	0.0	0.0
Mo	42	-0.2	-0.2	-0.2	-0.2
Ru	44	0.0	0.0	0.0	0.0
Rh	45	-0.1	-0.1	-0.1	-0.2
Pd	46	0.0	0.0	0.0	0.0
Ag*	47	-0.1	0.0	0.0	0.0
Sn	50	0.0	0.0	0.0	0.0
Tb*	65	-0.1	0.0	0.0	0.0
Tm*	69	0.0	0.0	0.0	0.0
Hf	72	-0.2	-0.2	-0.2	-0.2
Ta	73	-0.4	-0.5	-0.4	-0.3
W	74	-0.35	-0.4	-0.3	-0.2
Re	75	0.0	-0.1	-0.1	-0.2
Os	76	-0.2	-0.2	-0.2	-0.2
Ir	77	-0.2	-0.2	-0.2	-0.2
Pt	78	-0.2	-0.2	-0.2	-0.2
Au*	79	0.0	-0.1	-0.1	-0.2
Th	90	-0.2	-0.1	-0.2	-0.2
U	92	-0.2	-0.2	-0.2	-0.2

* The OR local model of the electronic energy loss is used for all projectile-target combinations.

Table 2 The surface binding energies U_s and best-fit values of $Q(Z_2)$, $W(Z_2)$ and $s(Z_2)$

target	Z_2	U_s	Q	W	s
Be	4	3.32	1.66	2.32	2.5
B	5	5.77	2.62	4.39	2.5
C	6	7.37	1.70	1.84	2.5
Al	13	3.39	1.0	2.17	2.5
Si	14	4.63	0.66	2.32	2.5
Ti	22	4.85	0.54	2.57	2.5
V	23	5.31	0.72	2.39	2.5
Cr	24	4.10	0.93	1.44	2.5
Mn	25	2.92	0.95	0.88	2.5
Fe	26	4.28	0.75	1.20	2.5
Co	27	4.39	1.02	1.54	2.5
Ni	28	4.44	0.94	1.33	2.5
Cu	29	3.49	1.0	0.73	2.5
Ge	32	3.85	0.59	2.08	2.5
Zr	40	6.25	0.54	2.50	2.8
Nb	41	7.57	0.93	2.65	2.8
Mo	42	6.82	0.85	2.39	2.8
Ru	44	6.74	1.31	2.36	2.5
Rh	45	5.75	1.14	2.59	2.5
Pd	46	3.89	0.85	1.36	2.5
Ag	47	2.95	1.08	1.03	2.8
Sn	50	3.14	0.47	0.88	2.5
Tb	65	4.05	0.90	1.42	2.5
Tm	69	2.42	0.65	0.85	2.5
Hf	72	6.44	0.65	2.25	2.5
Ta	73	8.1	0.56	2.84	2.8
W	74	8.9	0.72	2.14	2.8
Re	75	8.03	1.03	2.81	2.5
Os	76	8.17	1.11	2.86	2.5
Ir	77	6.94	0.96	2.43	2.5
Pt	78	5.84	1.03	3.21	2.5
Au	79	3.81	1.08	1.64	2.8
Th	90	6.2	0.63	2.79	2.5
U	92	5.55	0.66	2.78	2.5

Table 3 Ion-target combinations and the number of experimental references represented in each graphical display

Target \ Ion		^{1}H	^{2}D	^{4}He
		1	1	2
Be	4	3	3	5
B	5	1	1	2
C	6	8	5	7
Al	13	2	3	4
Si	14	1	1	3
Ti	22	2	4	8
V	23	1	1	6
Cr	24			1
Mn	25			
Fe	26	3	3	3
Co	27			1
Ni	28	5	1	6
Cu	29	4	4	6
Ge	32			1
Zr	40	1	1	3
Nb	41	2	3	3
Mo	42	7	3	10
Ru	44			
Rh	45			1
Pd	46			1
Ag	47	4	3	4
Sn	50			
Tb	65			
Tm	69			
Hf	72			1
Ta	73	3	3	5
W	74	3	3	5
Re	75			
Os	76			1
Ir	77			1
Pt	78			1
Au	79	4	3	4
Th	90			1
U	92			1

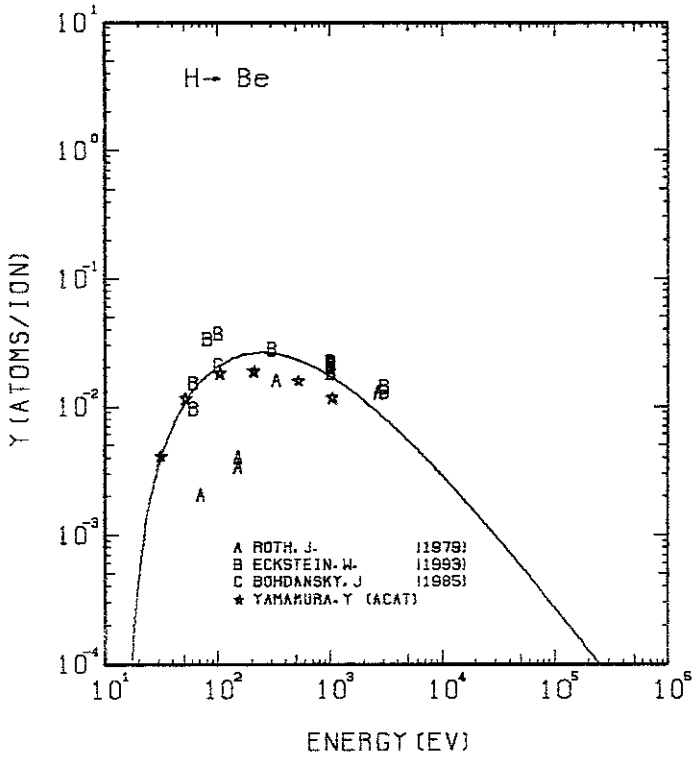

FIG. 1 ENERGY DEPENDENCE OF THE SPUTTERING YIELD OF BE WITH H^+.
A= 8.94, Q= 1.66, Us= 3.32EV, s= 2.50,
W= 0.70Us.

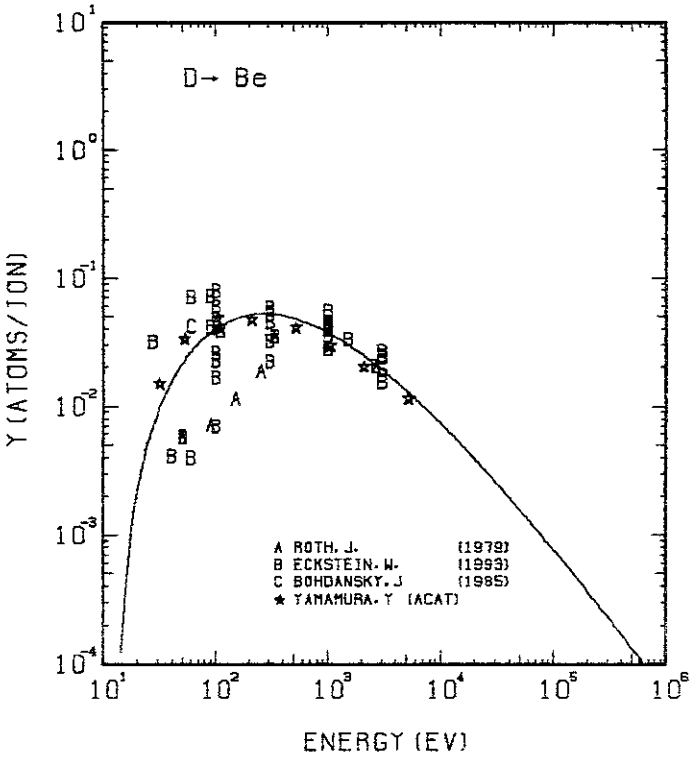

FIG. 2 ENERGY DEPENDENCE OF THE SPUTTERING YIELD OF BE WITH D^+.
A= 4.47, Q= 1.66, Us= 3.32EV, s= 2.50,
W= 0.70Us.

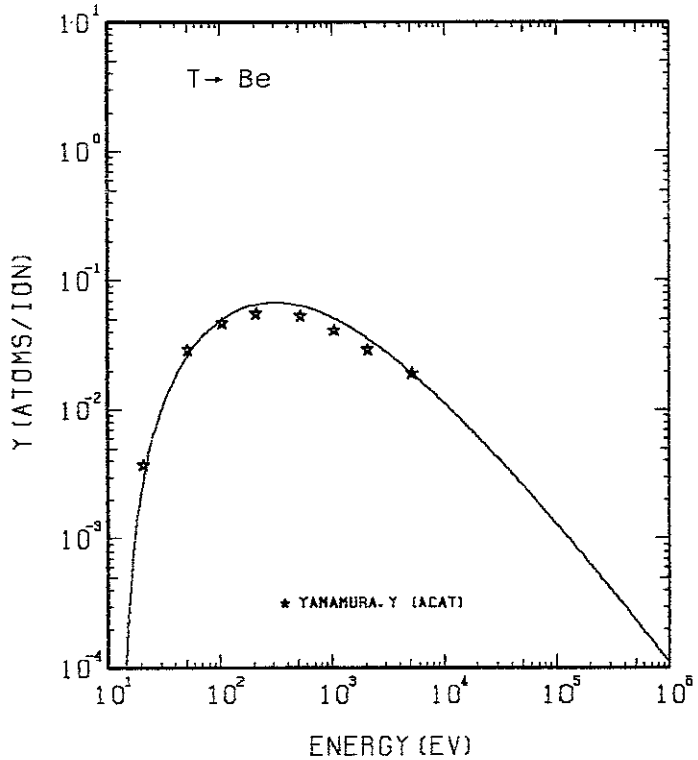

FIG. 3 ENERGY DEPENDENCE OF THE SPUTTERING YIELD OF BE WITH T^+.
A= 2.99, Q= 1.66, Us= 3.32EV, s= 2.50,
W= 0.70Us.

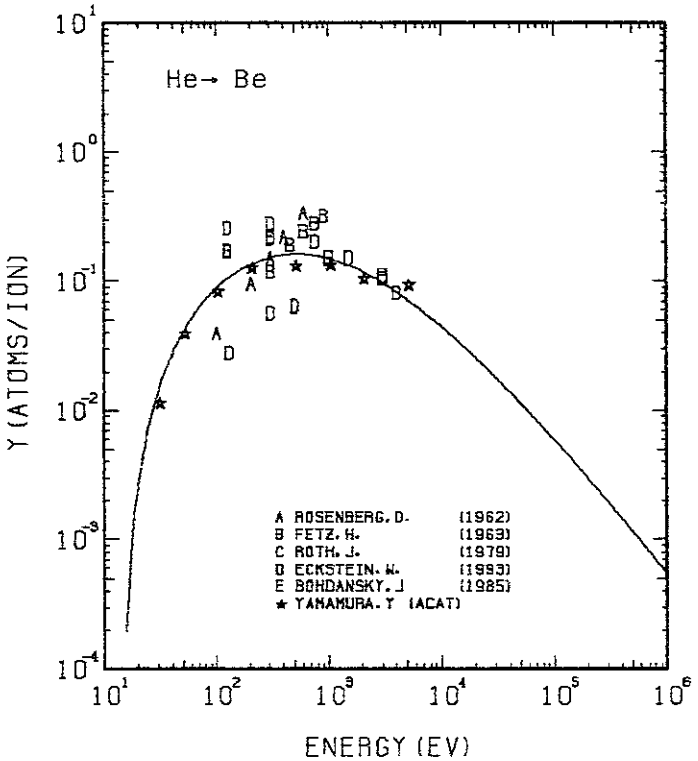

FIG. 4 ENERGY DEPENDENCE OF THE SPUTTERING YIELD OF BE WITH HE^+.
A= 2.25, Q= 1.66, Us= 3.32EV, s= 2.50,
W= 0.70Us.

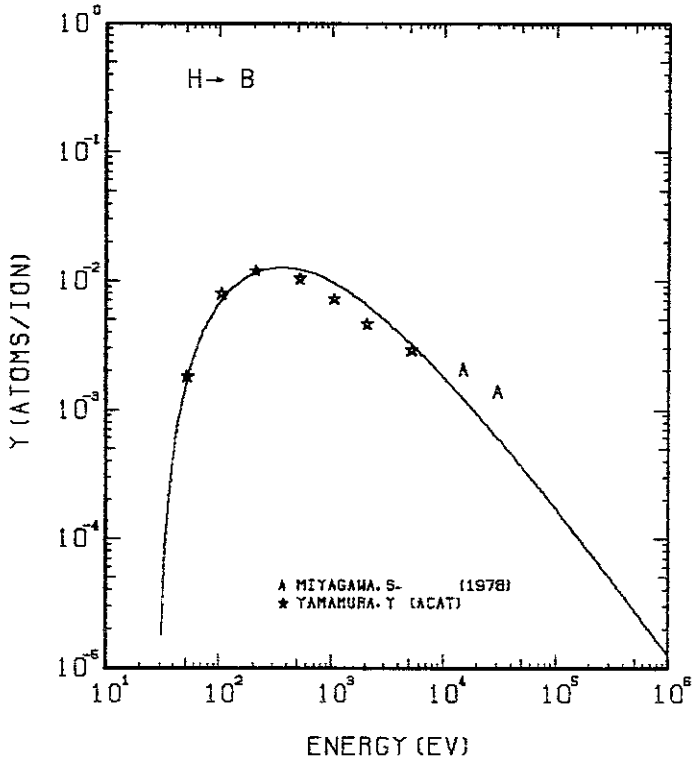

FIG. 5 ENERGY DEPENDENCE OF THE SPUTTERING YIELD OF B WITH H^+.
A= 10.72, Q= 2.62, Us= 5.77EV, s= 2.50,
W= 0.76Us.

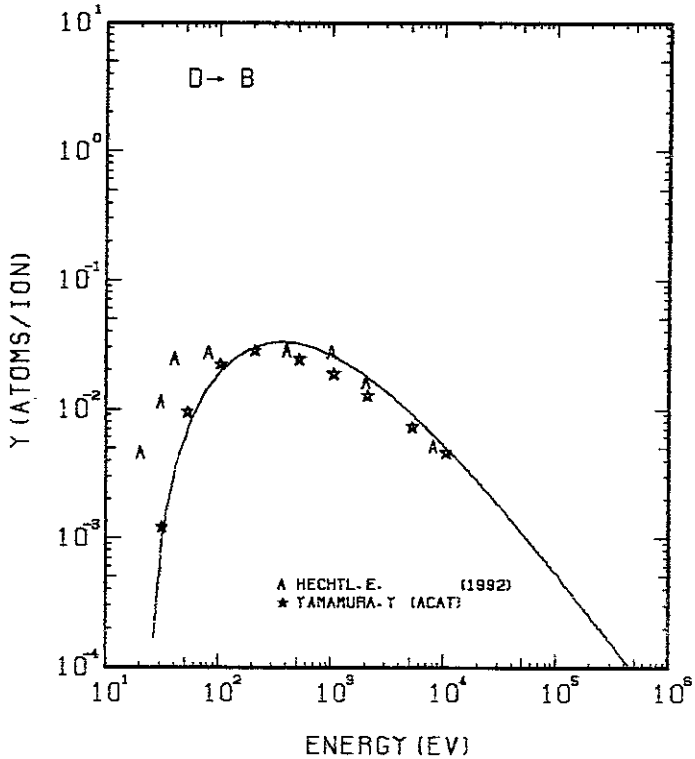

FIG. 6 ENERGY DEPENDENCE OF THE SPUTTERING YIELD OF B WITH D^+.
A= 5.37, Q= 2.62, Us= 5.77EV, s= 2.50,
W= 0.76Us.

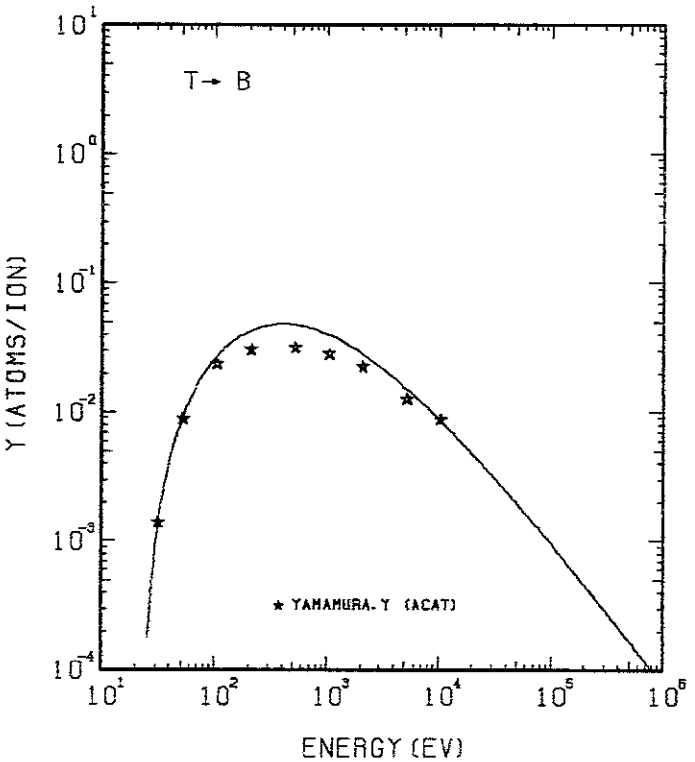

FIG. 7 ENERGY DEPENDENCE OF THE SPUTTERING YIELD OF B WITH T^+.
A= 3.58, Q= 2.62, Us= 5.77EV, s= 2.50,
W= 0.76Us.

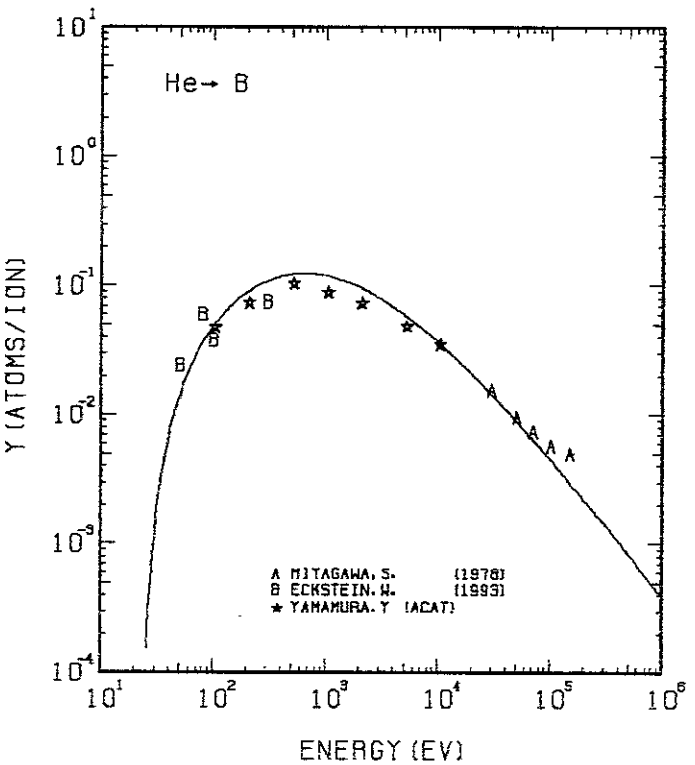

FIG. 8 ENERGY DEPENDENCE OF THE SPUTTERING YIELD OF B WITH HE^+.
A= 2.70, Q= 2.62, Us= 5.77EV, s= 2.50,
W= 0.76Us.

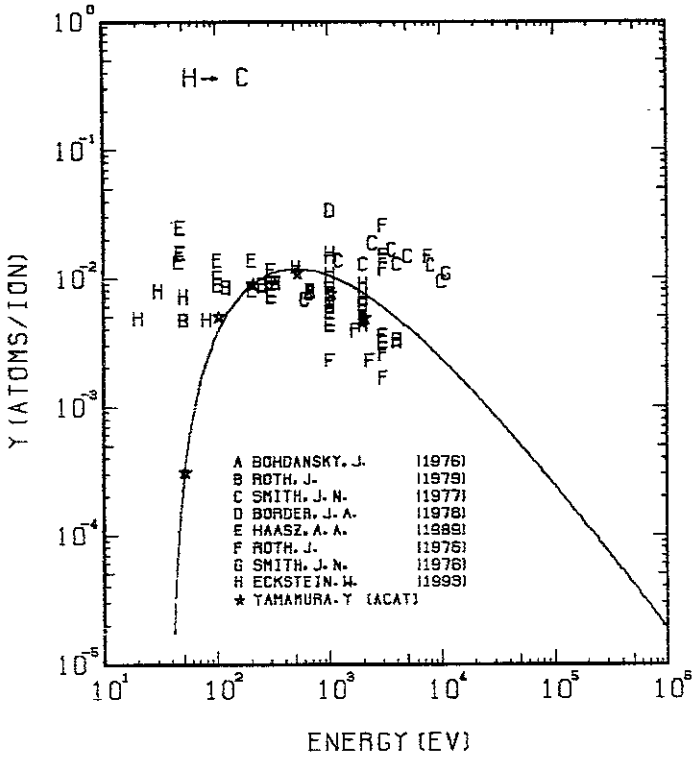

FIG. 9 ENERGY DEPENDENCE OF THE SPUTTERING YIELD OF C WITH H^+. A= 11.91, Q= 1.70, Us= 7.37EV, S= 2.50, W= 0.25Us. EXPERIMENTAL DATA FOR DIFFERENT KINDS OF GRAPHITE ARE INCLUDED. THE CHEMICAL EROSION IS FOUND EVEN AT ROOM TEMPERATURE.

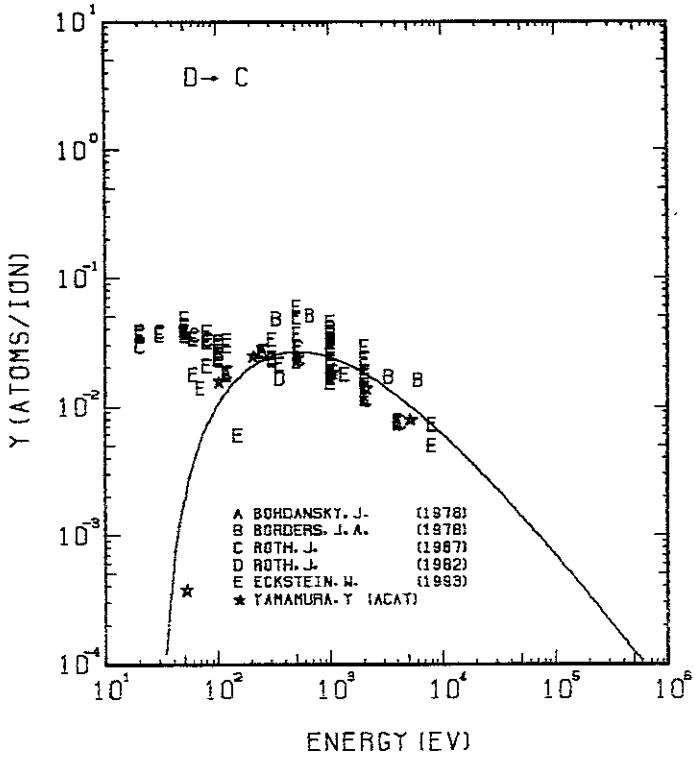

FIG. 10 ENERGY DEPENDENCE OF THE SPUTTERING YIELD OF C WITH D^+. A= 5.96, Q= 1.70, Us= 7.37EV, S= 2.50, W= 0.25Us. EXPERIMENTAL DATA FOR DIFFERENT KINDS OF GRAPHITE ARE INCLUDED. THE CHEMICAL EROSION IS FOUND EVEN AT ROOM TEMPERATURE.

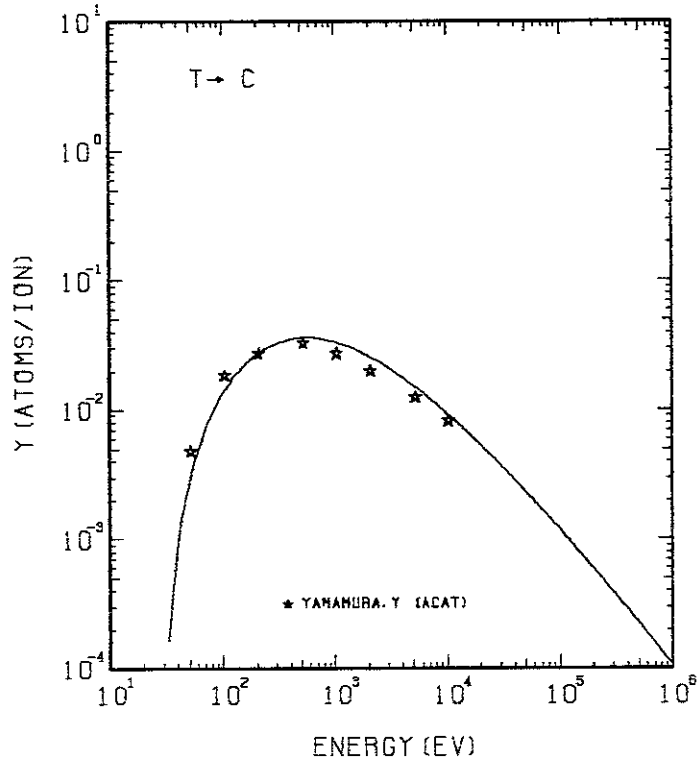

FIG. 11 ENERGY DEPENDENCE OF THE SPUTTERING YIELD OF C WITH T^+. A= 3.98, Q= 1.70, Us= 7.37EV, S= 2.50, W= 0.25Us. EXPERIMENTAL DATA FOR DIFFERENT KINDS OF GRAPHITE ARE INCLUDED.

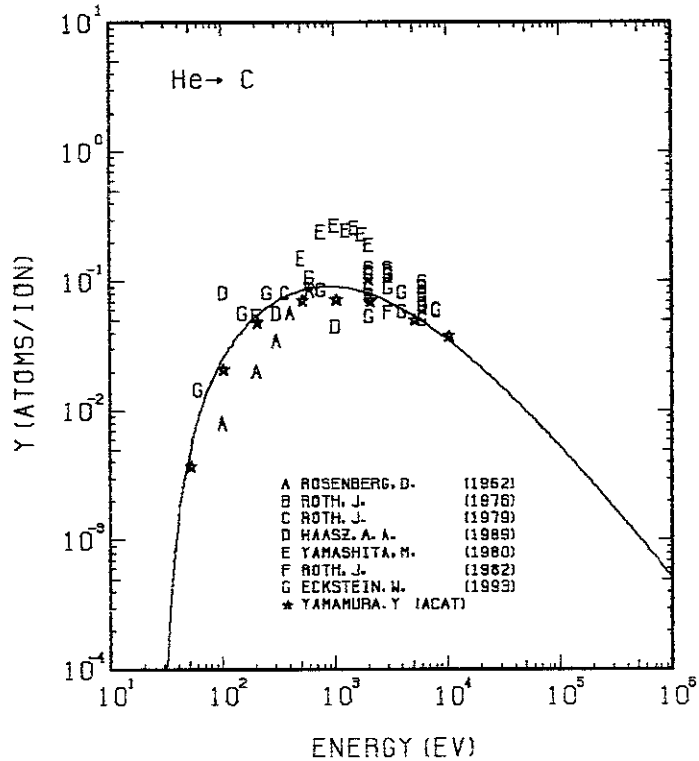

FIG. 12 ENERGY DEPENDENCE OF THE SPUTTERING YIELD OF C WITH HE^+. A= 3.00, Q= 1.70, Us= 7.37EV, S= 2.50, W= 0.25Us. EXPERIMENTAL DATA FOR DIFFERENT KINDS OF GRAPHITE ARE INCLUDED.

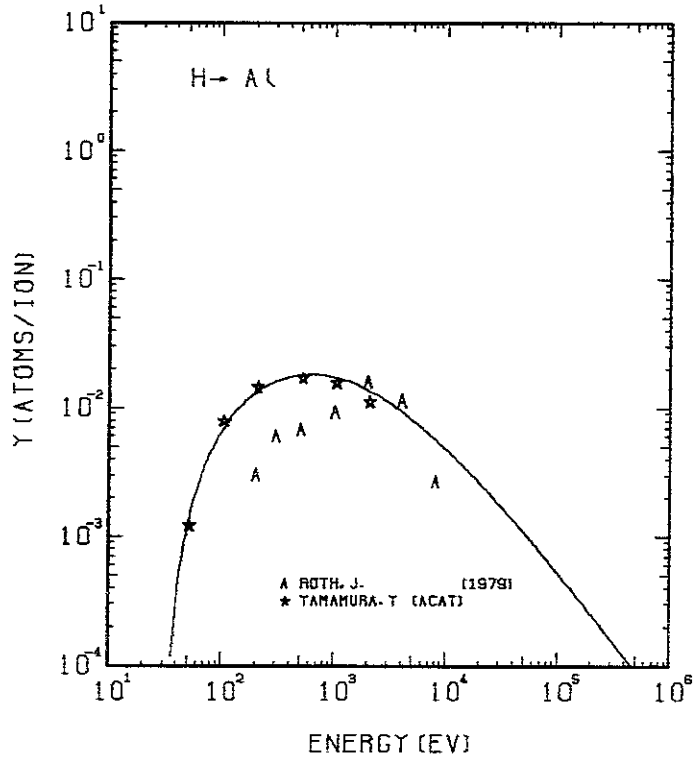

FIG. 13 ENERGY DEPENDENCE OF THE SPUTTERING YIELD OF AL WITH H^+. A= 26.77, Q= 1.00, Us= 3.39EV, s= 2.50, W= 0.64Us. EXPERIMENTAL DATA MIGHT BE AFFCTED BY OXIDE FORMAION DURING SPUTTERING.

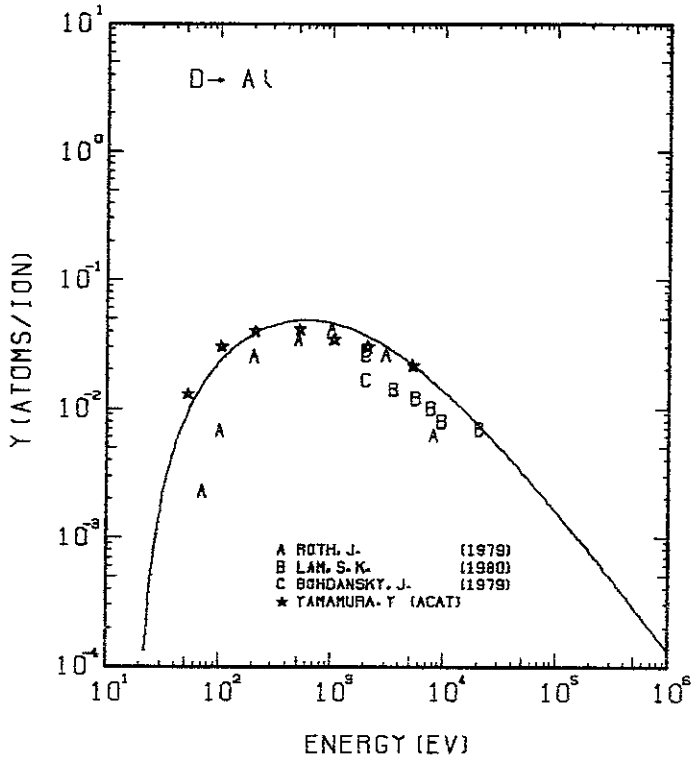

FIG. 14 ENERGY DEPENDENCE OF THE SPUTTERING YIELD OF AL WITH D^+. A= 13.40, Q= 1.00, Us= 3.39EV, s= 2.50, W= 0.64Us. EXPERIMENTAL DATA MIGHT BE AFFCTED BY OXIDE FORMAION DURING SPUTTERING.

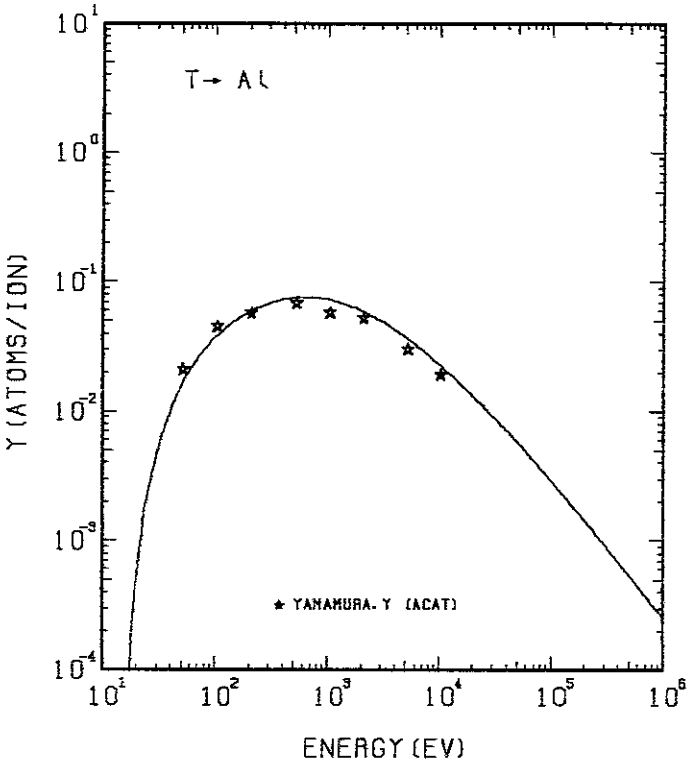

FIG. 15 ENERGY DEPENDENCE OF THE SPUTTERING YIELD OF AL WITH T^+. A= 8.94, Q= 1.00, Us= 3.39EV, s= 2.50, W= 0.64Us. EXPERIMENTAL DATA MIGHT BE AFFCTED BY OXIDE FORMAION DURING SPUTTERING.

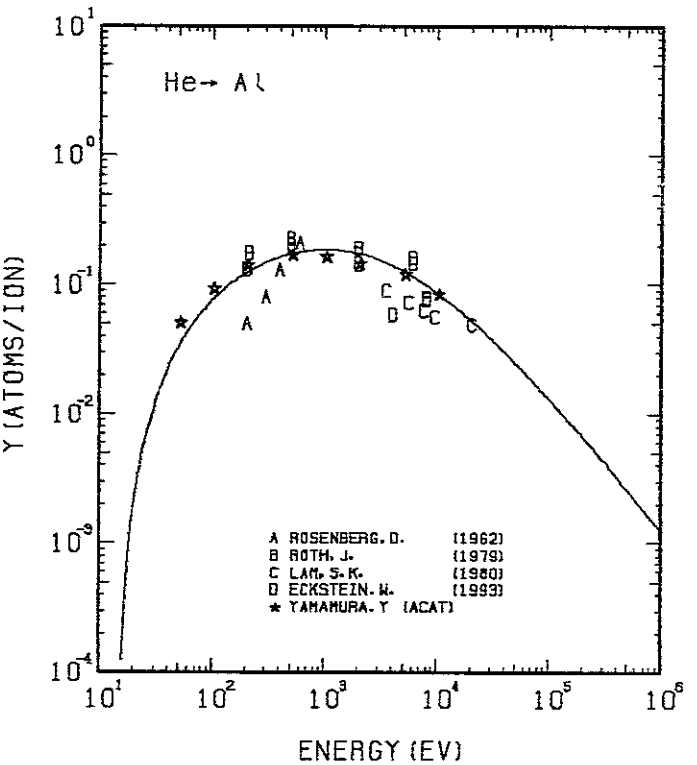

FIG. 16 ENERGY DEPENDENCE OF THE SPUTTERING YIELD OF AL WITH HE^+. A= 6.74, Q= 1.00, Us= 3.39EV, s= 2.50, W= 0.64Us. EXPERIMENTAL DATA MIGHT BE AFFCTED BY OXIDE FORMAION DURING SPUTTERING.

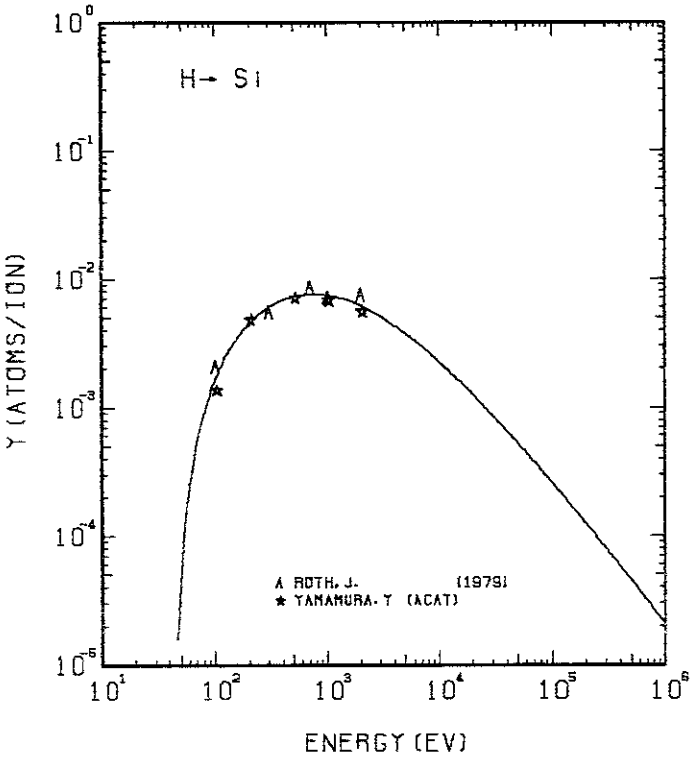

FIG. 17 ENERGY DEPENDENCE OF THE SPUTTERING YIELD OF SI WITH H^+.
A= 27.86, Q= 0.66, Us= 4.63EV, s= 2.50,
W= 0.50Us.

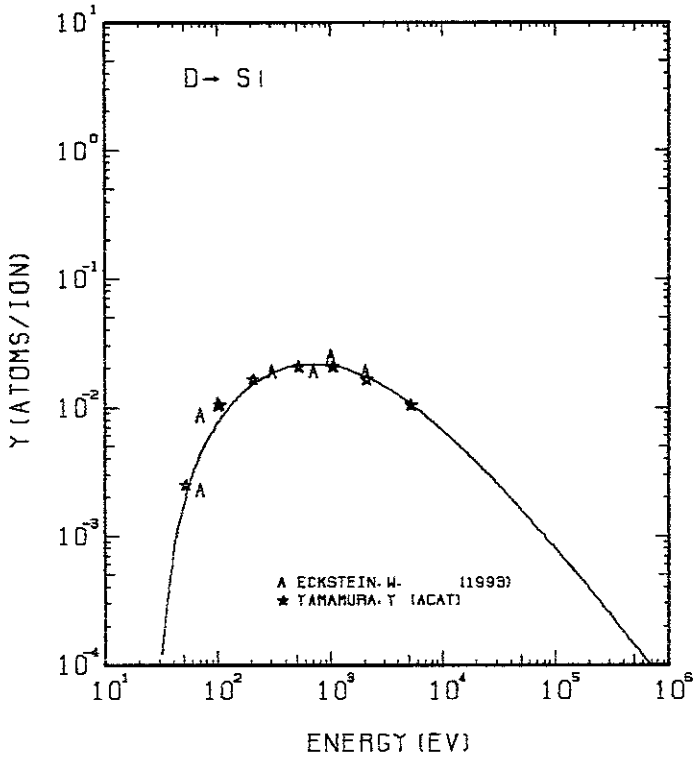

FIG. 18 ENERGY DEPENDENCE OF THE SPUTTERING YIELD OF SI WITH D^+.
A= 13.94, Q= 0.66, Us= 4.63EV, s= 2.50,
W= 0.50Us.

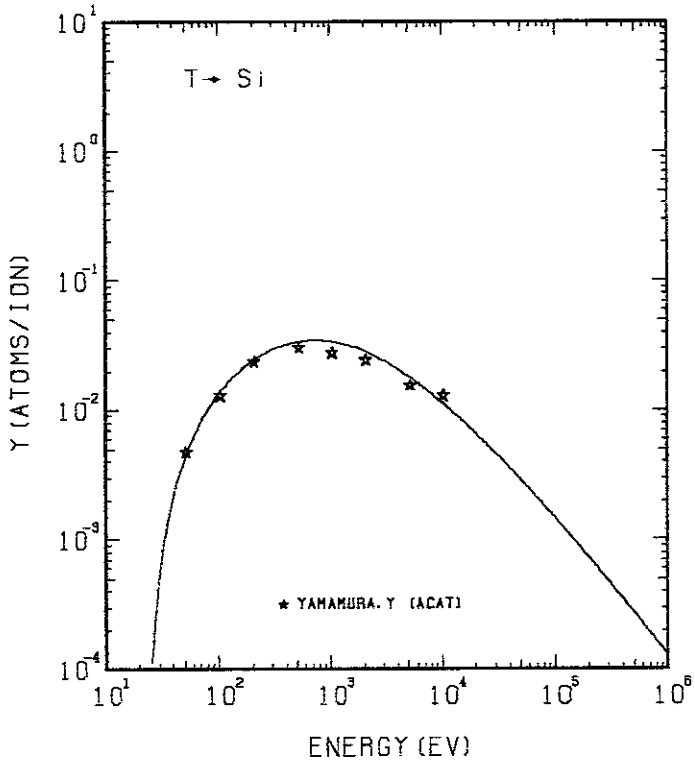

FIG. 19 ENERGY DEPENDENCE OF THE SPUTTERING YIELD OF SI WITH T^+.
A= 9.31, Q= 0.66, Us= 4.63EV, s= 2.50,
W= 0.50Us.

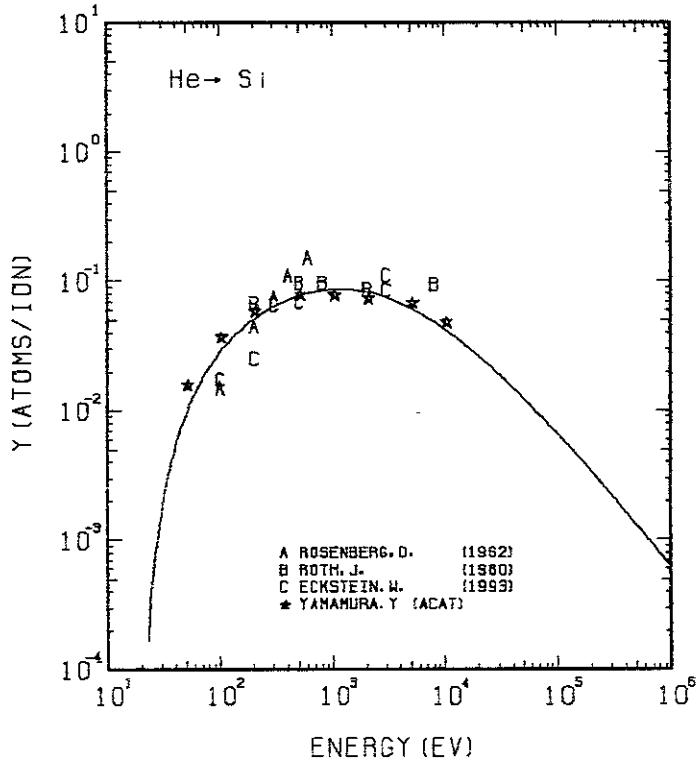

FIG. 20 ENERGY DEPENDENCE OF THE SPUTTERING YIELD OF SI WITH HE^+.
A= 7.01, Q= 0.66, Us= 4.63EV, s= 2.50,
W= 0.50Us.

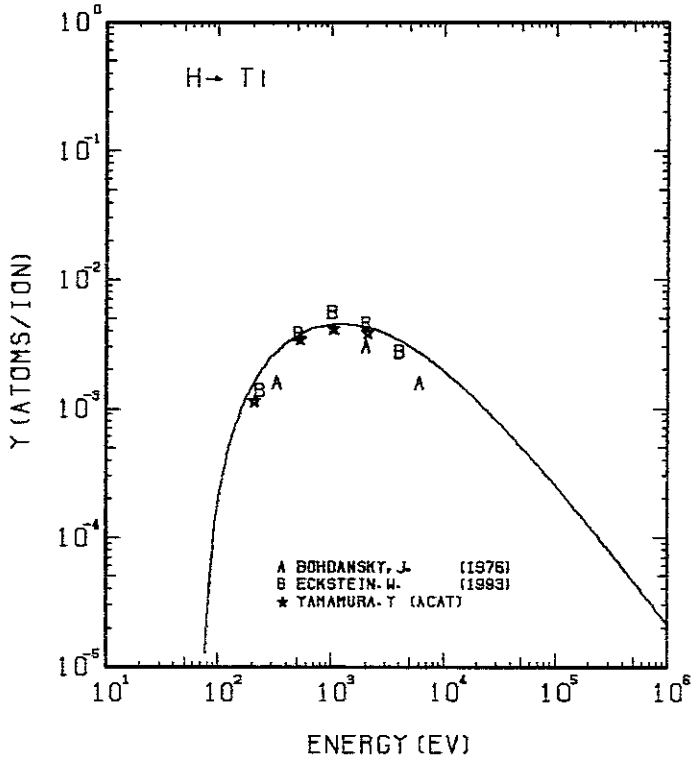

FIG. 21 ENERGY DEPENDENCE OF THE SPUTTERING YIELD OF TI WITH H^+.
A= 47.52, Q= 0.54, Us= 4.85EV, s= 2.50,
W= 0.53Us.

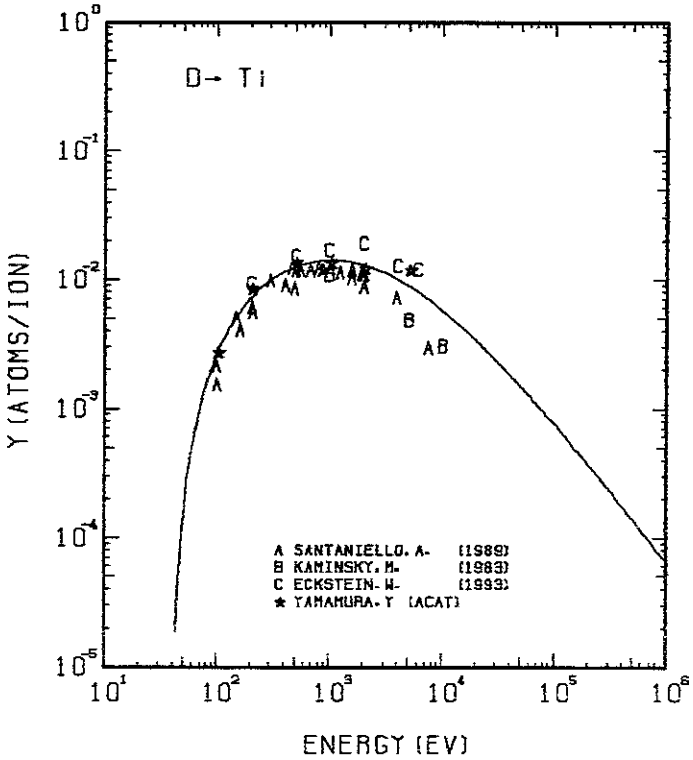

FIG. 22 ENERGY DEPENDENCE OF THE SPUTTERING YIELD OF TI WITH D^+.
A= 23.78, Q= 0.54, Us= 4.85EV, s= 2.50,
W= 0.53Us.

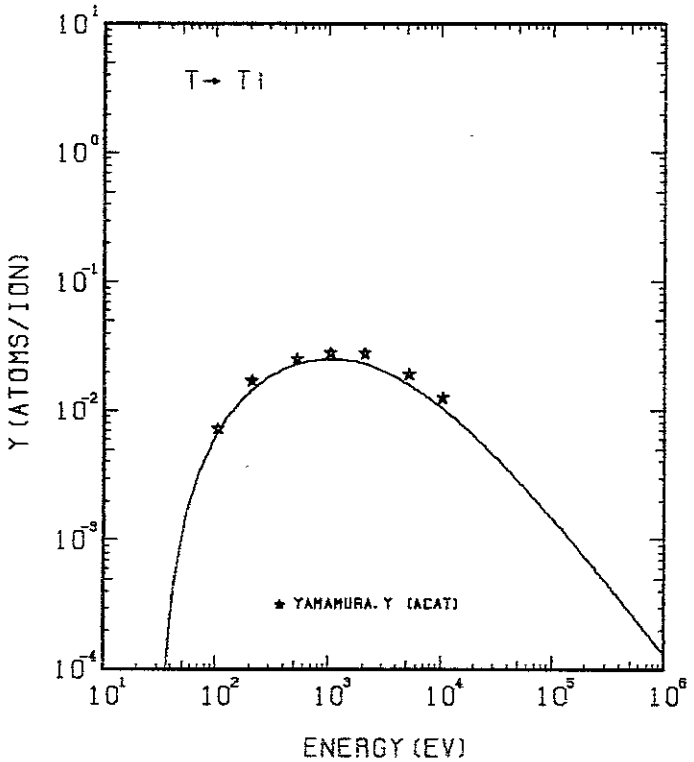

FIG. 23 ENERGY DEPENDENCE OF THE SPUTTERING YIELD OF TI WITH T^+.
A= 15.88, Q= 0.54, Us= 4.85EV, s= 2.50,
W= 0.53Us.

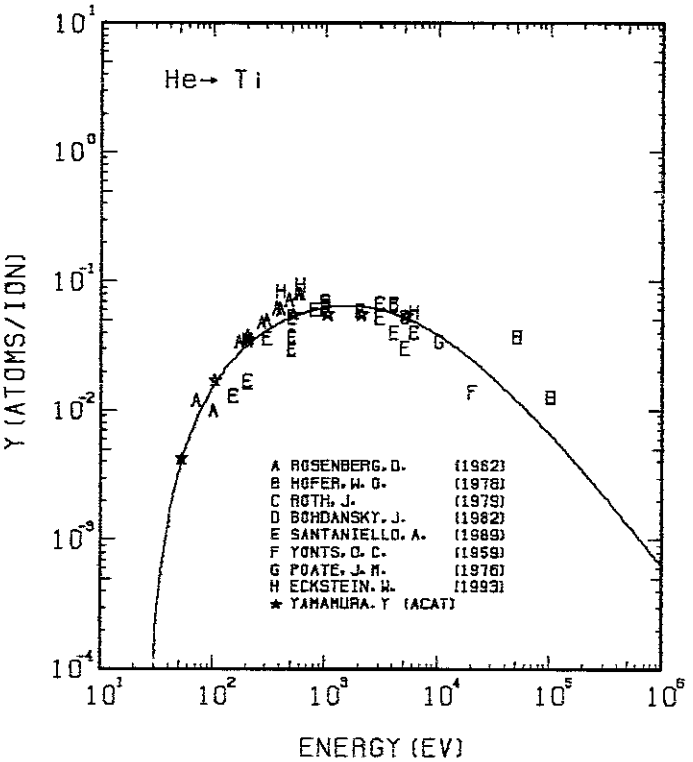

FIG. 24 ENERGY DEPENDENCE OF THE SPUTTERING YIELD OF TI WITH HE^+.
A= 11.97, Q= 0.54, Us= 4.85EV, s= 2.50,
W= 0.53Us.

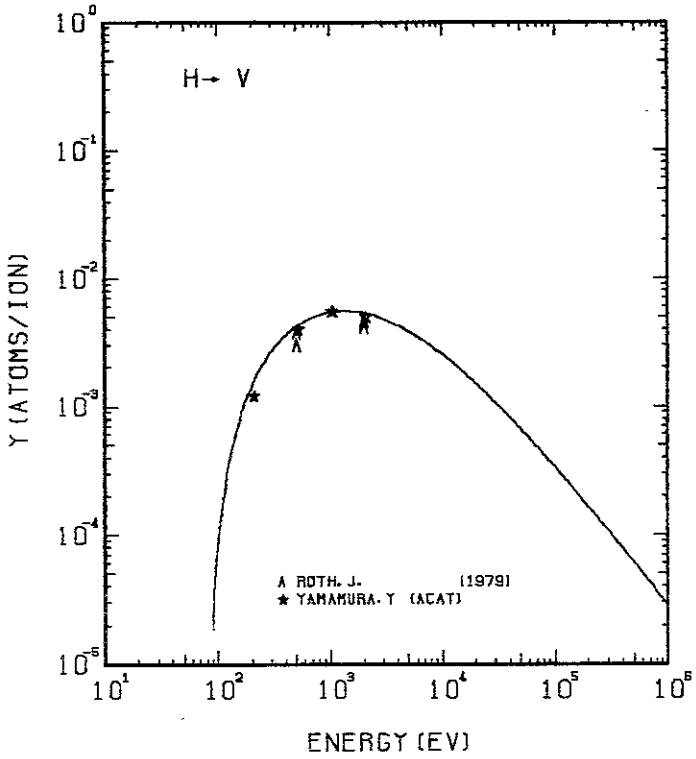

FIG. 25 ENERGY DEPENDENCE OF THE SPUTTERING YIELD OF V WITH H^+.
A= 50.54, Q= 0.72, Us= 5.31 EV, s= 2.50, W= 0.45Us.

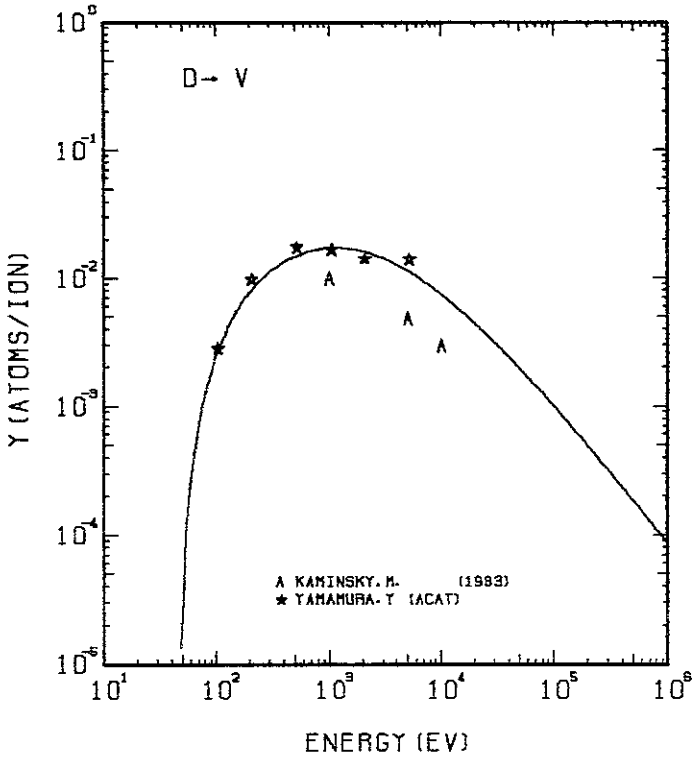

FIG. 26 ENERGY DEPENDENCE OF THE SPUTTERING YIELD OF V WITH D^+.
A= 25.29, Q= 0.72, Us= 5.31 EV, s= 2.50, W= 0.45Us.

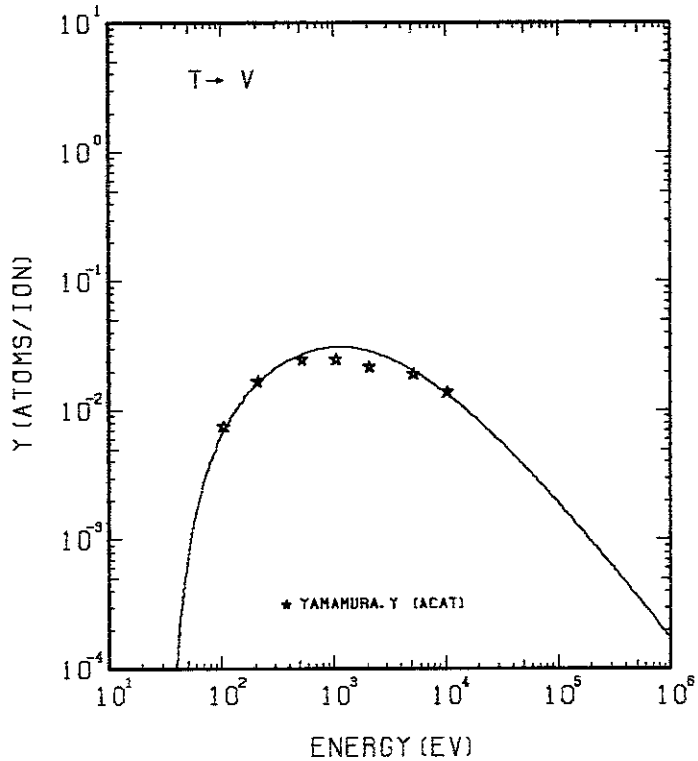

FIG. 27 ENERGY DEPENDENCE OF THE SPUTTERING YIELD OF V WITH T^+.
A= 16.88, Q= 0.72, Us= 5.31 EV, s= 2.50, W= 0.45Us.

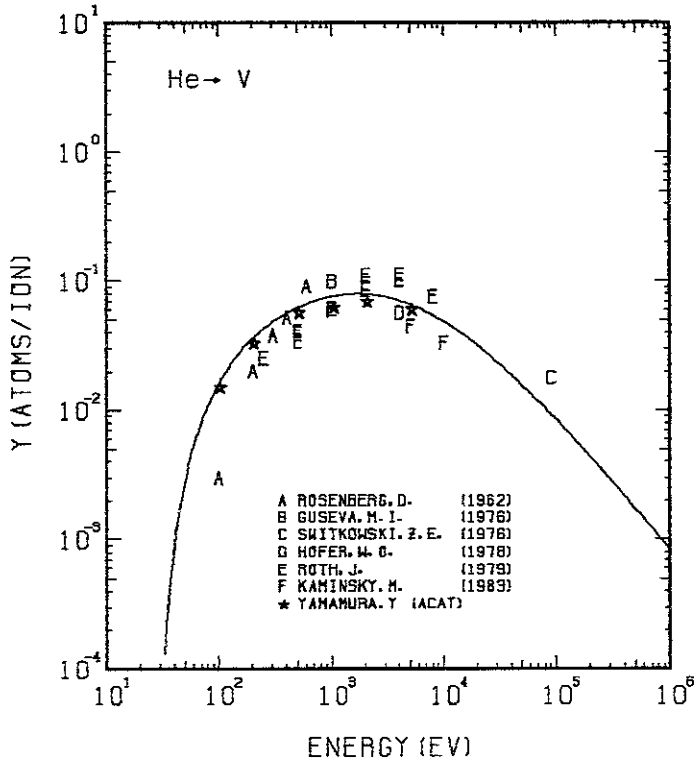

FIG. 28 ENERGY DEPENDENCE OF THE SPUTTERING YIELD OF V WITH HE^+.
A= 12.73, Q= 0.72, Us= 5.31 EV, s= 2.50, W= 0.45Us.

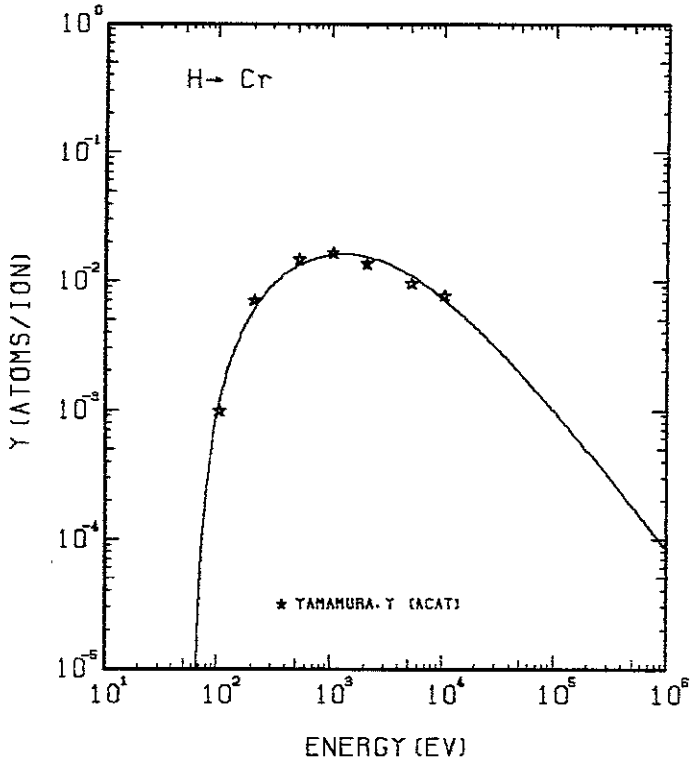

FIG. 29 ENERGY DEPENDENCE OF THE SPUTTERING YIELD OF CR WITH H^+.
A= 51.59, 0= 0.93, Us= 4.10EV, s= 2.50,
W= 0.35Us.

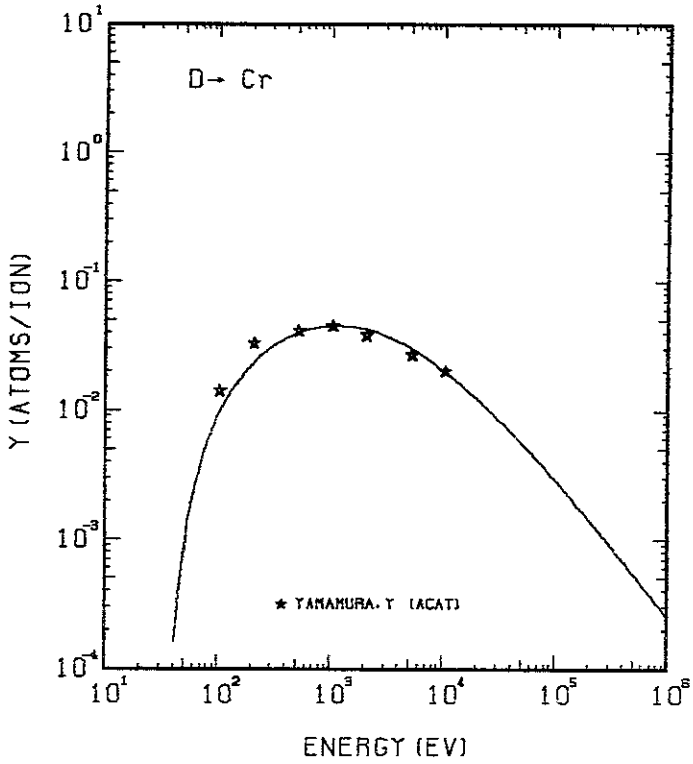

FIG. 30 ENERGY DEPENDENCE OF THE SPUTTERING YIELD OF CR WITH D^+.
A= 25.82, 0= 0.93, Us= 4.10EV, s= 2.50,
W= 0.35Us.

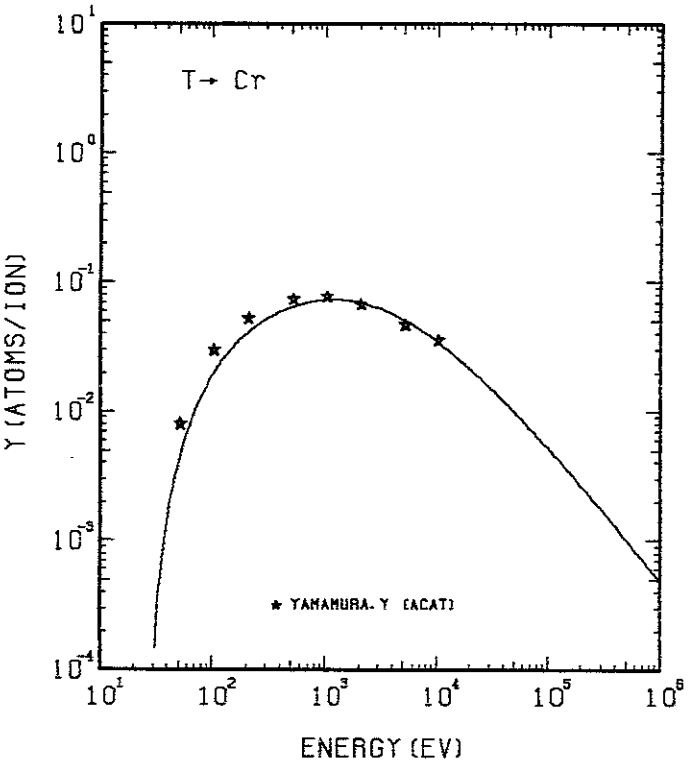

FIG. 31 ENERGY DEPENDENCE OF THE SPUTTERING YIELD OF CR WITH T^+.
A= 17.24, 0= 0.93, Us= 4.10EV, s= 2.50,
W= 0.35Us.

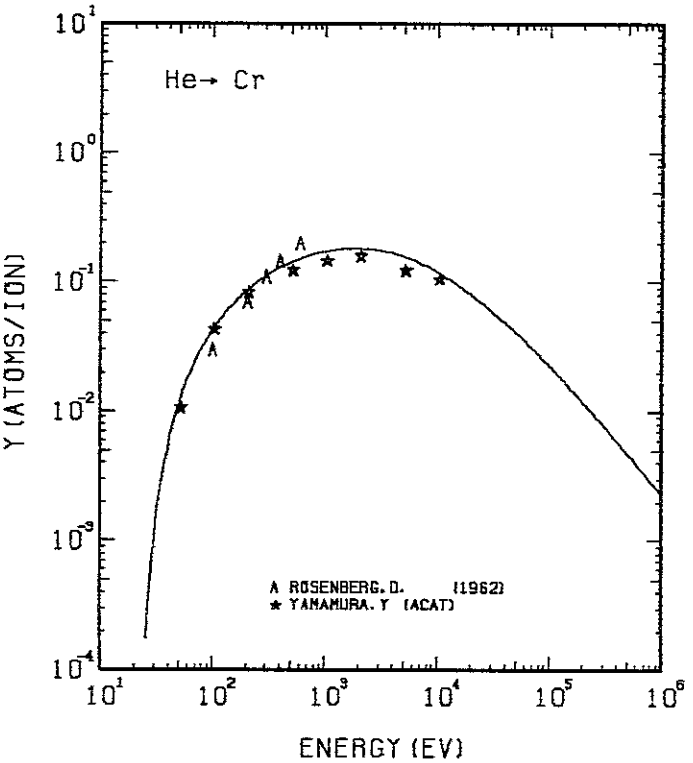

FIG. 32 ENERGY DEPENDENCE OF THE SPUTTERING YIELD OF CR WITH HE^+.
A= 12.99, 0= 0.93, Us= 4.10EV, s= 2.50,
W= 0.35Us.

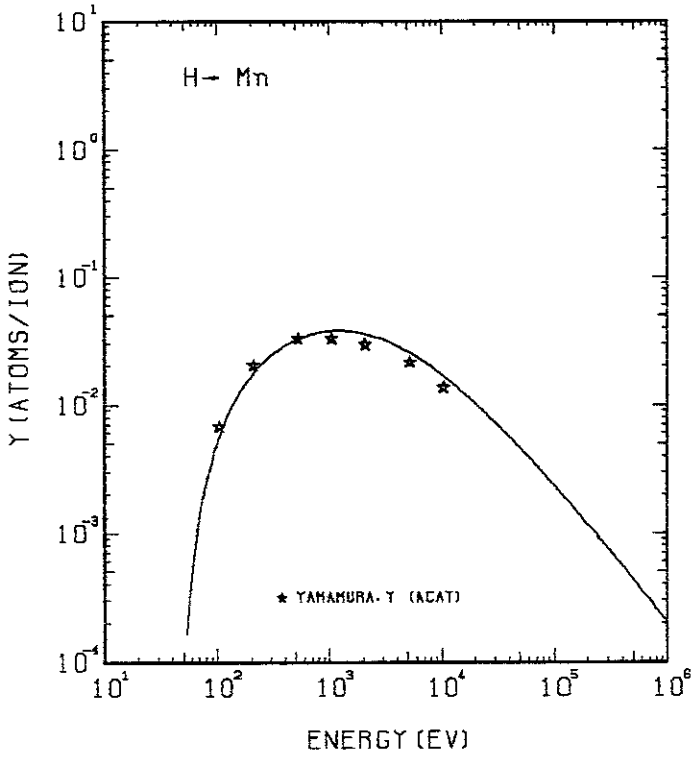

FIG. 33 ENERGY DEPENDENCE OF THE SPUTTERING YIELD OF MN WITH H^+.
A= 54.48, Q= 0.95, Us= 2.92EV, s= 2.50,
W= 0.30Us.

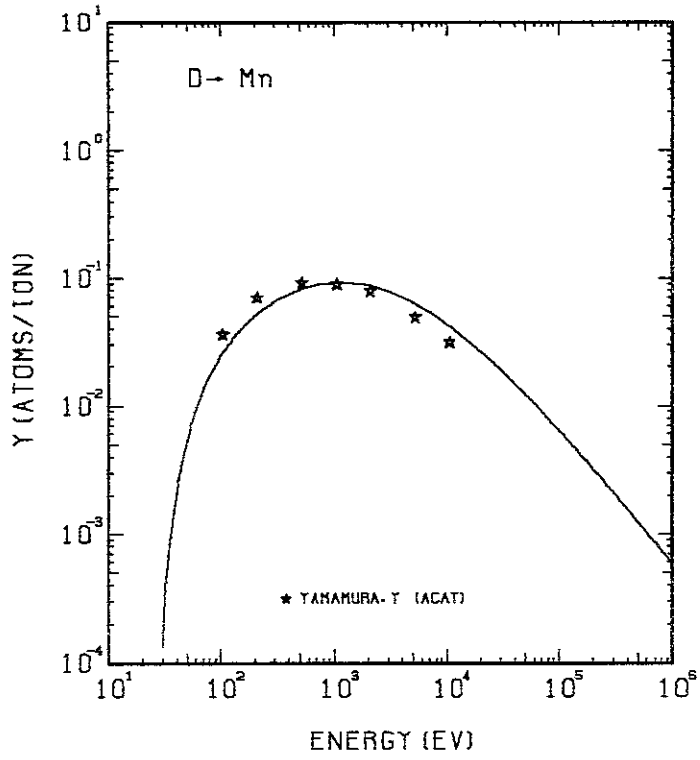

FIG. 34 ENERGY DEPENDENCE OF THE SPUTTERING YIELD OF MN WITH D^+.
A= 27.27, Q= 0.95, Us= 2.92EV, s= 2.50,
W= 0.30Us.

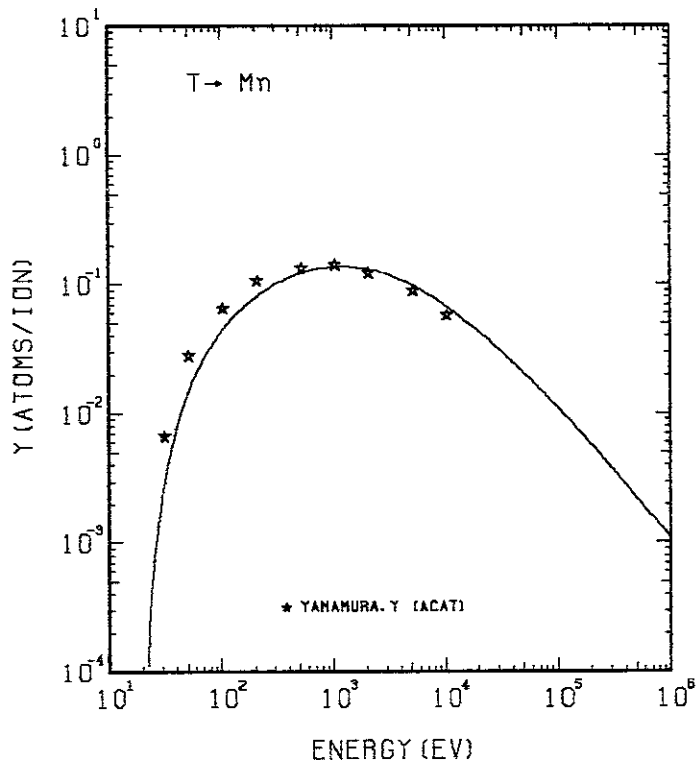

FIG. 35 ENERGY DEPENDENCE OF THE SPUTTERING YIELD OF MN WITH T^+.
A= 18.21, Q= 0.95, Us= 2.92EV, s= 2.50,
W= 0.30Us.

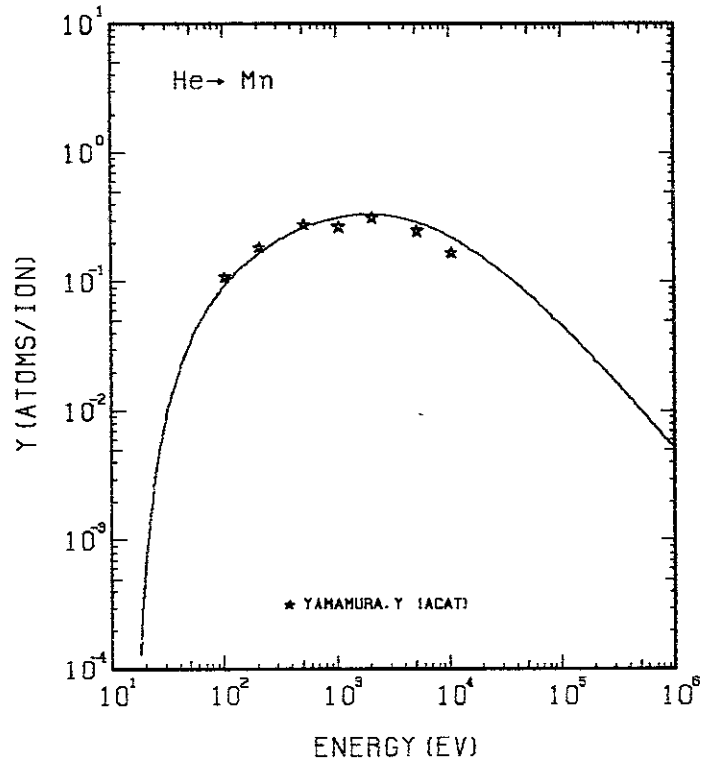

FIG. 36 ENERGY DEPENDENCE OF THE SPUTTERING YIELD OF MN WITH HE^+.
A= 13.72, Q= 0.95, Us= 2.92EV, s= 2.50,
W= 0.30Us.

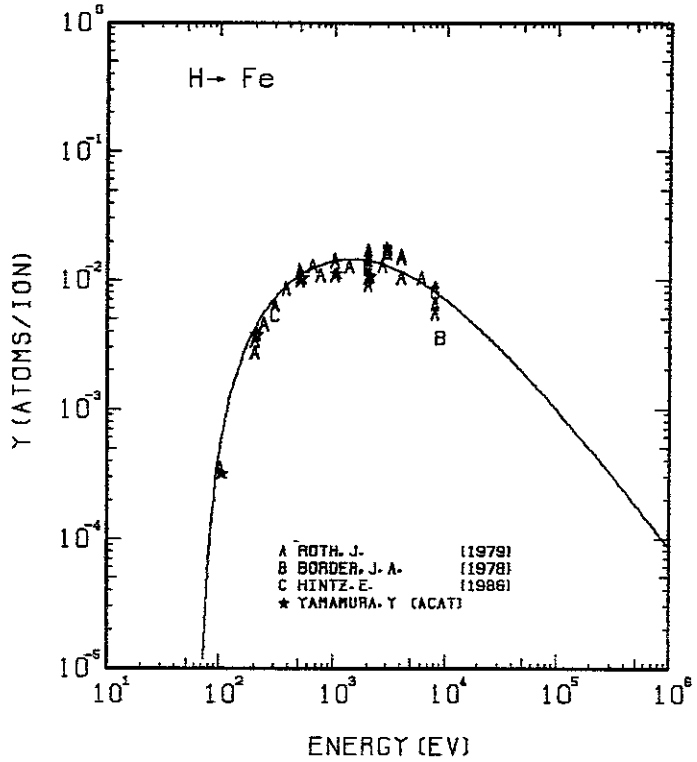

FIG. 37 ENERGY DEPENDENCE OF THE SPUTTERING YIELD OF FE WITH H^+.
A= 55.41, Q= 0.75, Us= 4.28EV, s= 2.50,
W= 0.28Us.

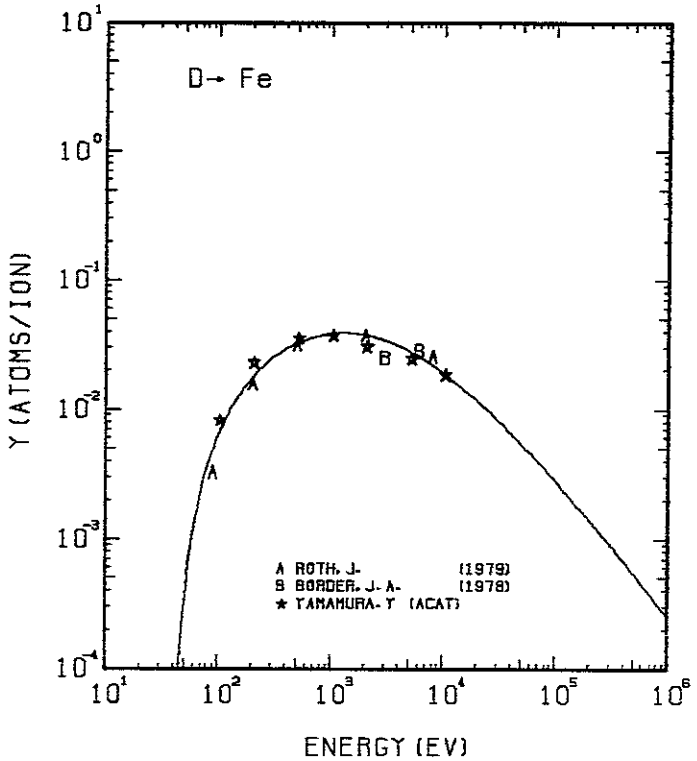

FIG. 38 ENERGY DEPENDENCE OF THE SPUTTERING YIELD OF FE WITH D^+.
A= 27.73, Q= 0.75, Us= 4.28EV, s= 2.50,
W= 0.28Us.

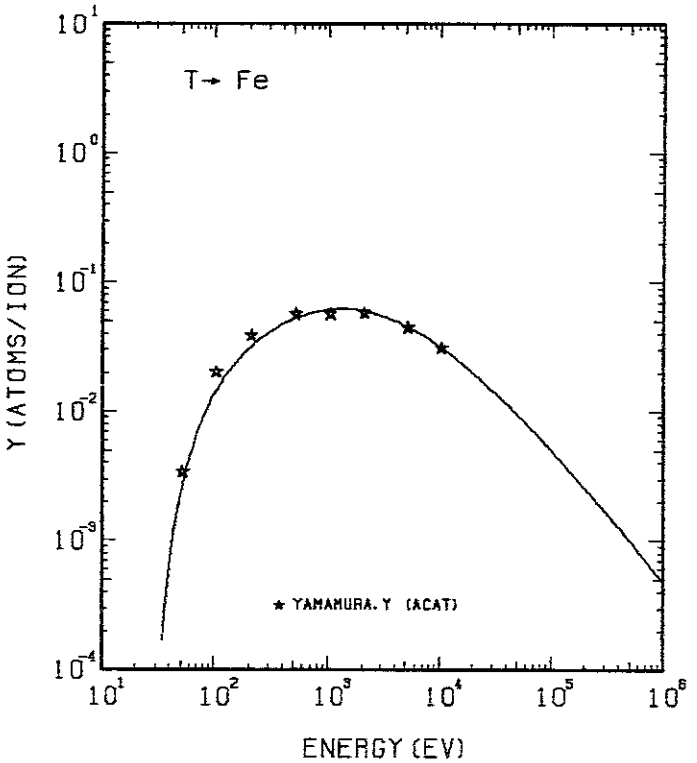

FIG. 39 ENERGY DEPENDENCE OF THE SPUTTERING YIELD OF FE WITH T^+.
A= 18.51, Q= 0.75, Us= 4.28EV, s= 2.50,
W= 0.28Us.

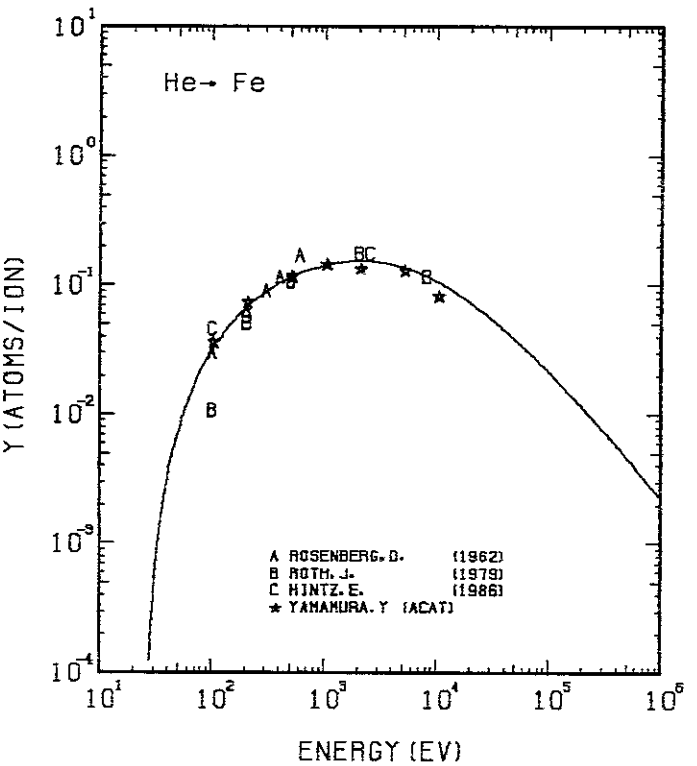

FIG. 40 ENERGY DEPENDENCE OF THE SPUTTERING YIELD OF FE WITH HE^+.
A= 13.95, Q= 0.75, Us= 4.28EV, s= 2.50,
W= 0.28Us.

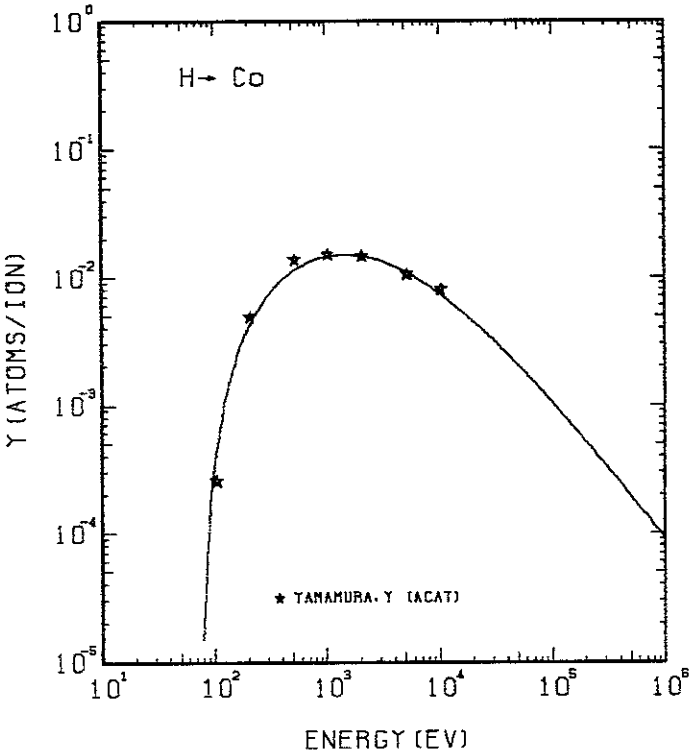

FIG. 41 ENERGY DEPENDENCE OF THE SPUTTERING YIELD OF CO WITH H^+.
A= 58.46, Q= 1.02, Us= 4.39EV, s= 2.50,
W= 0.35Us.

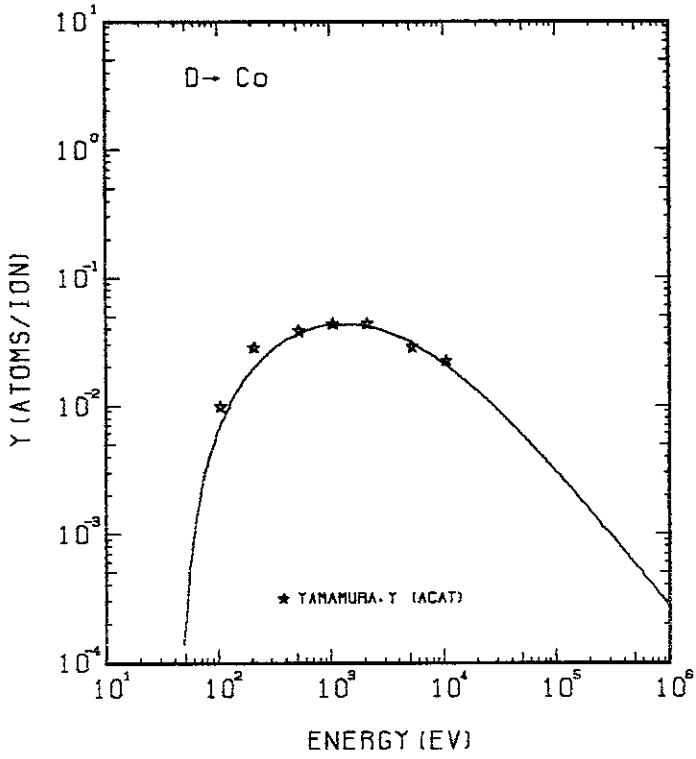

FIG. 42 ENERGY DEPENDENCE OF THE SPUTTERING YIELD OF CO WITH D^+.
A= 29.26, Q= 1.02, Us= 4.39EV, s= 2.50,
W= 0.35Us.

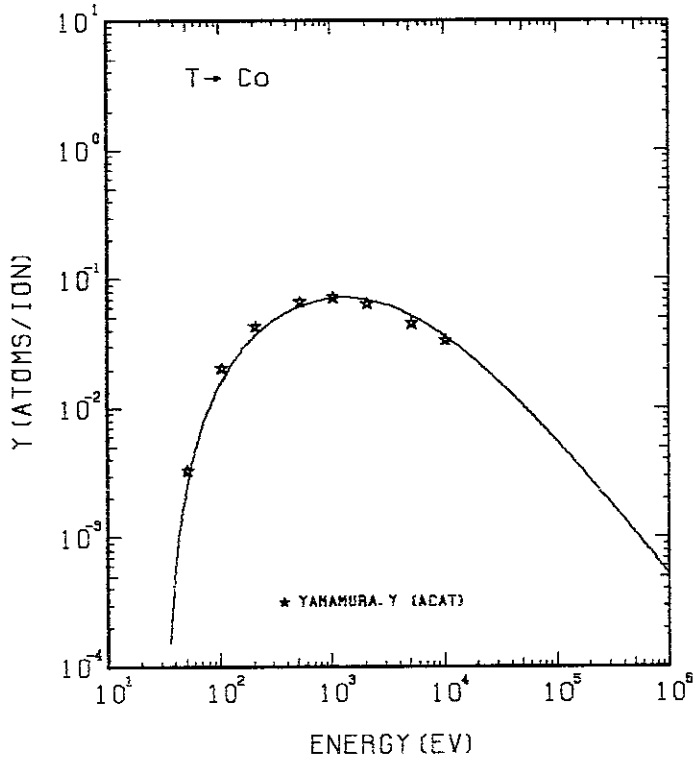

FIG. 43 ENERGY DEPENDENCE OF THE SPUTTERING YIELD OF CO WITH T^+.
A= 19.53, Q= 1.02, Us= 4.39EV, s= 2.50,
W= 0.35Us.

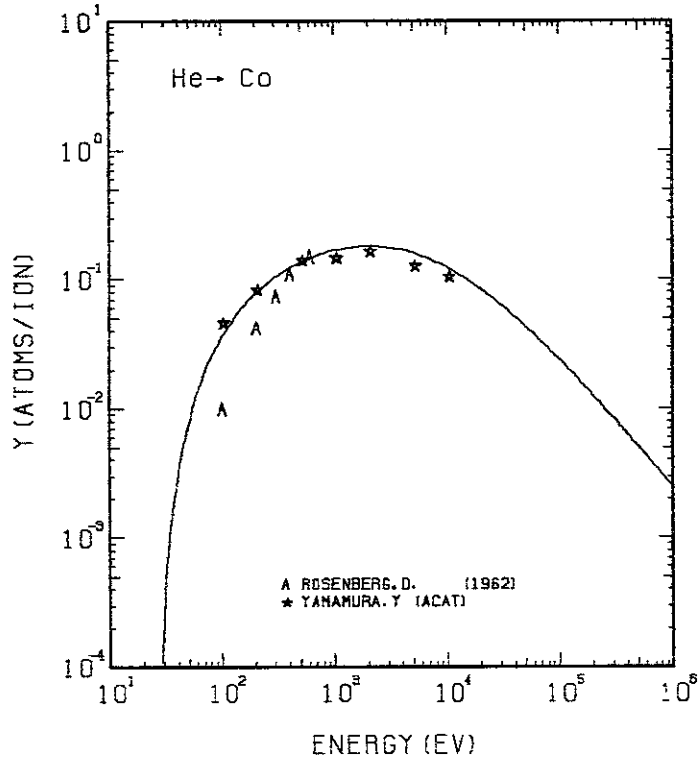

FIG. 44 ENERGY DEPENDENCE OF THE SPUTTERING YIELD OF CO WITH HE^+.
A= 14.72, Q= 1.02, Us= 4.39EV, s= 2.50,
W= 0.35Us.

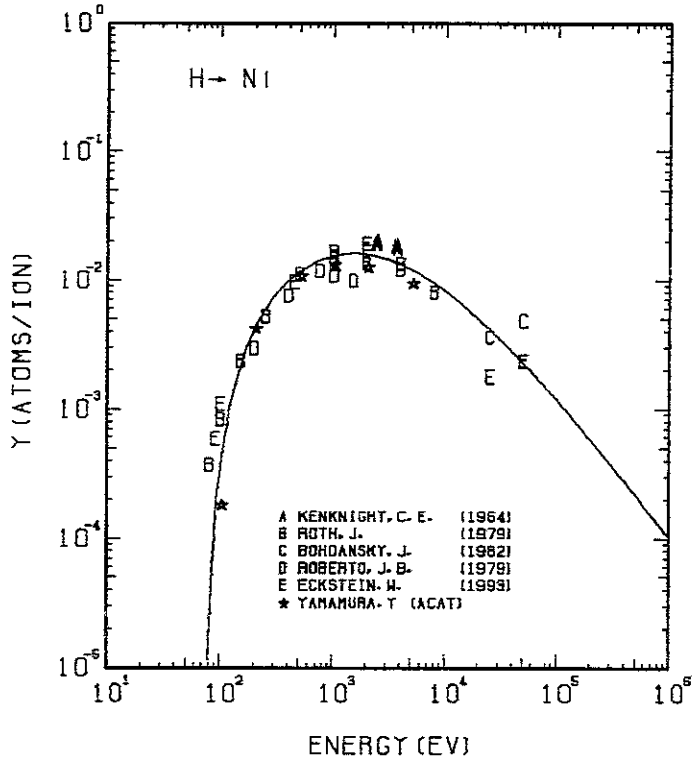

FIG. 45 ENERGY DEPENDENCE OF THE SPUTTERING YIELD OF NI WITH H^+.
A= 58.24, Q= 0.94, Us= 4.44EV, S= 2.50, W= 0.30Us.

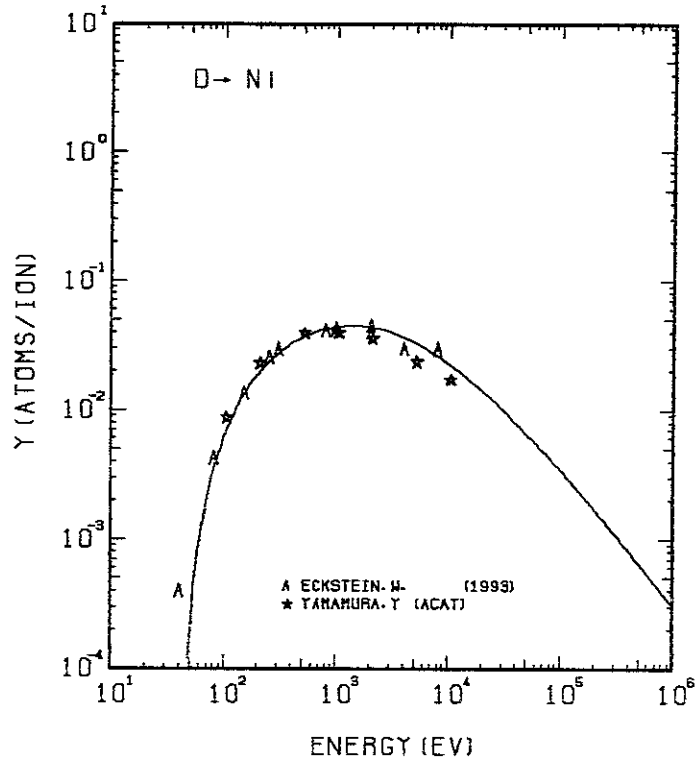

FIG. 46 ENERGY DEPENDENCE OF THE SPUTTERING YIELD OF NI WITH D^+.
A= 29.15, Q= 0.94, Us= 4.44EV, S= 2.50, W= 0.30Us.

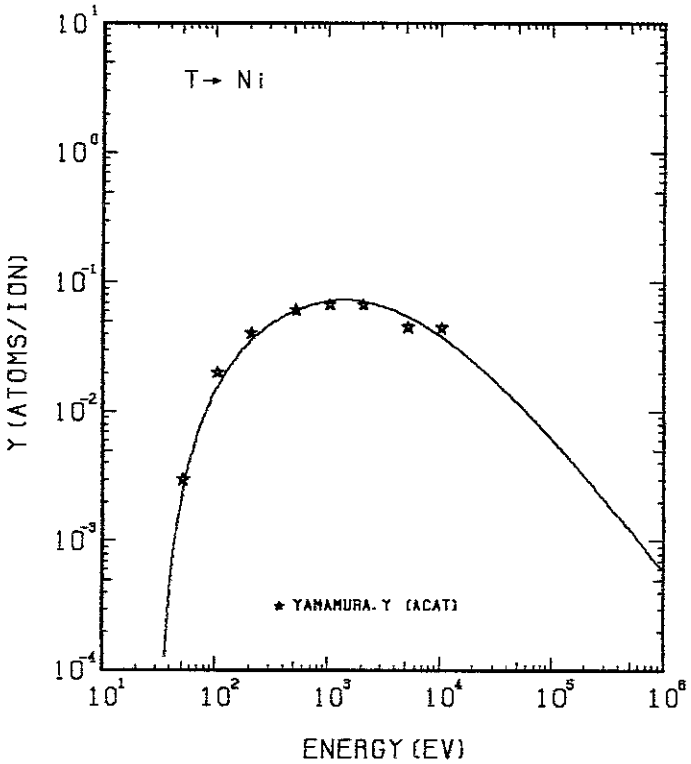

FIG. 47 ENERGY DEPENDENCE OF THE SPUTTERING YIELD OF NI WITH T^+.
A= 19.46, Q= 0.94, Us= 4.44EV, S= 2.50, W= 0.30Us.

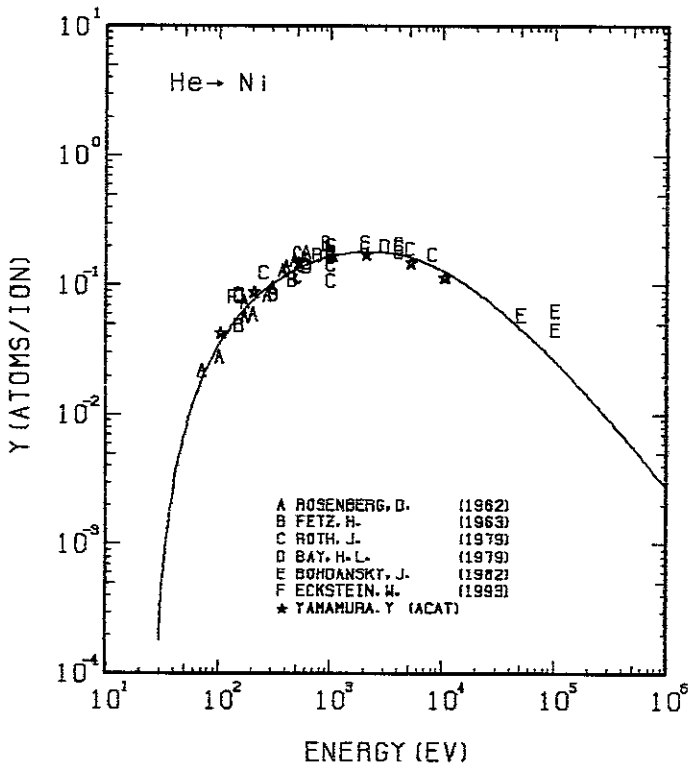

FIG. 48 ENERGY DEPENDENCE OF THE SPUTTERING YIELD OF NI WITH HE^+.
A= 14.67, Q= 0.94, Us= 4.44EV, S= 2.50, W= 0.30Us.

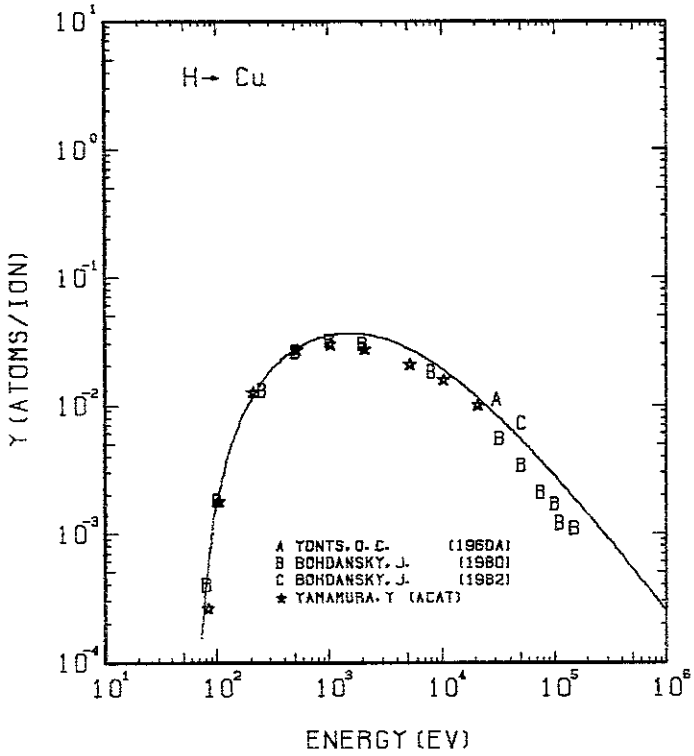

FIG. 49 ENERGY DEPENDENCE OF THE SPUTTERING YIELD OF CU WITH H^+.
A= 63.05, Q= 1.00, Us= 3.49EV, s= 2.50,
W= 0.21Us.

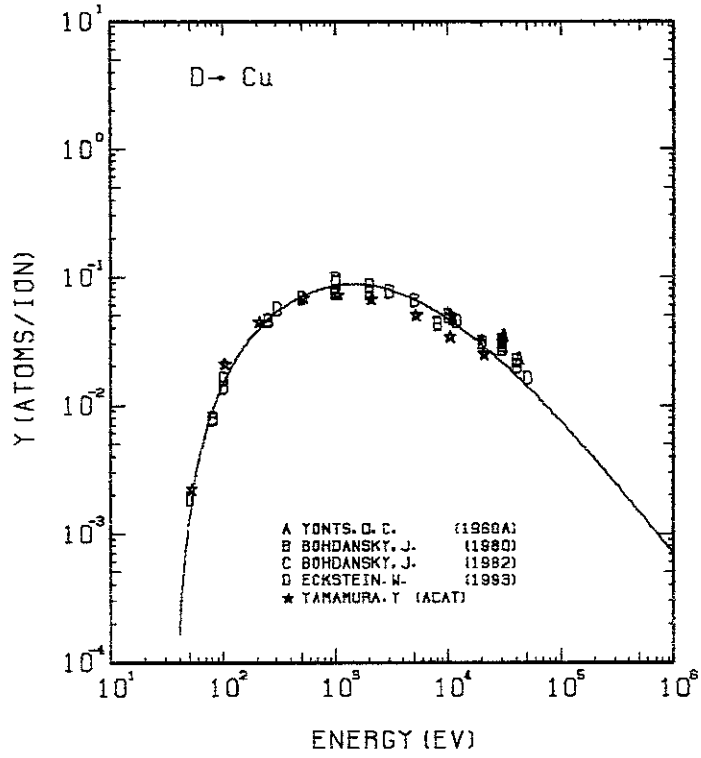

FIG. 50 ENERGY DEPENDENCE OF THE SPUTTERING YIELD OF CU WITH D^+.
A= 31.55, Q= 1.00, Us= 3.49EV, s= 2.50,
W= 0.21Us.

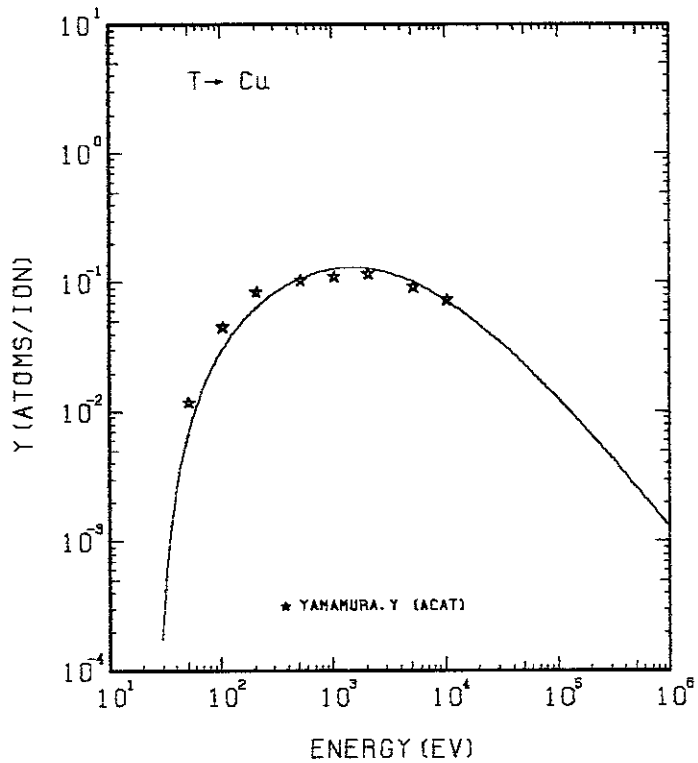

FIG. 51 ENERGY DEPENDENCE OF THE SPUTTERING YIELD OF CU WITH T^+.
A= 21.06, Q= 1.00, Us= 3.49EV, s= 2.50,
W= 0.21Us.

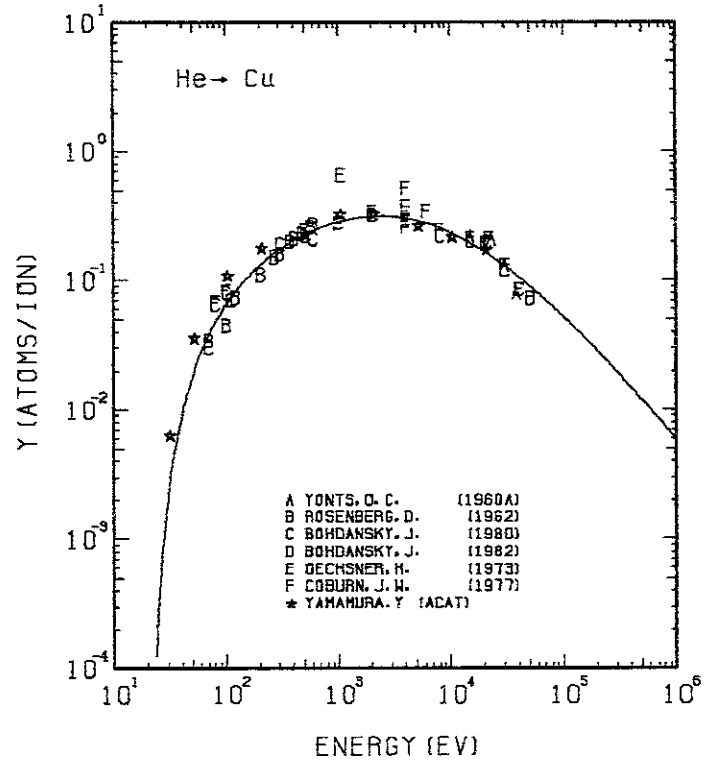

FIG. 52 ENERGY DEPENDENCE OF THE SPUTTERING YIELD OF CU WITH HE^+.
A= 15.88, Q= 1.00, Us= 3.49EV, s= 2.50,
W= 0.21Us.

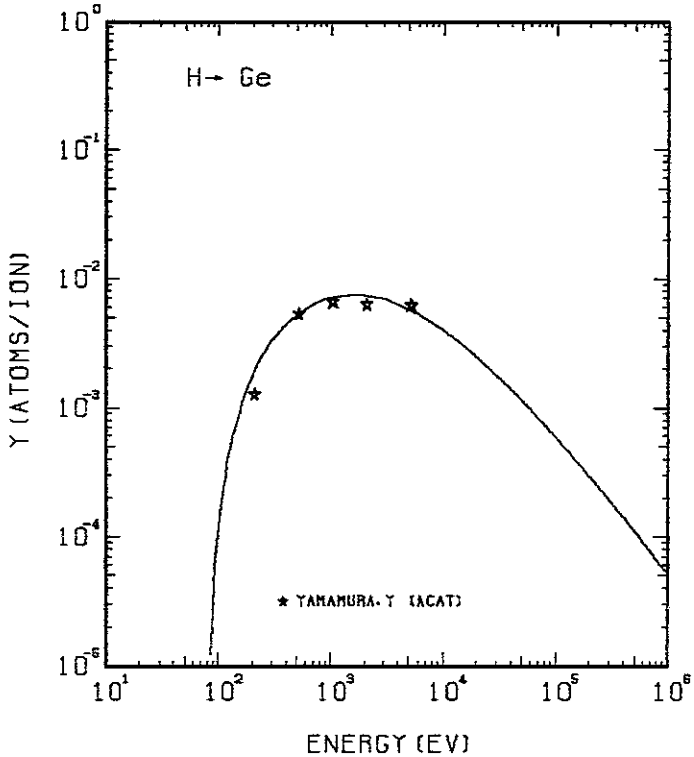

FIG. 53 ENERGY DEPENDENCE OF THE SPUTTERING YIELD OF GE WITH H^+.
A= 72.01, Q= 0.59, Us= 3.85EV, s= 2.50,
W= 0.54Us.

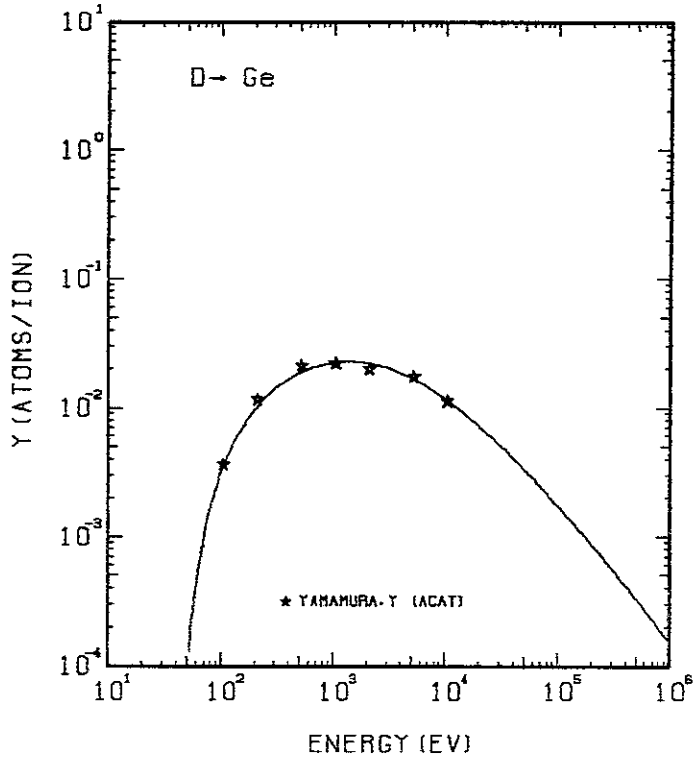

FIG. 54 ENERGY DEPENDENCE OF THE SPUTTERING YIELD OF GE WITH D^+.
A= 36.04, Q= 0.59, Us= 3.85EV, s= 2.50,
W= 0.54Us.

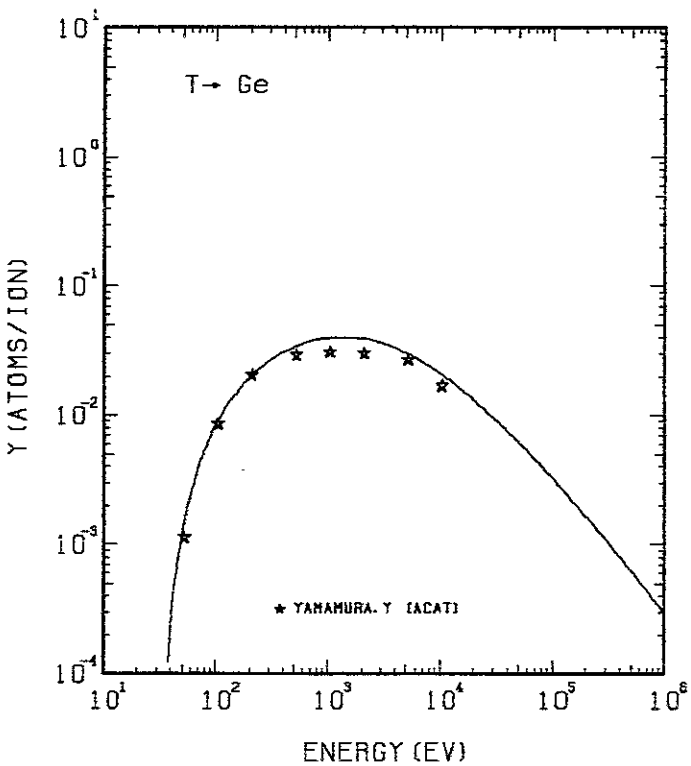

FIG. 55 ENERGY DEPENDENCE OF THE SPUTTERING YIELD OF GE WITH T^+.
A= 24.06, Q= 0.59, Us= 3.85EV, s= 2.50,
W= 0.54Us.

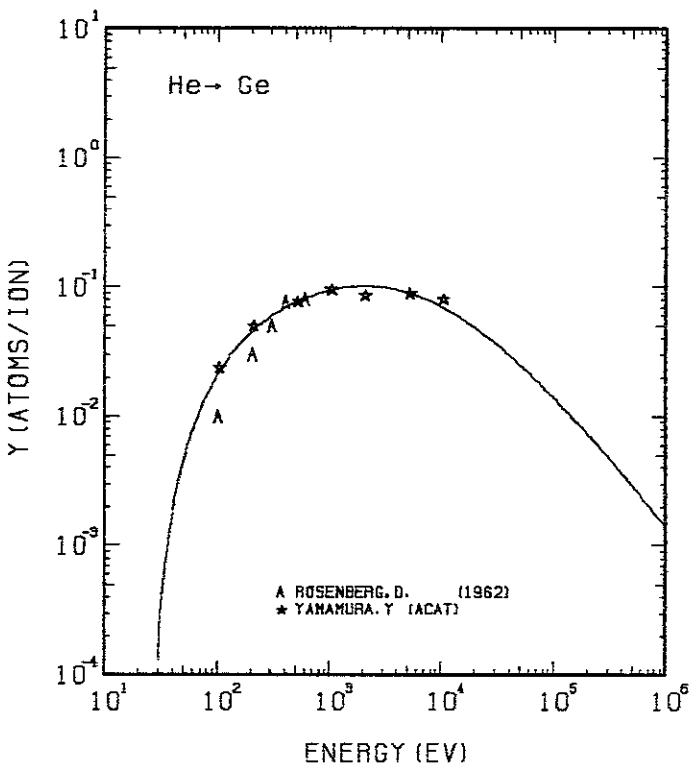

FIG. 56 ENERGY DEPENDENCE OF THE SPUTTERING YIELD OF GE WITH HE^+.
A= 18.13, Q= 0.59, Us= 3.85EV, s= 2.50,
W= 0.54Us.

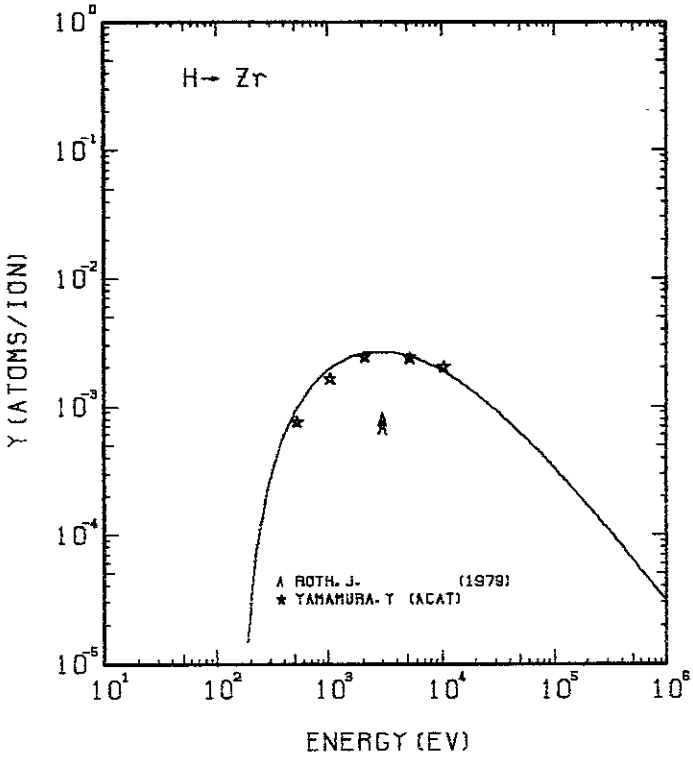

FIG. 57 ENERGY DEPENDENCE OF THE SPUTTERING YIELD OF ZR WITH H^+.
A= 90.50, Q= 0.54, Us= 6.25EV, s= 2.80, W= 0.40Us.

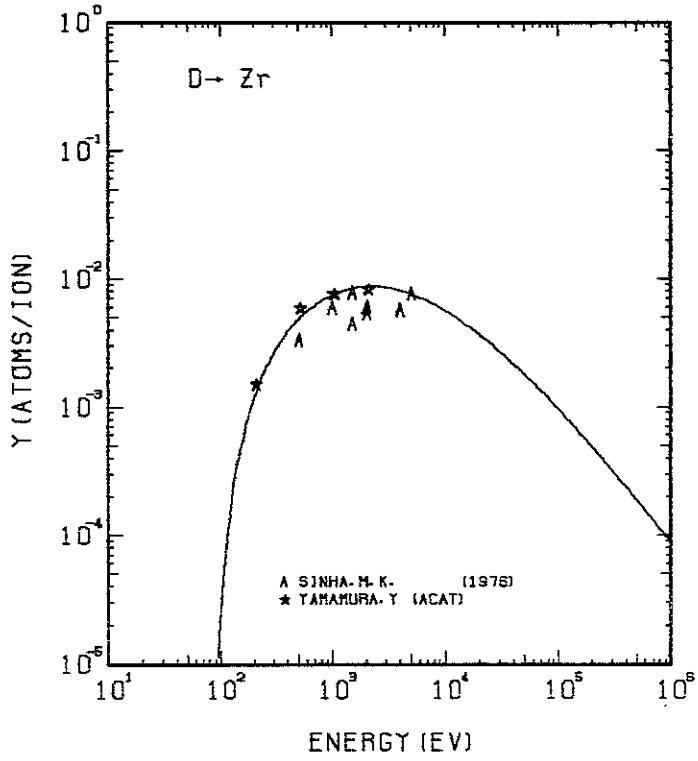

FIG. 58 ENERGY DEPENDENCE OF THE SPUTTERING YIELD OF ZR WITH D^+.
A= 45.29, Q= 0.54, Us= 6.25EV, s= 2.80, W= 0.40Us.

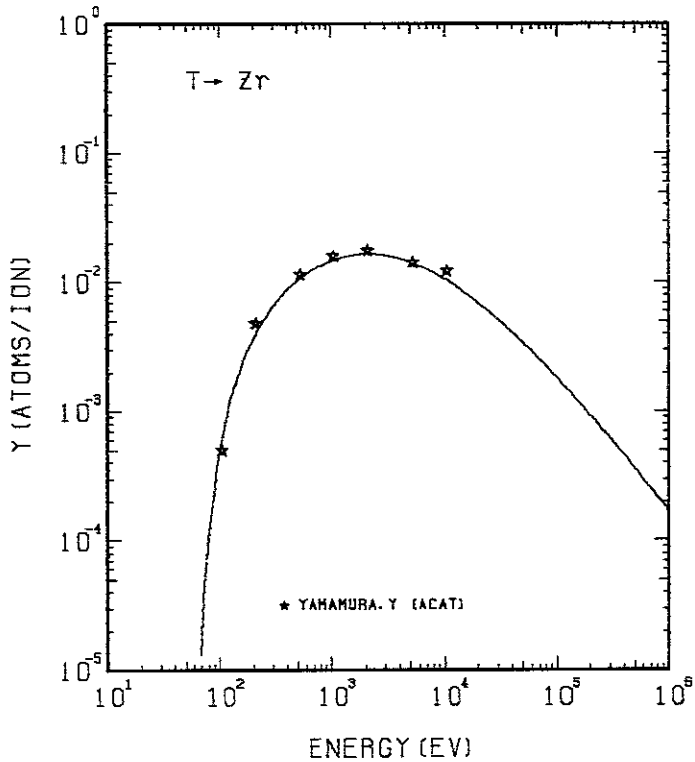

FIG. 59 ENERGY DEPENDENCE OF THE SPUTTERING YIELD OF ZR WITH T^+.
A= 30.24, Q= 0.54, Us= 6.25EV, s= 2.80, W= 0.40Us.

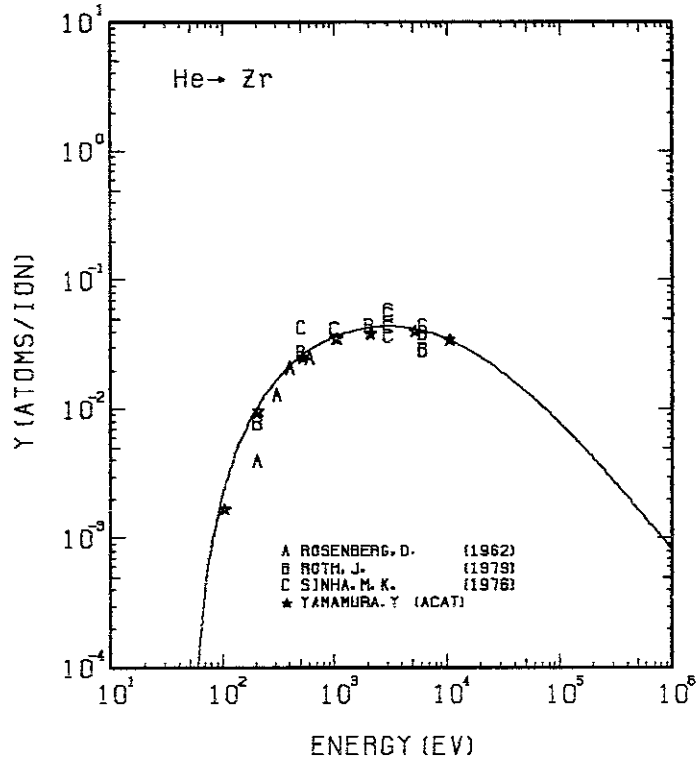

FIG. 60 ENERGY DEPENDENCE OF THE SPUTTERING YIELD OF ZR WITH HE^+.
A= 22.79, Q= 0.54, Us= 6.25EV, s= 2.80, W= 0.40Us.

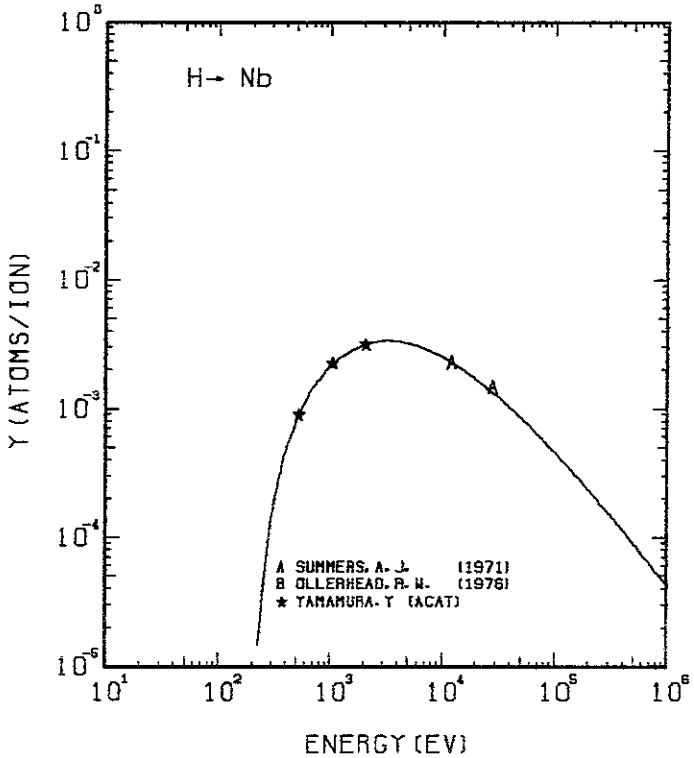

FIG. 61 ENERGY DEPENDENCE OF THE SPUTTERING YIELD OF NB WITH H^+.
A= 92.17, Q= 0.93, Us= 7.57EV, s= 2.80,
W= 0.35Us.

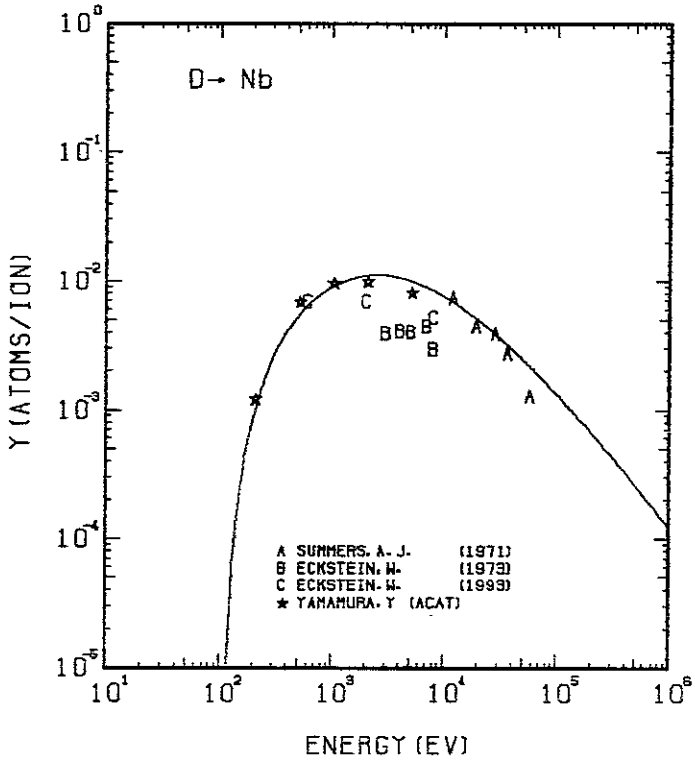

FIG. 62 ENERGY DEPENDENCE OF THE SPUTTERING YIELD OF NB WITH D^+.
A= 46.13, Q= 0.93, Us= 7.57EV, s= 2.80,
W= 0.35Us.

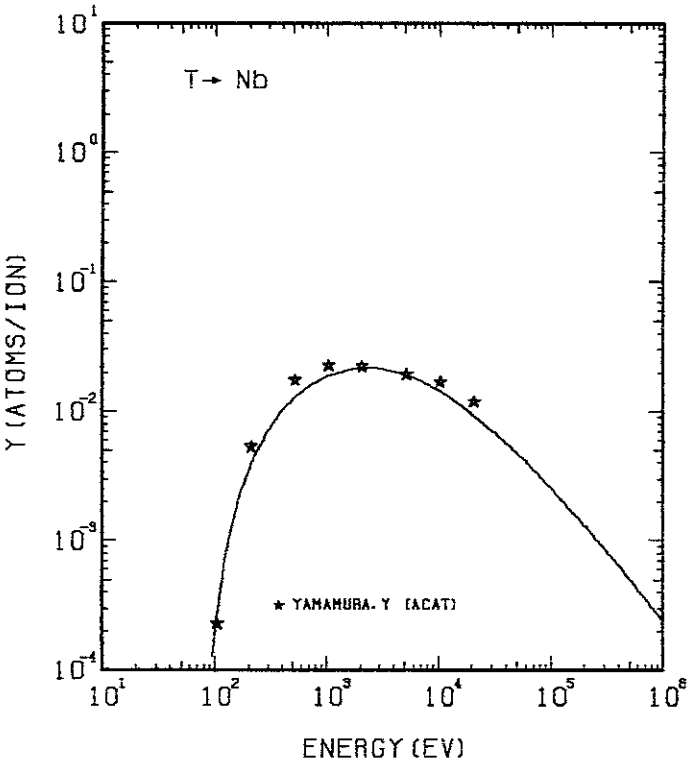

FIG. 63 ENERGY DEPENDENCE OF THE SPUTTERING YIELD OF NB WITH T^+.
A= 30.80, Q= 0.93, Us= 7.57EV, s= 2.80,
W= 0.35Us.

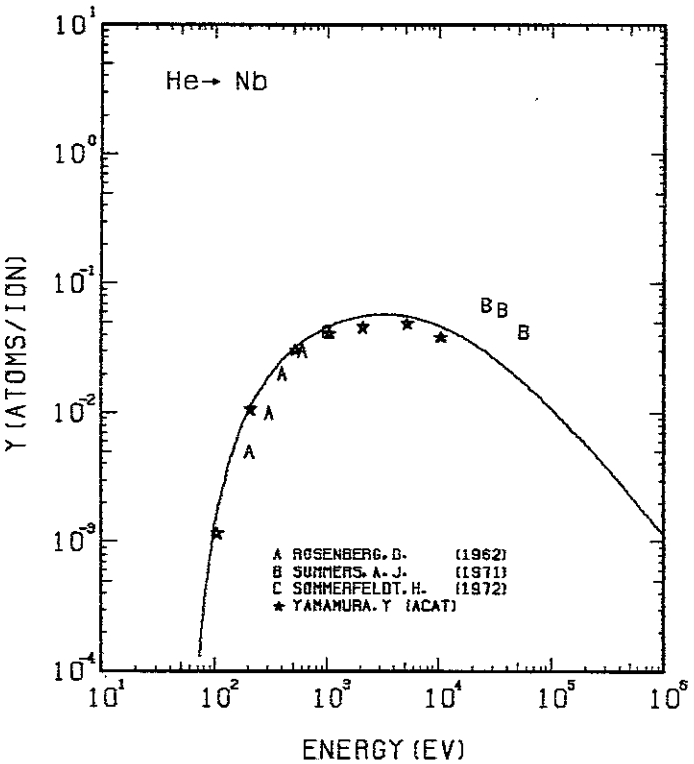

FIG. 64 ENERGY DEPENDENCE OF THE SPUTTERING YIELD OF NB WITH HE^+.
A= 23.21, Q= 0.93, Us= 7.57EV, s= 2.80,
W= 0.35Us.

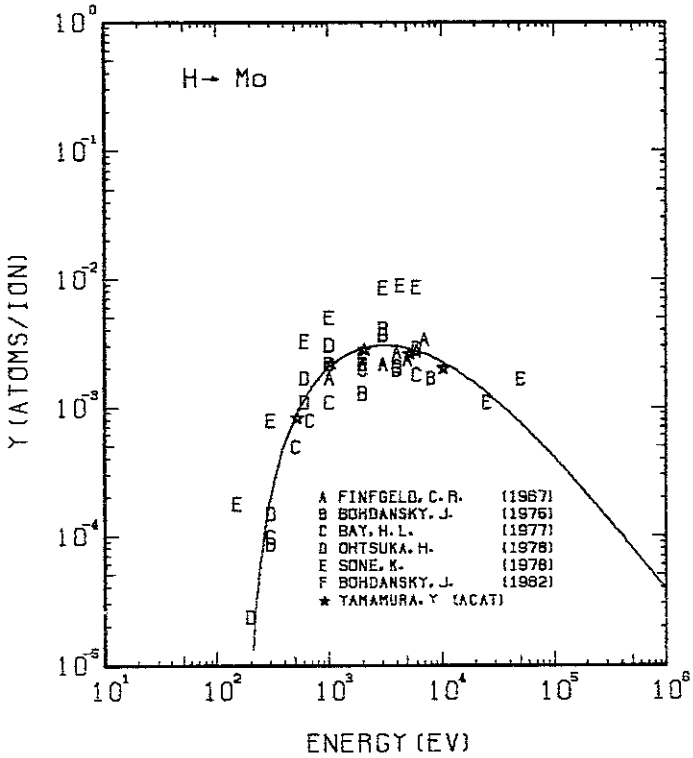

FIG. 65 ENERGY DEPENDENCE OF THE SPUTTERING YIELD OF MO WITH H^+.
A= 95.18, Q= 0.85, Us= 6.82EV, s= 2.80, W= 0.45Us.

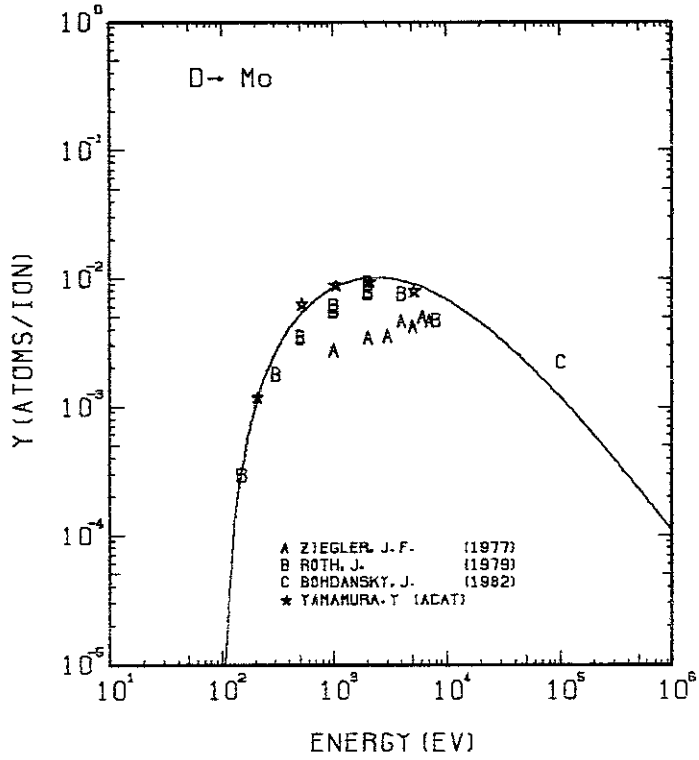

FIG. 66 ENERGY DEPENDENCE OF THE SPUTTERING YIELD OF MO WITH D^+.
A= 47.64, Q= 0.85, Us= 6.82EV, s= 2.80, W= 0.45Us.

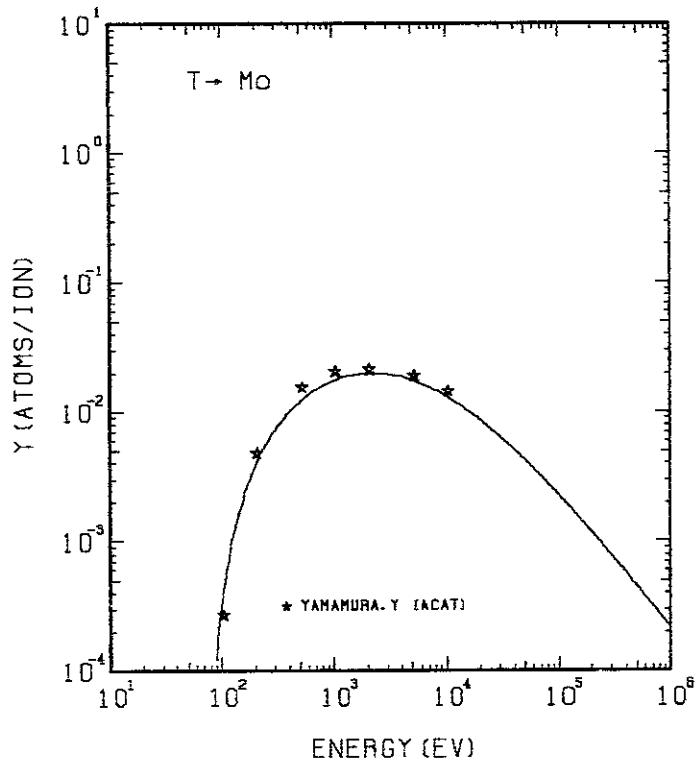

FIG. 67 ENERGY DEPENDENCE OF THE SPUTTERING YIELD OF MO WITH T^+.
A= 31.80, Q= 0.85, Us= 6.82EV, s= 2.80, W= 0.45Us.

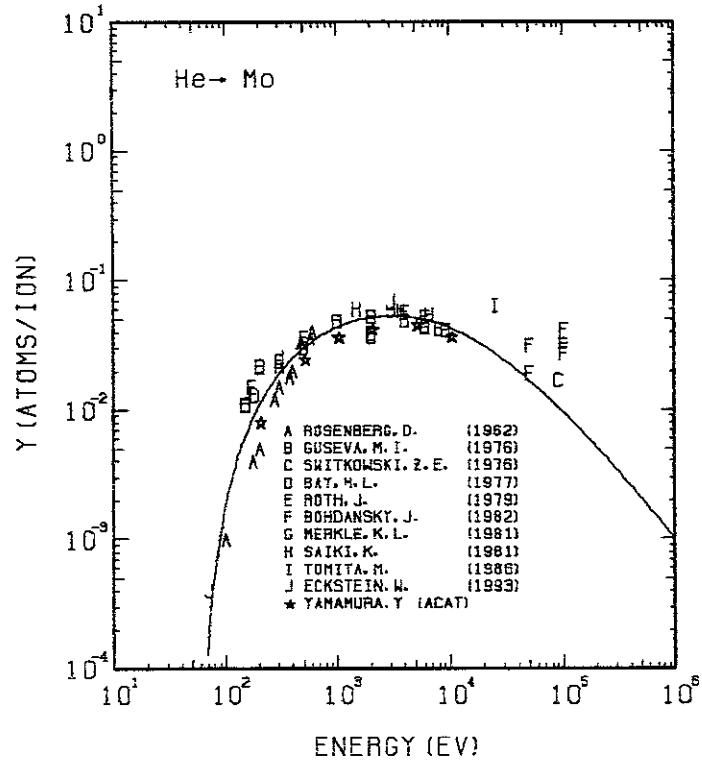

FIG. 68 ENERGY DEPENDENCE OF THE SPUTTERING YIELD OF MO WITH HE^+.
A= 23.97, Q= 0.85, Us= 6.82EV, s= 2.80, W= 0.45Us.

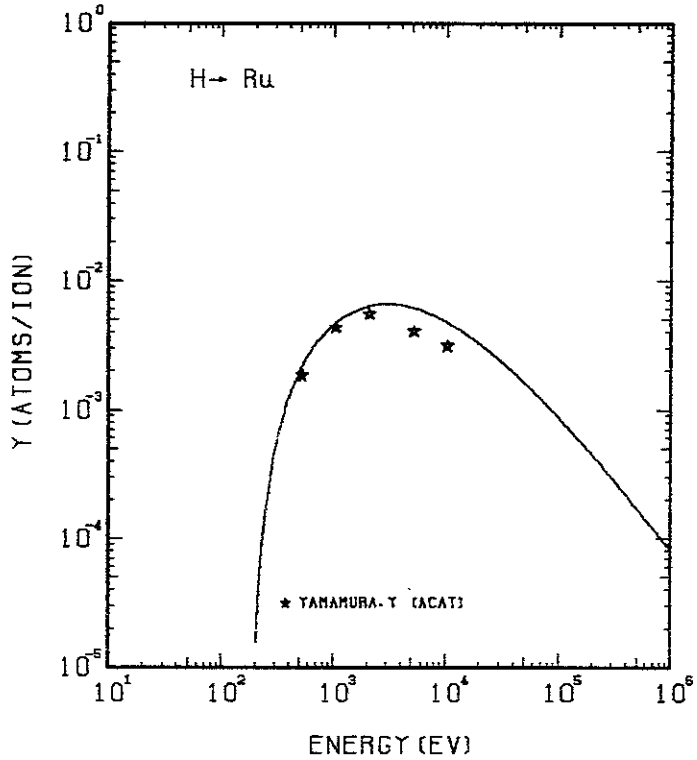

FIG. 69 ENERGY DEPENDENCE OF THE SPUTTERING YIELD OF RU WITH H^+.
A= 100.20, Q= 1.31, Us= 6.74EV, s= 2.50,
W= 0.35Us.

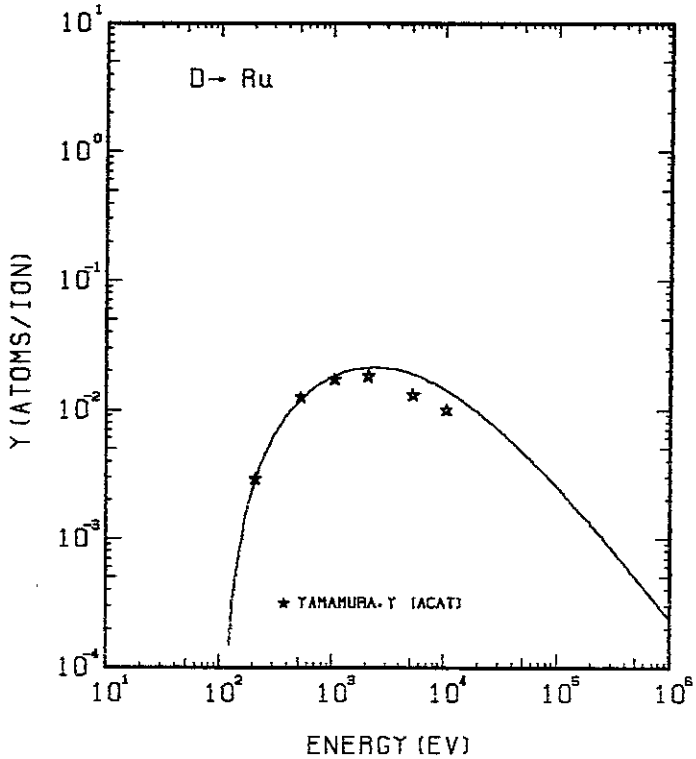

FIG. 70 ENERGY DEPENDENCE OF THE SPUTTERING YIELD OF RU WITH D^+.
A= 50.15, Q= 1.31, Us= 6.74EV, s= 2.50,
W= 0.35Us.

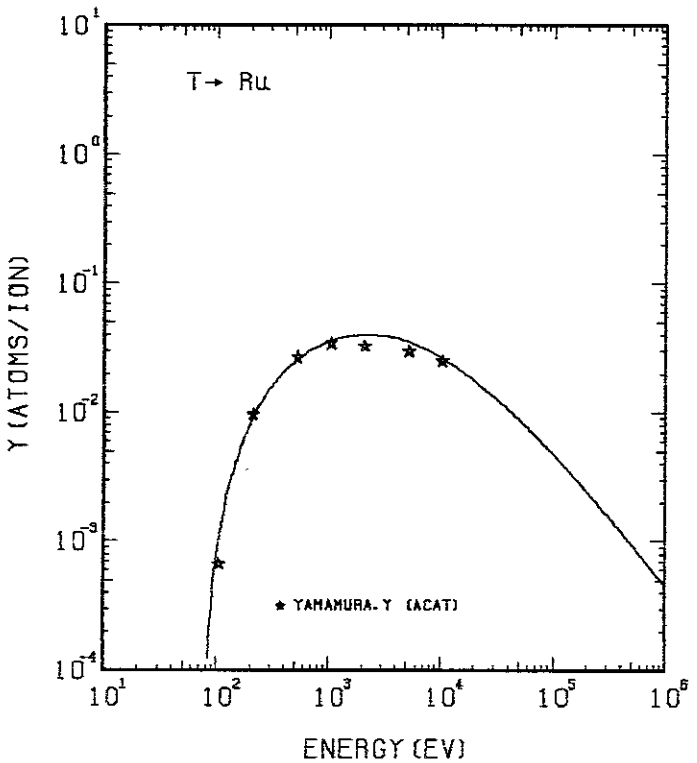

FIG. 71 ENERGY DEPENDENCE OF THE SPUTTERING YIELD OF RU WITH T^+.
A= 33.48, Q= 1.31, Us= 6.74EV, s= 2.50,
W= 0.35Us.

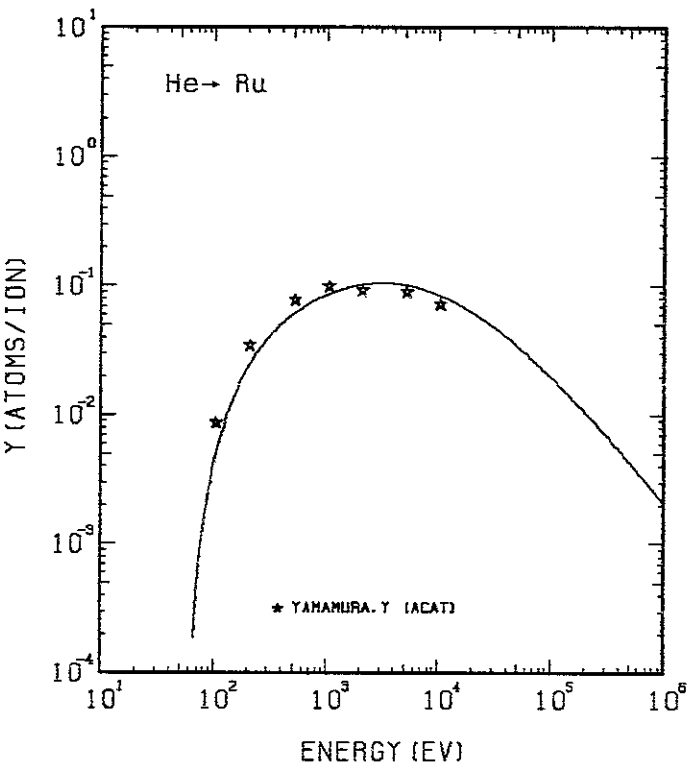

FIG. 72 ENERGY DEPENDENCE OF THE SPUTTERING YIELD OF RU WITH HE^+.
A= 25.23, Q= 1.31, Us= 6.74EV, s= 2.50,
W= 0.35Us.

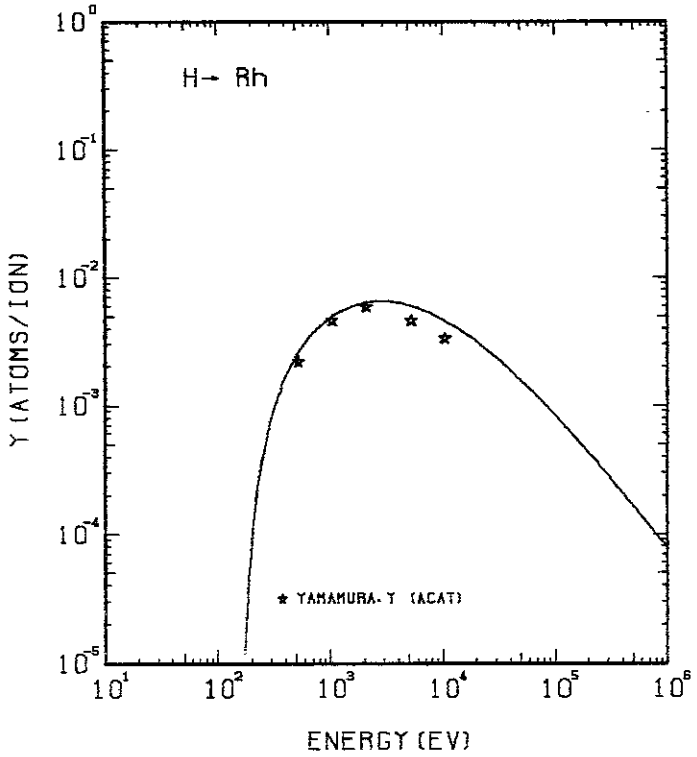

FIG. 73 ENERGY DEPENDENCE OF THE SPUTTERING YIELD OF RH WITH H^+.
A= 102.08, Z= 1.14, Us= 5.75EV, s= 2.50, W= 0.45Us.

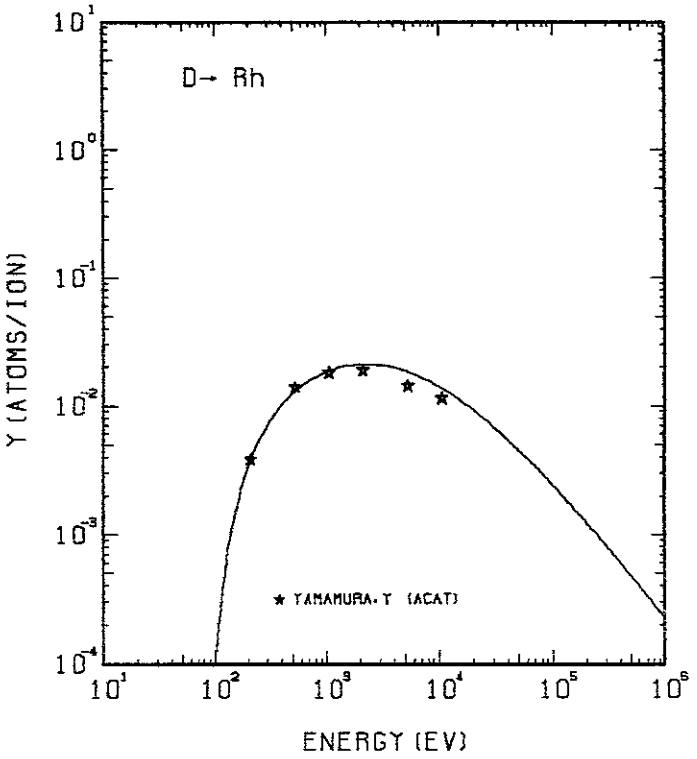

FIG. 74 ENERGY DEPENDENCE OF THE SPUTTERING YIELD OF RH WITH D^+.
A= 51.09, Z= 1.14, Us= 5.75EV, s= 2.50, W= 0.45Us.

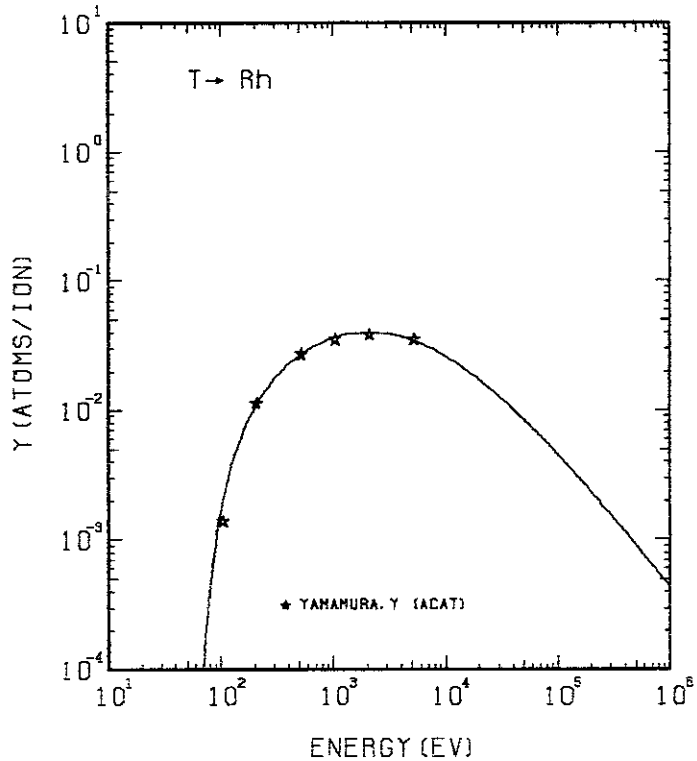

FIG. 75 ENERGY DEPENDENCE OF THE SPUTTERING YIELD OF RH WITH T^+.
A= 34.11, Z= 1.14, Us= 5.75EV, s= 2.50, W= 0.45Us.

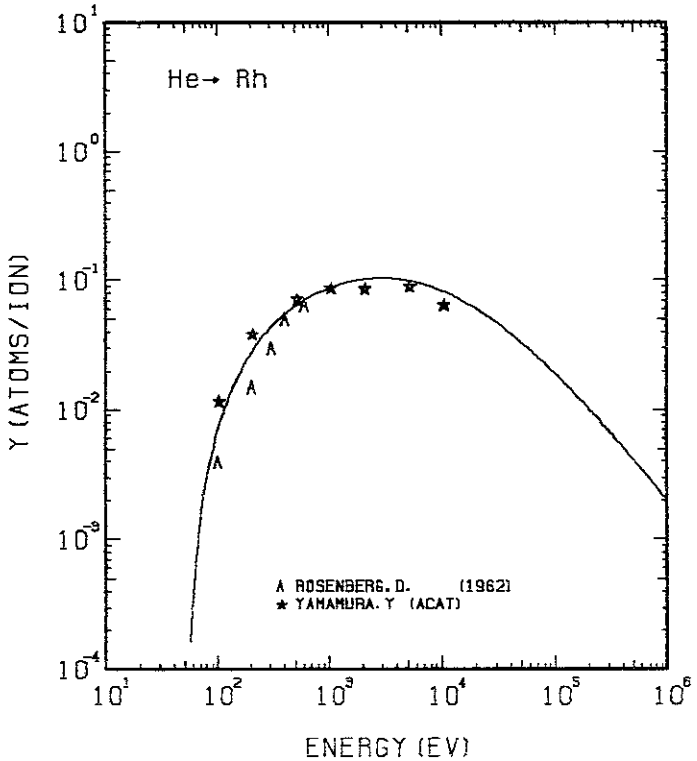

FIG. 76 ENERGY DEPENDENCE OF THE SPUTTERING YIELD OF RH WITH HE^+.
A= 25.71, Z= 1.14, Us= 5.75EV, s= 2.50, W= 0.45Us.

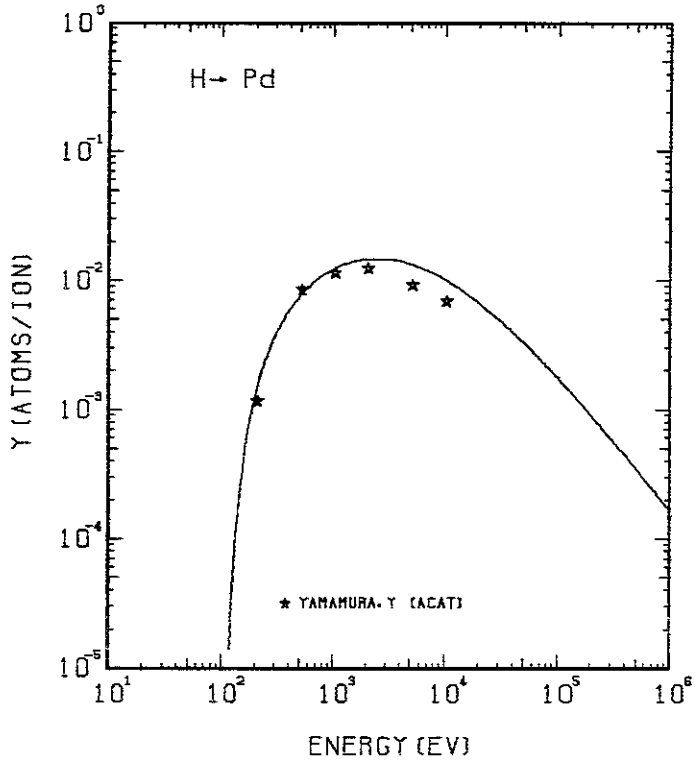

FIG. 77 ENERGY DEPENDENCE OF THE SPUTTERING YIELD OF PD WITH H^+.
A= 105.56, Z= 0.85, Us= 3.89EV, S= 2.50,
W= 0.35Us.

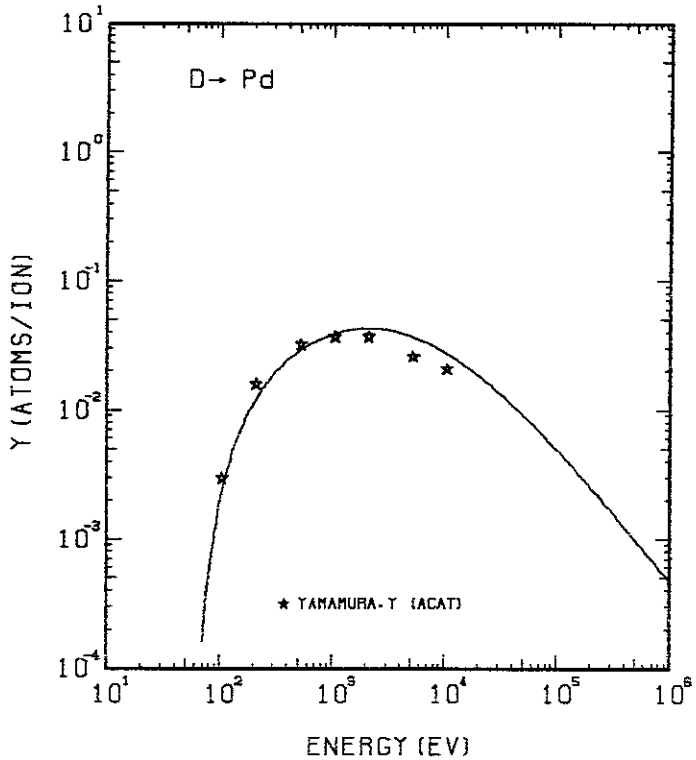

FIG. 78 ENERGY DEPENDENCE OF THE SPUTTERING YIELD OF PD WITH D^+.
A= 52.83, Z= 0.85, Us= 3.89EV, S= 2.50,
W= 0.35Us.

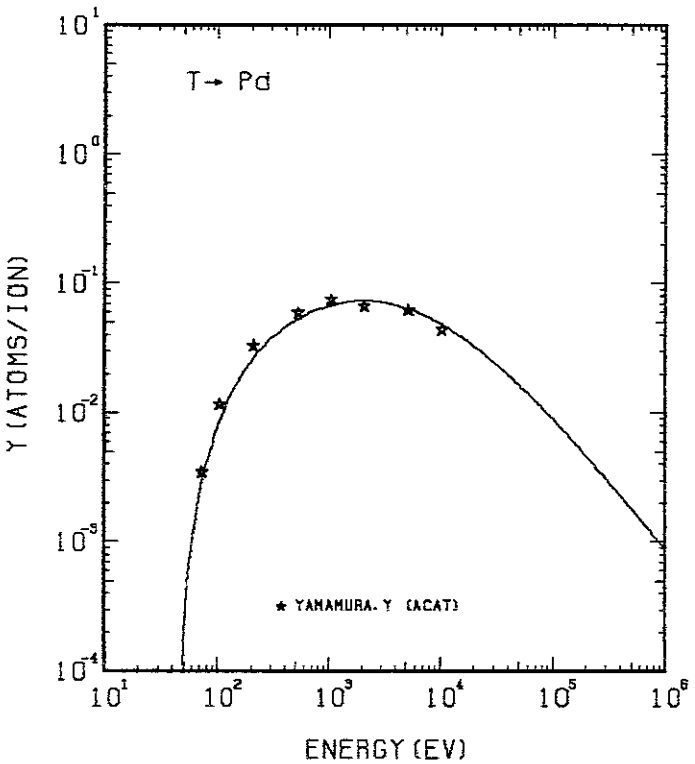

FIG. 79 ENERGY DEPENDENCE OF THE SPUTTERING YIELD OF PD WITH T^+.
A= 35.27, Z= 0.85, Us= 3.89EV, S= 2.50,
W= 0.35Us.

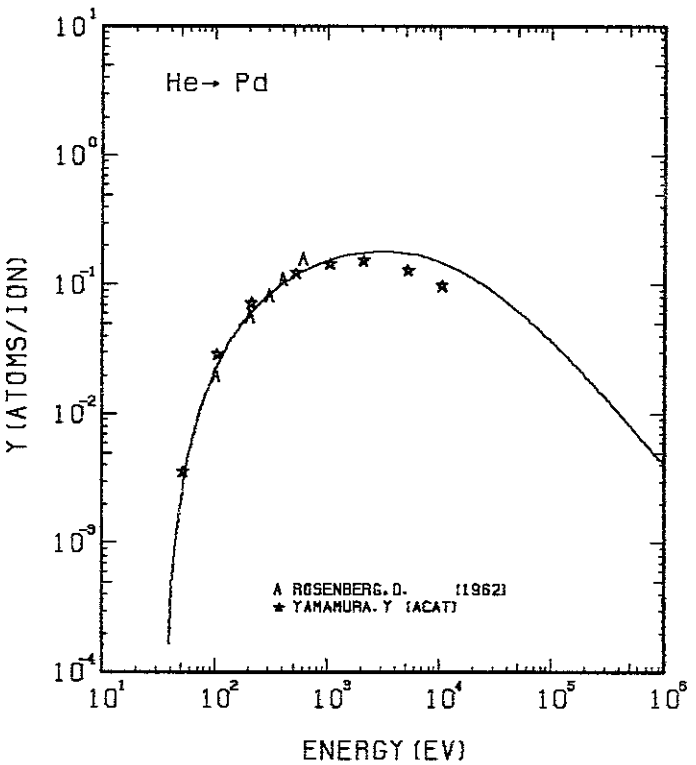

FIG. 80 ENERGY DEPENDENCE OF THE SPUTTERING YIELD OF PD WITH HE^+.
A= 26.58, Z= 0.85, Us= 3.89EV, S= 2.50,
W= 0.35Us.

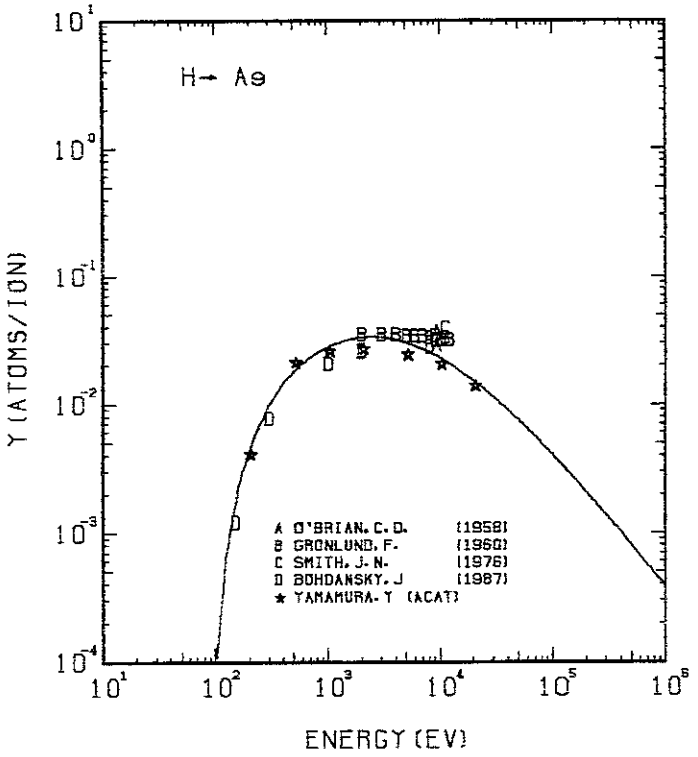

FIG. 81 ENERGY DEPENDENCE OF THE SPUTTERING YIELD OF AG WITH H^+.
A= 106.94, Q= 1.08, Us= 2.95EV, s= 2.80, W= 0.35Us.

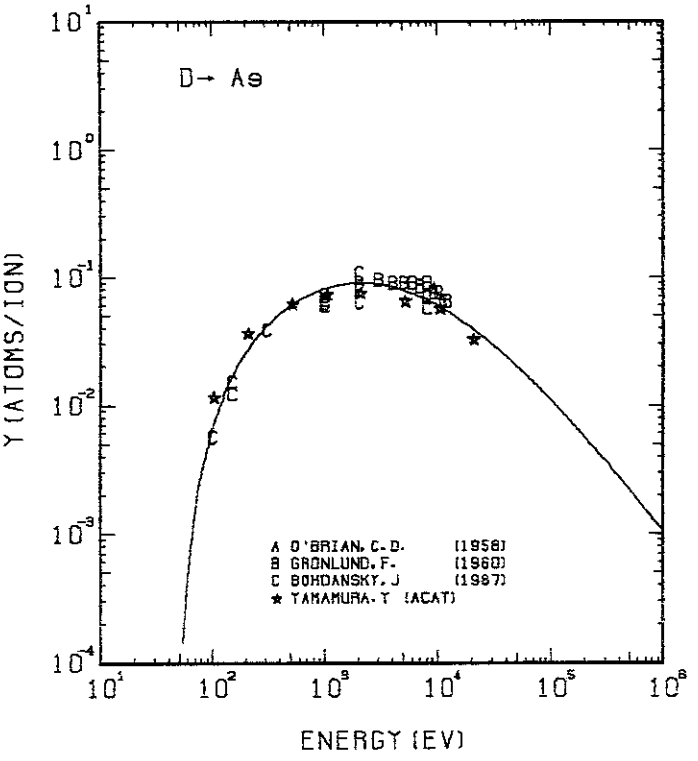

FIG. 82 ENERGY DEPENDENCE OF THE SPUTTERING YIELD OF AG WITH D^+.
A= 53.53, Q= 1.08, Us= 2.95EV, s= 2.80, W= 0.35Us.

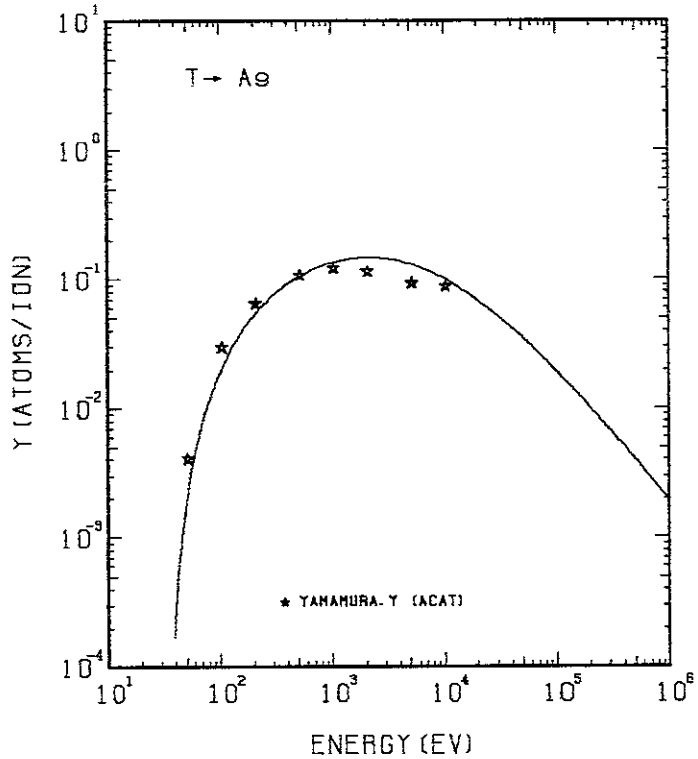

FIG. 83 ENERGY DEPENDENCE OF THE SPUTTERING YIELD OF AG WITH T^+.
A= 35.73, Q= 1.08, Us= 2.95EV, s= 2.80, W= 0.35Us.

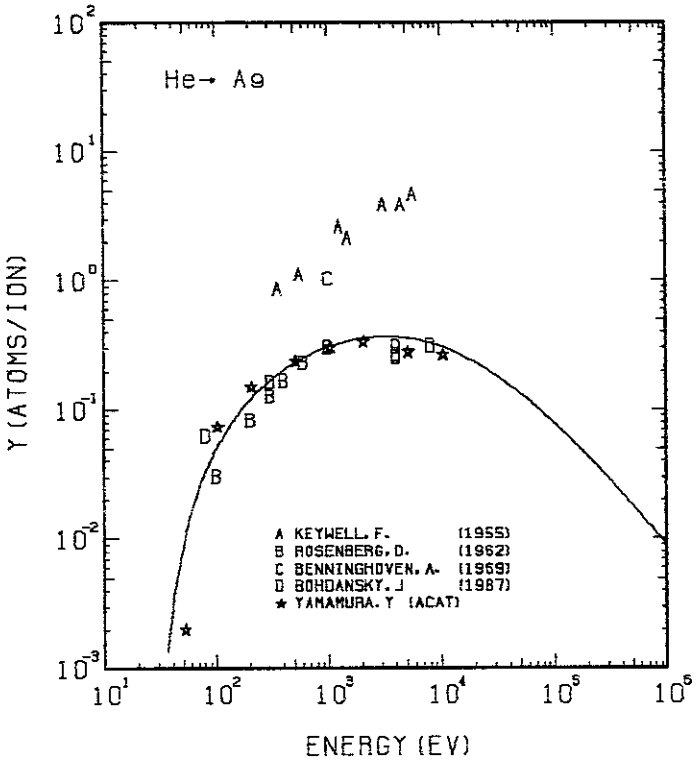

FIG. 84 ENERGY DEPENDENCE OF THE SPUTTERING YIELD OF AG WITH HE^+.
A= 26.93, Q= 1.08, Us= 2.95EV, s= 2.80, W= 0.35Us.

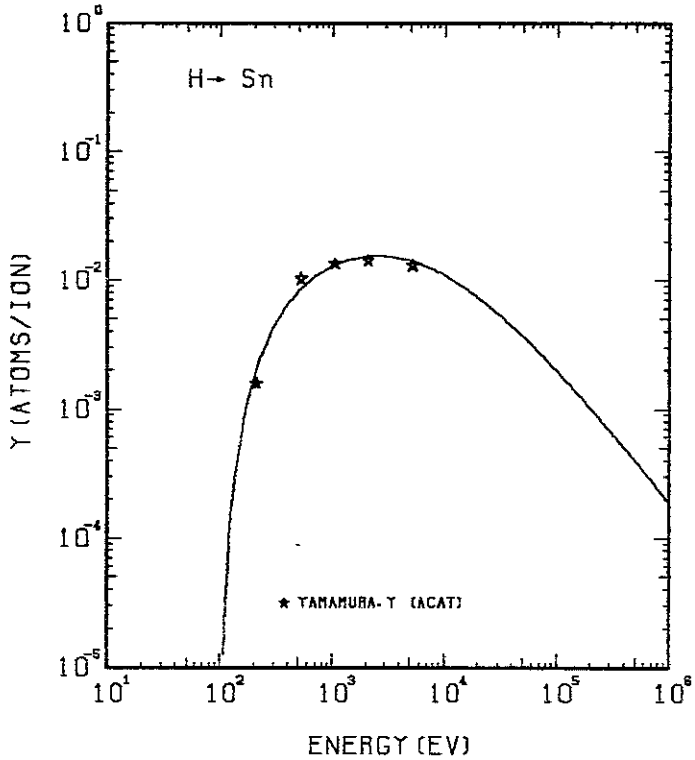

FIG. 85 ENERGY DEPENDENCE OF THE SPUTTERING YIELD OF SN WITH H^+.
A= 117.66, Q= 0.47, Us= 3.14EV, s= 2.50,
W= 0.28Us.

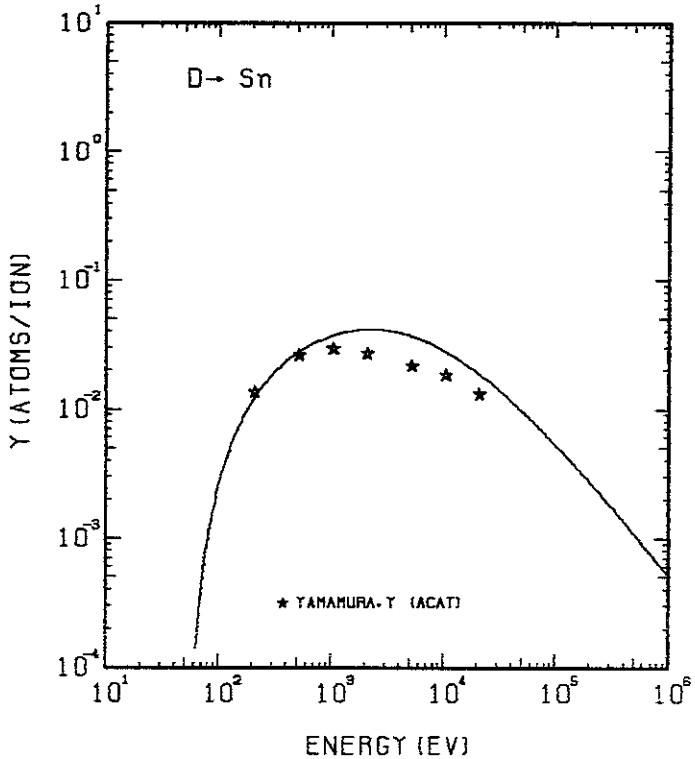

FIG. 86 ENERGY DEPENDENCE OF THE SPUTTERING YIELD OF SN WITH D^+.
A= 58.89, Q= 0.47, Us= 3.14EV, s= 2.50,
W= 0.28Us.

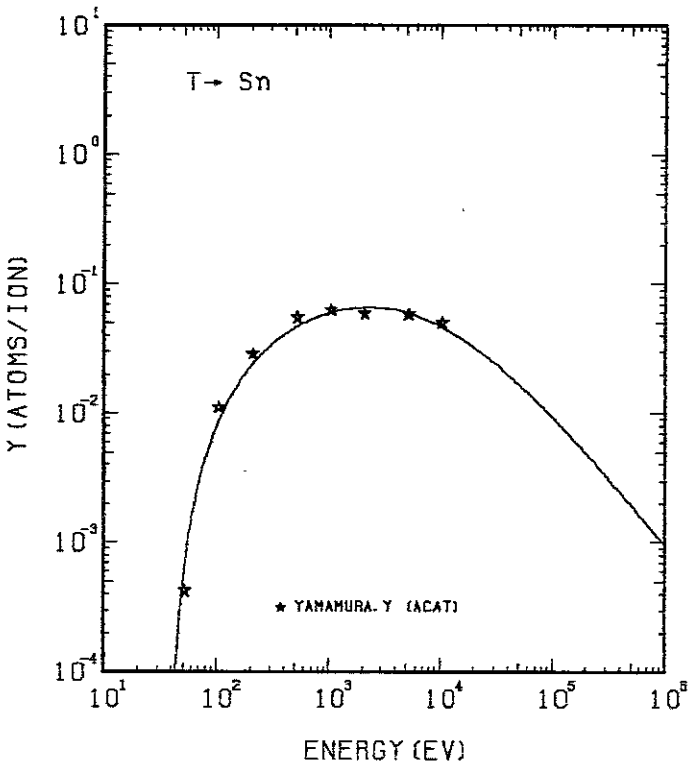

FIG. 87 ENERGY DEPENDENCE OF THE SPUTTERING YIELD OF SN WITH T^+.
A= 39.31, Q= 0.47, Us= 3.14EV, s= 2.50,
W= 0.28Us.

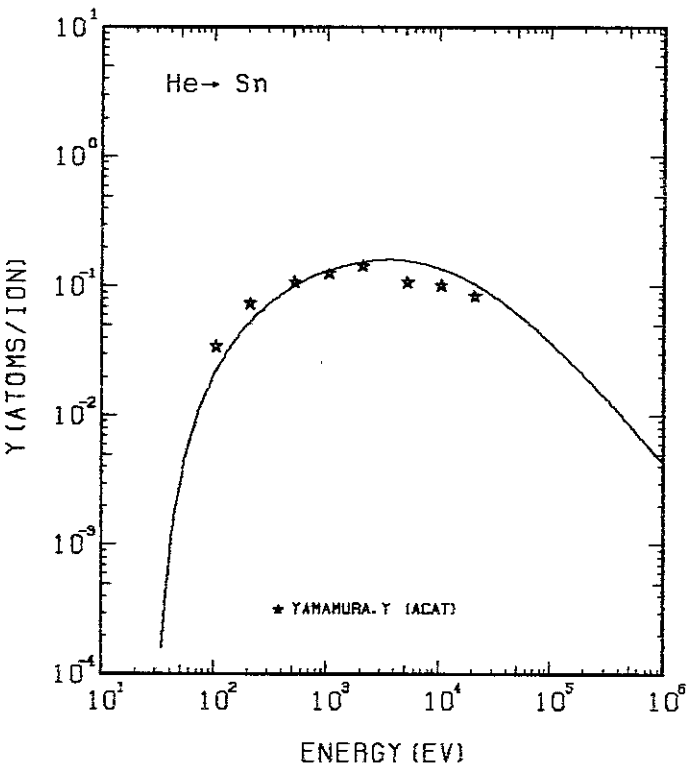

FIG. 88 ENERGY DEPENDENCE OF THE SPUTTERING YIELD OF SN WITH HE^+.
A= 29.63, Q= 0.47, Us= 3.14EV, s= 2.50,
W= 0.28Us.

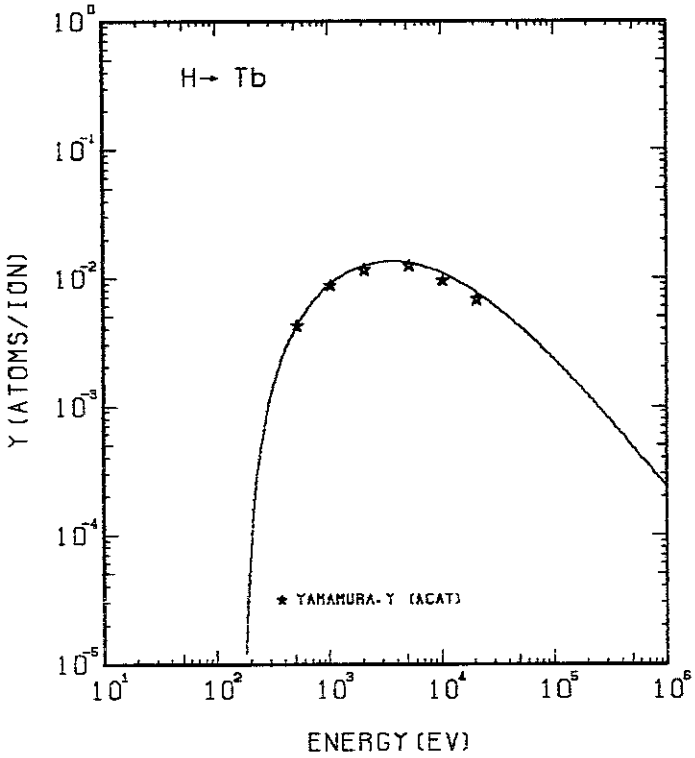

FIG. 89 ENERGY DEPENDENCE OF THE SPUTTERING YIELD OF TB WITH H^+.
A= 157.64, Q= 0.90, Us= 4.05EV, s= 2.50,
W= 0.35Us.

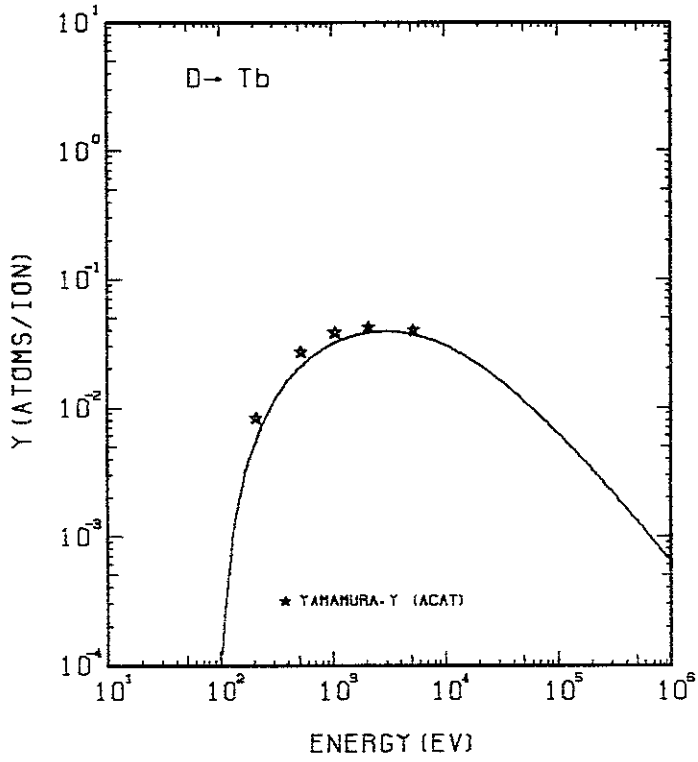

FIG. 90 ENERGY DEPENDENCE OF THE SPUTTERING YIELD OF TB WITH D^+.
A= 78.90, Q= 0.90, Us= 4.05EV, s= 2.50,
W= 0.35Us.

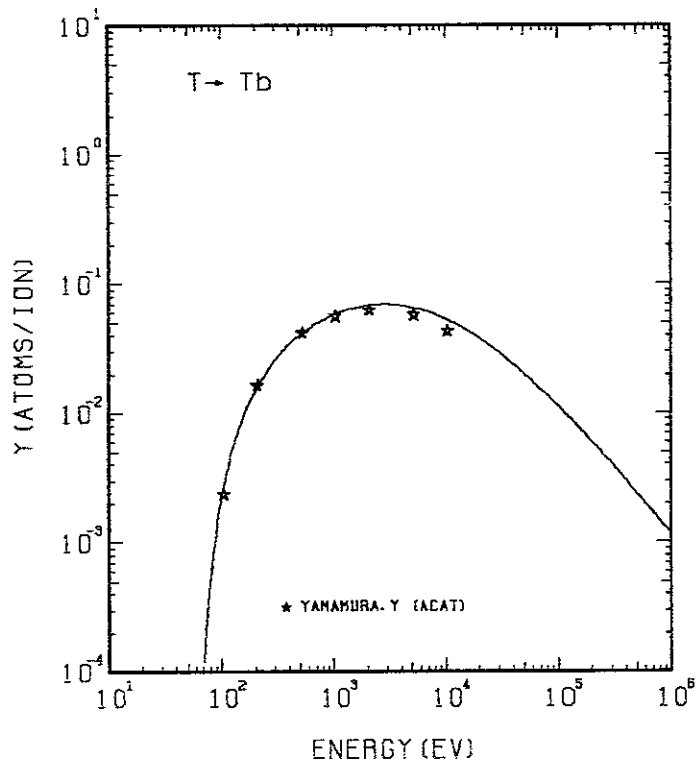

FIG. 91 ENERGY DEPENDENCE OF THE SPUTTERING YIELD OF TB WITH T^+.
A= 52.67, Q= 0.90, Us= 4.05EV, s= 2.50,
W= 0.35Us.

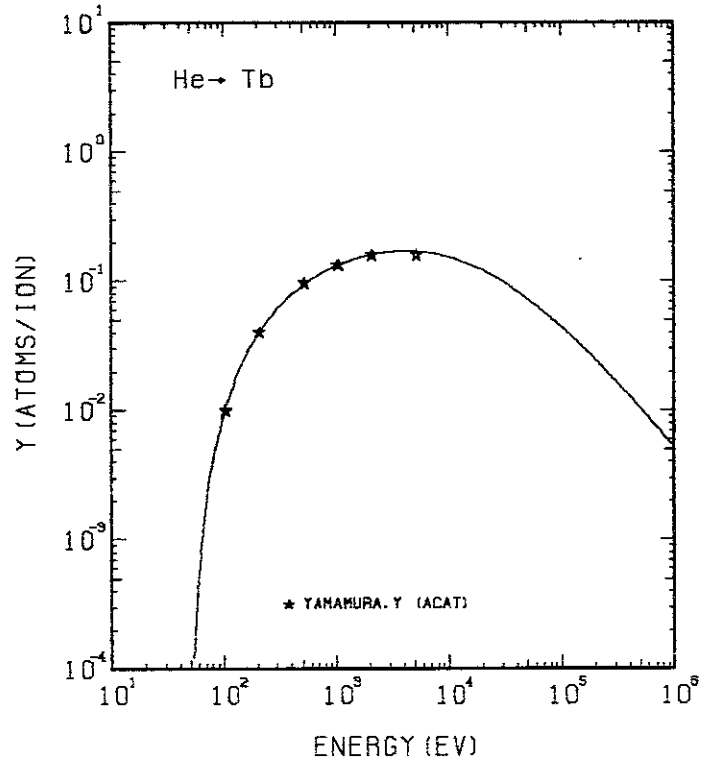

FIG. 92 ENERGY DEPENDENCE OF THE SPUTTERING YIELD OF TB WITH HE^+.
A= 39.70, Q= 0.90, Us= 4.05EV, s= 2.50,
W= 0.35Us.

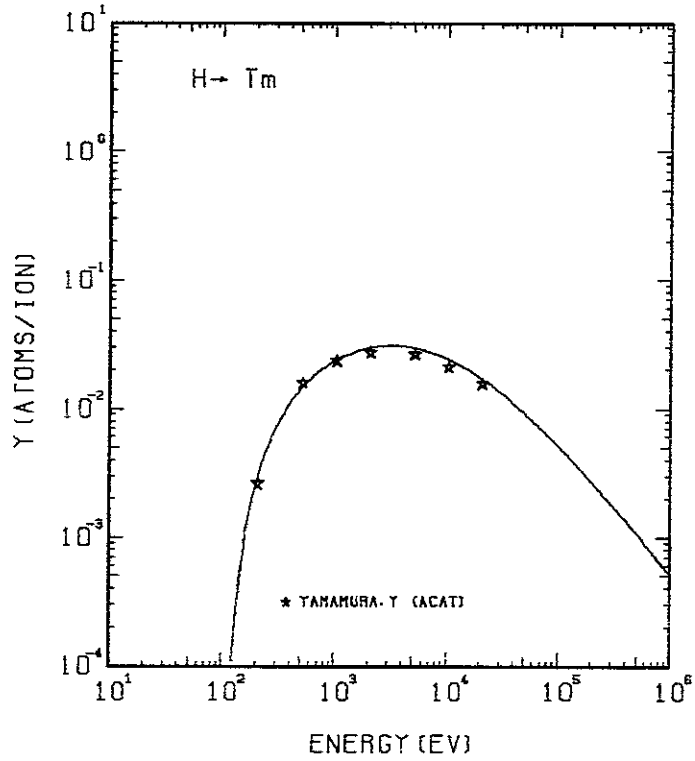

FIG. 93 ENERGY DEPENDENCE OF THE SPUTTERING YIELD OF TM WITH H^+.
A= 167.56, Q= 0.65, Us= 2.42EV, s= 2.50,
W= 0.35Us.

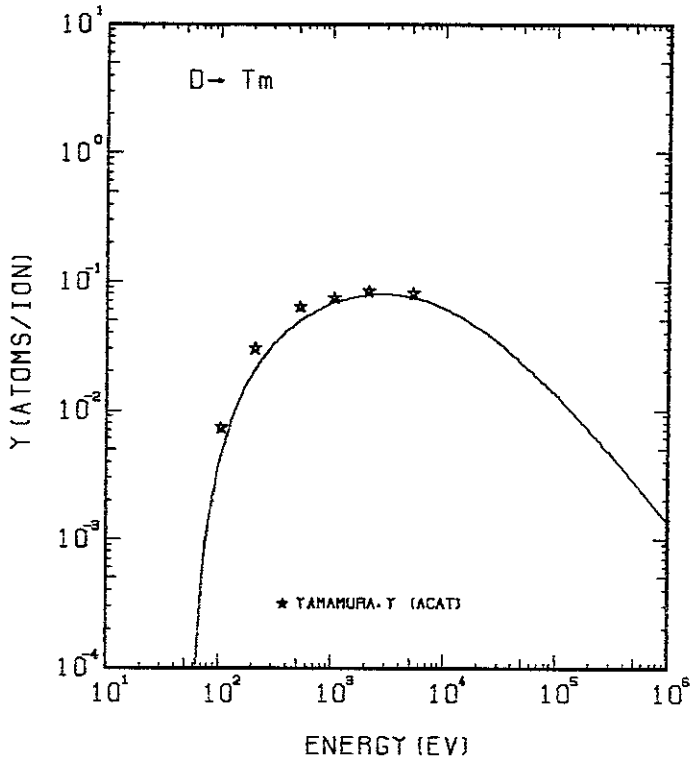

FIG. 94 ENERGY DEPENDENCE OF THE SPUTTERING YIELD OF TM WITH D^+.
A= 83.86, Q= 0.65, Us= 2.42EV, s= 2.50,
W= 0.35Us.

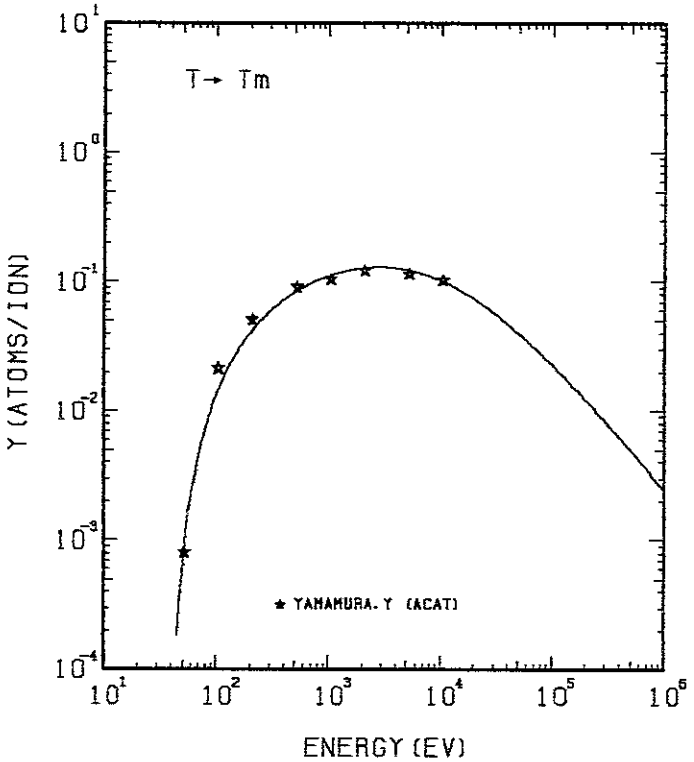

FIG. 95 ENERGY DEPENDENCE OF THE SPUTTERING YIELD OF TM WITH T^+.
A= 55.98, Q= 0.65, Us= 2.42EV, s= 2.50,
W= 0.35Us.

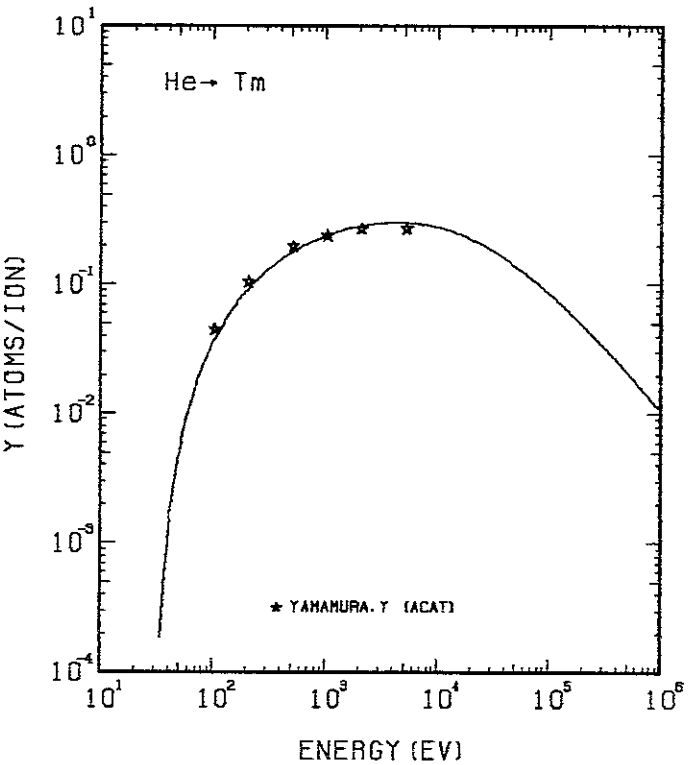

FIG. 96 ENERGY DEPENDENCE OF THE SPUTTERING YIELD OF TM WITH HE^+.
A= 42.19, Q= 0.65, Us= 2.42EV, s= 2.50,
W= 0.35Us.

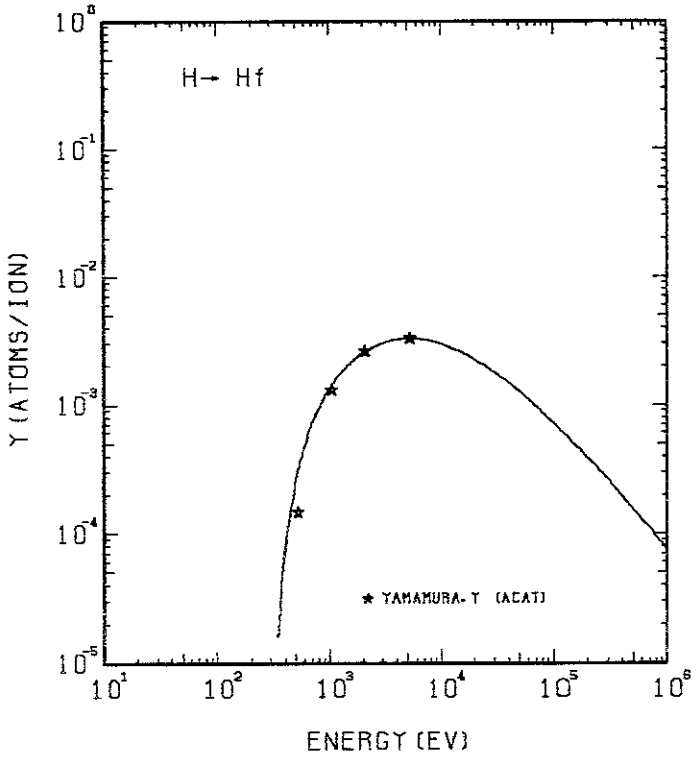

FIG. 97 ENERGY DEPENDENCE OF THE SPUTTERING YIELD OF HF WITH H^+.
A= 176.98, Q= 0.65, Us= 6.44EV, s= 2.50,
W= 0.35Us.

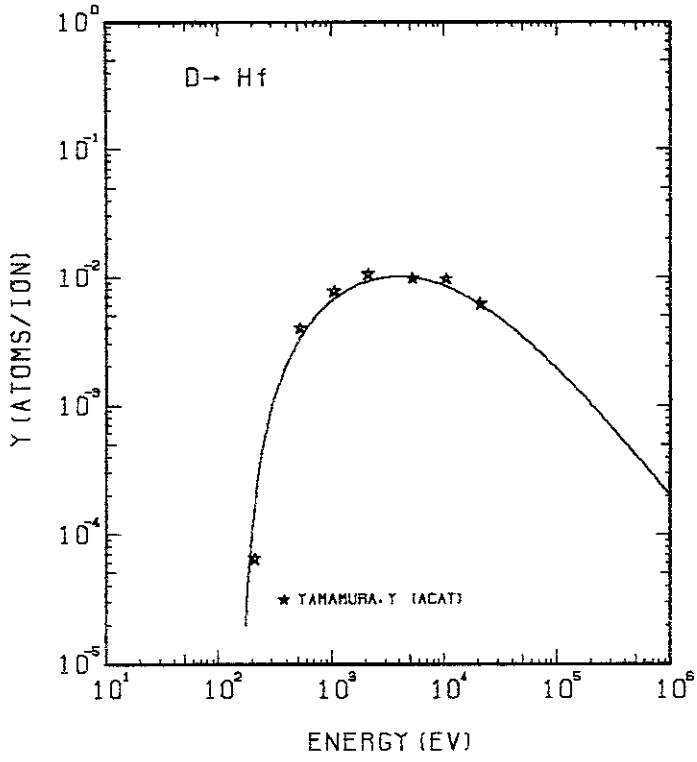

FIG. 98 ENERGY DEPENDENCE OF THE SPUTTERING YIELD OF HF WITH D^+.
A= 88.58, Q= 0.65, Us= 6.44EV, s= 2.50,
W= 0.35Us.

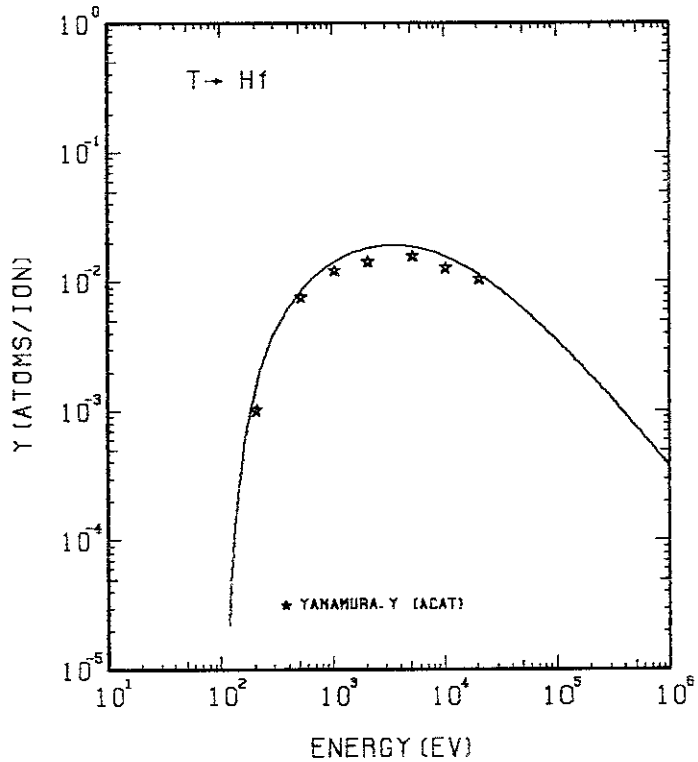

FIG. 99 ENERGY DEPENDENCE OF THE SPUTTERING YIELD OF HF WITH T^+.
A= 59.13, Q= 0.65, Us= 6.44EV, s= 2.50,
W= 0.35Us.

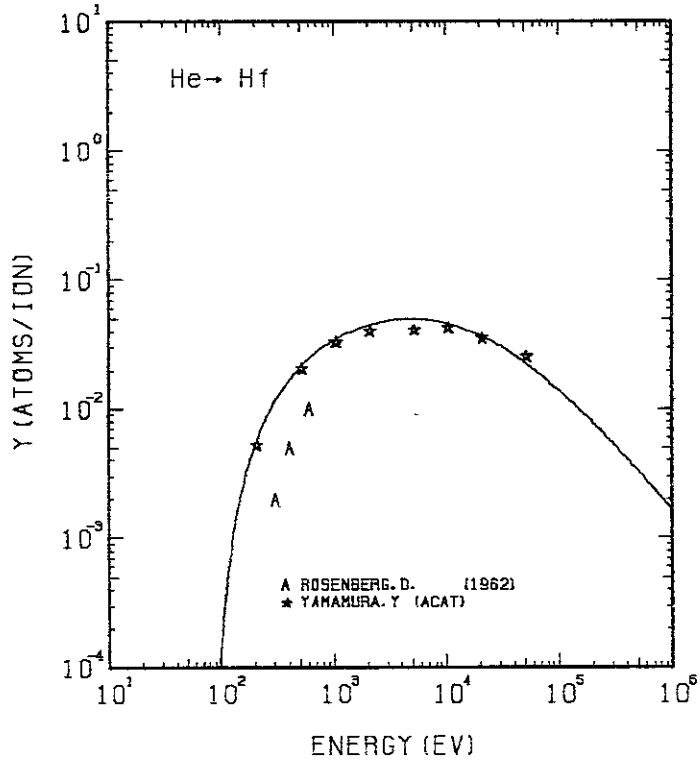

FIG. 100 ENERGY DEPENDENCE OF THE SPUTTERING YIELD OF HF WITH HE^+.
A= 44.57, Q= 0.65, Us= 6.44EV, s= 2.50,
W= 0.35Us.

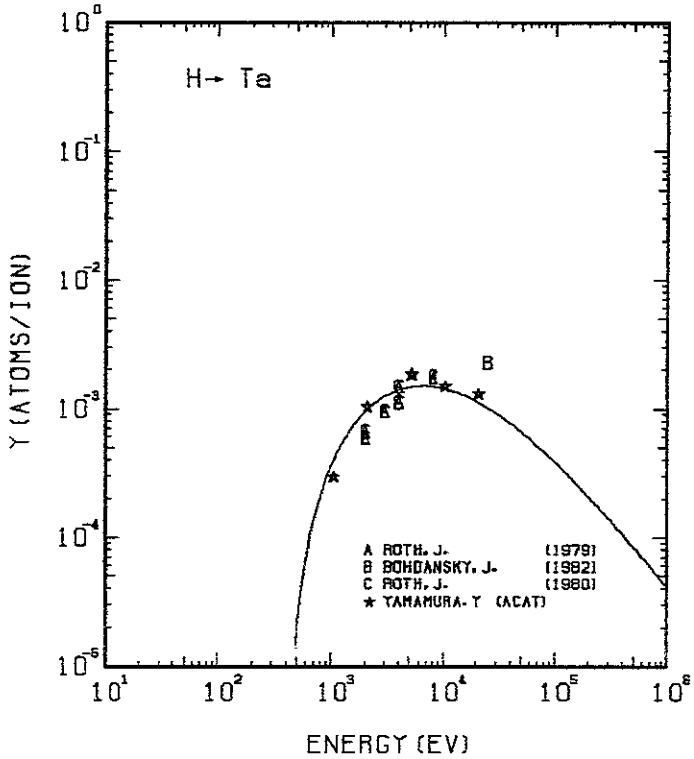

FIG. 101 ENERGY DEPENDENCE OF THE SPUTTERING YIELD OF TA WITH H^+.
A= 179.46, Q= 0.56, Us= 8.10EV, s= 2.80, W= 0.35Us.

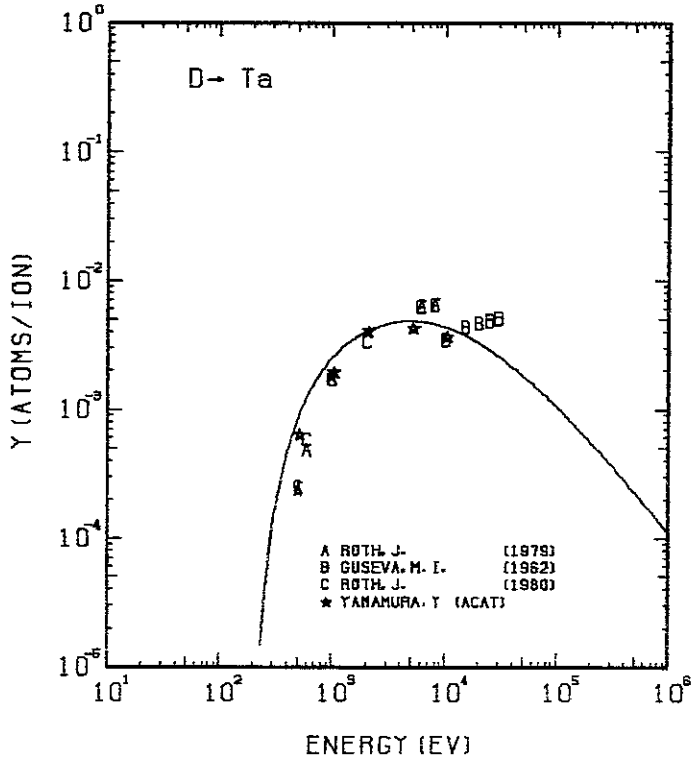

FIG. 102 ENERGY DEPENDENCE OF THE SPUTTERING YIELD OF TA WITH D^+.
A= 89.82, Q= 0.56, Us= 8.10EV, s= 2.80, W= 0.35Us.

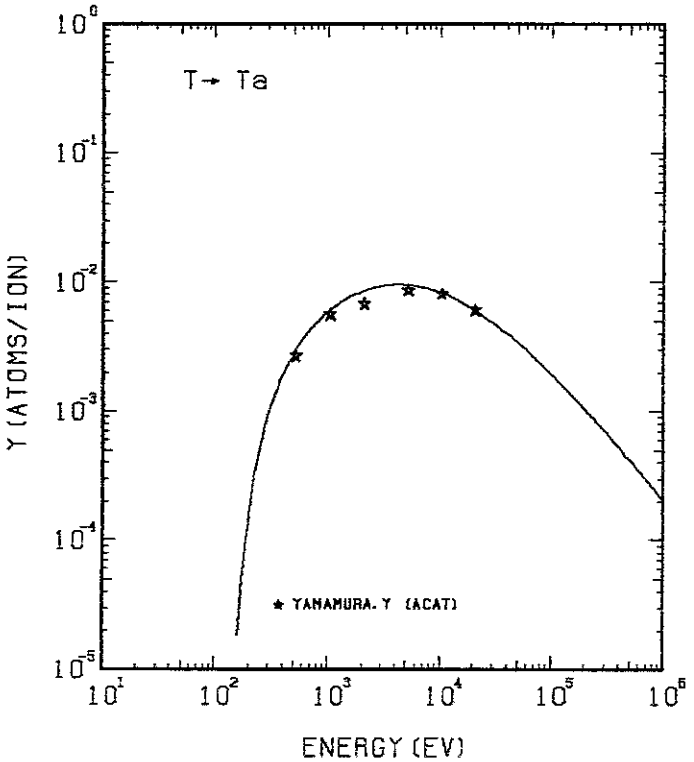

FIG. 103 ENERGY DEPENDENCE OF THE SPUTTERING YIELD OF TA WITH T^+.
A= 59.96, Q= 0.56, Us= 8.10EV, s= 2.80, W= 0.35Us.

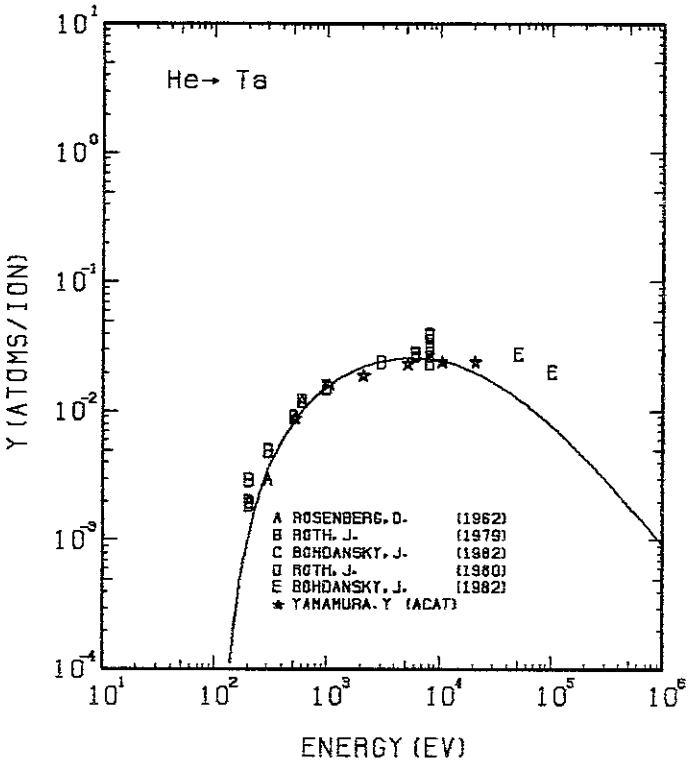

FIG. 104 ENERGY DEPENDENCE OF THE SPUTTERING YIELD OF TA WITH HE^+.
A= 45.19, Q= 0.56, Us= 8.10EV, s= 2.80, W= 0.35Us.

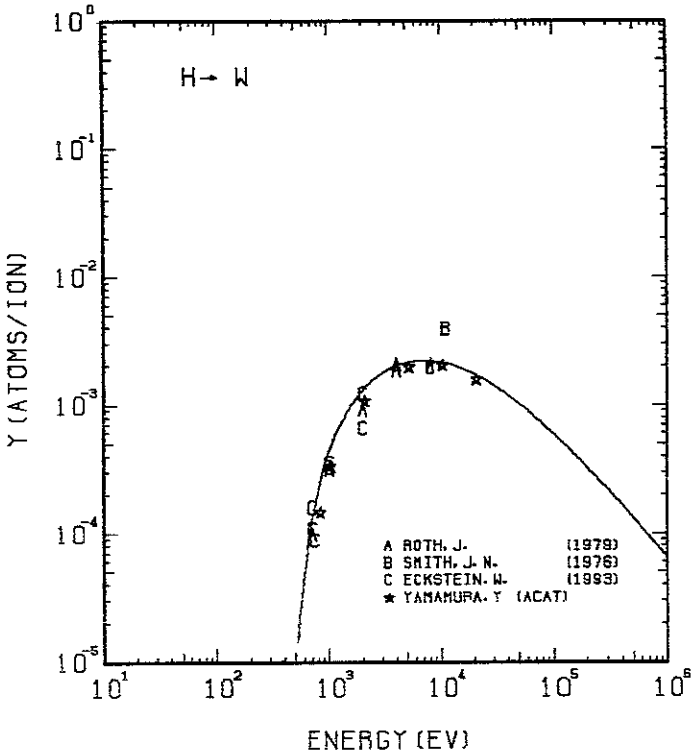

FIG. 105 ENERGY DEPENDENCE OF THE SPUTTERING YIELD OF W WITH H^+.
A= 182.34, Q= 0.72, Us= 8.90EV, S= 2.80, W= 0.24Us.

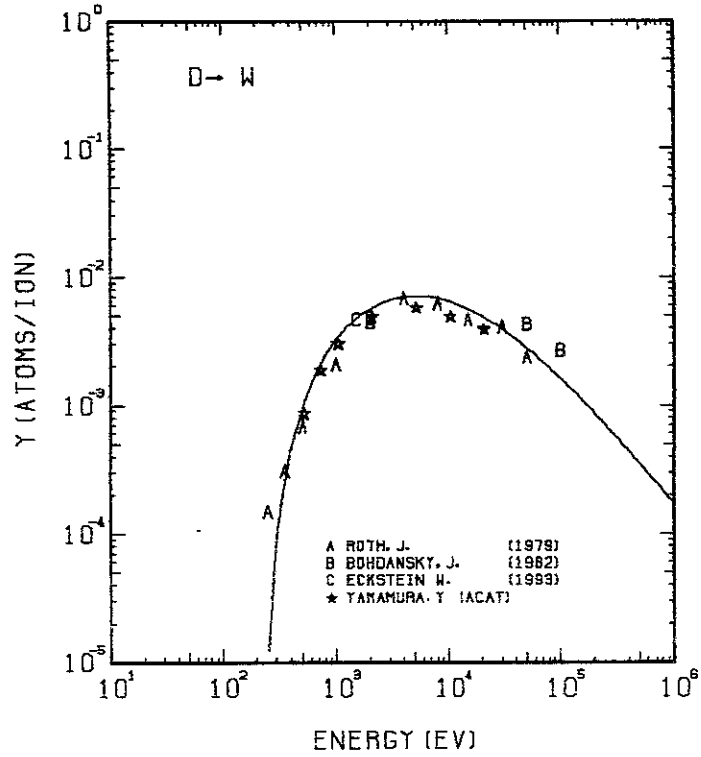

FIG. 106 ENERGY DEPENDENCE OF THE SPUTTERING YIELD OF W WITH D^+.
A= 91.26, Q= 0.72, Us= 8.90EV, S= 2.80, W= 0.24Us.

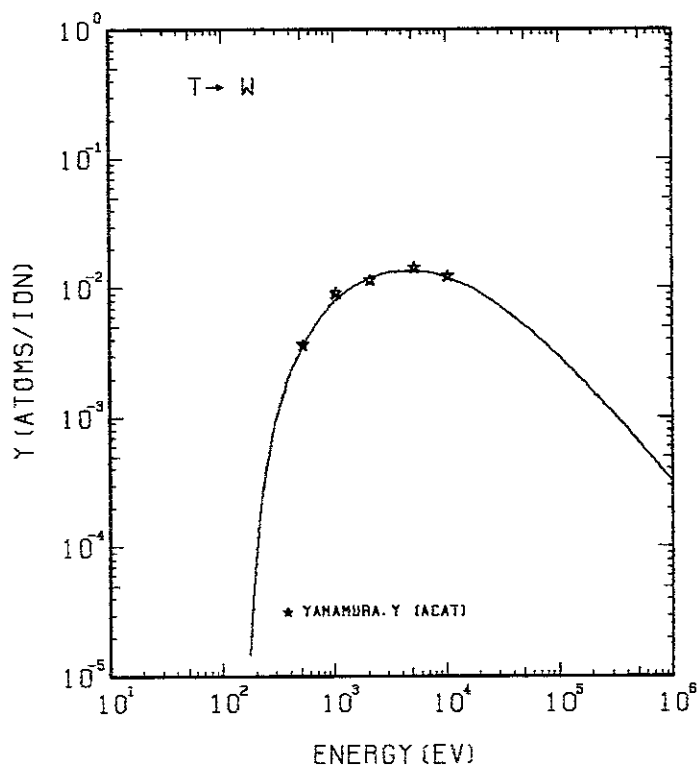

FIG. 107 ENERGY DEPENDENCE OF THE SPUTTERING YIELD OF W WITH T^+.
A= 60.92, Q= 0.72, Us= 8.90EV, S= 2.80, W= 0.24Us.

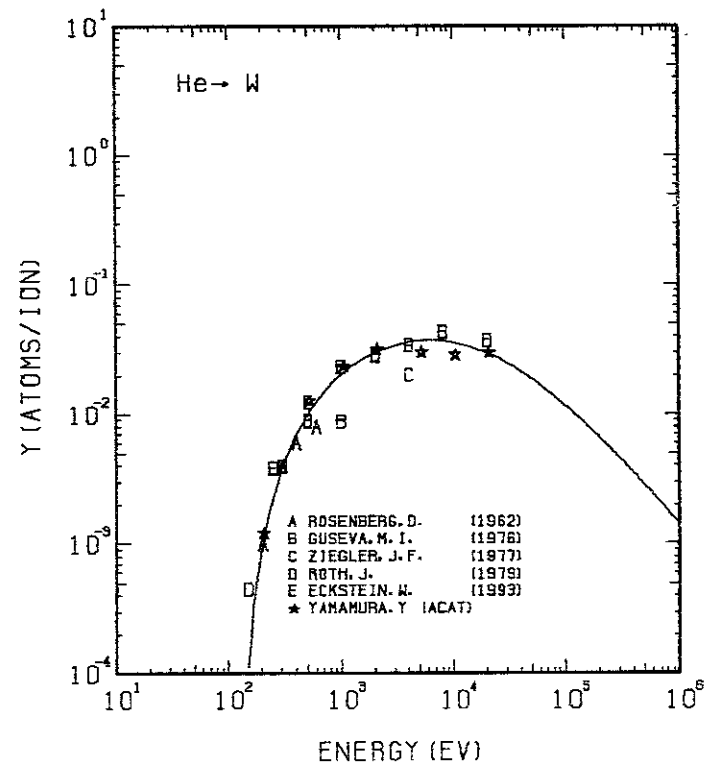

FIG. 108 ENERGY DEPENDENCE OF THE SPUTTERING YIELD OF W WITH HE^+.
A= 45.92, Q= 0.72, Us= 8.90EV, S= 2.80, W= 0.24Us.

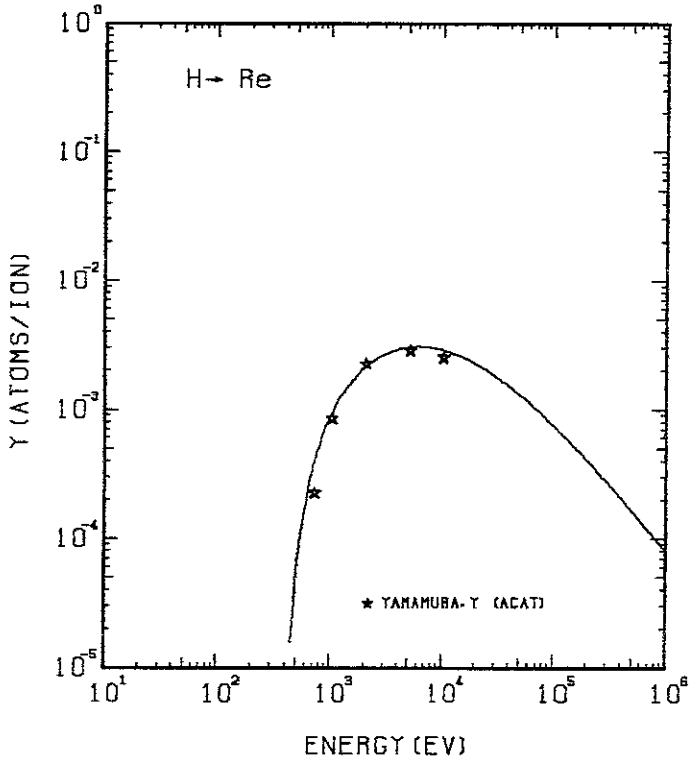

FIG. 109 ENERGY DEPENDENCE OF THE SPUTTERING YIELD OF RE WITH H^+.
A= 184.72, Q= 1.03, Us= 8.03EV, s= 2.50,
W= 0.35Us.

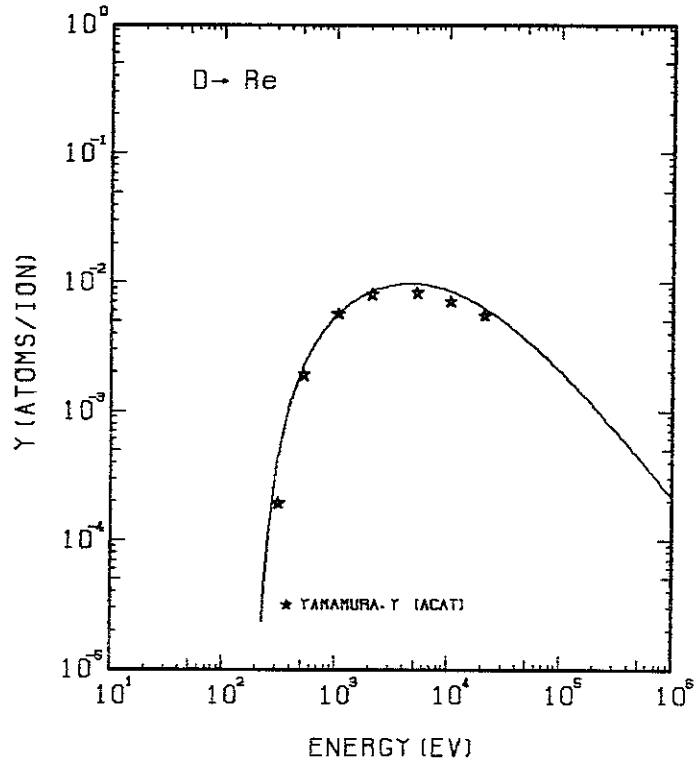

FIG. 110 ENERGY DEPENDENCE OF THE SPUTTERING YIELD OF RE WITH D^+.
A= 92.45, Q= 1.03, Us= 8.03EV, s= 2.50,
W= 0.35Us.

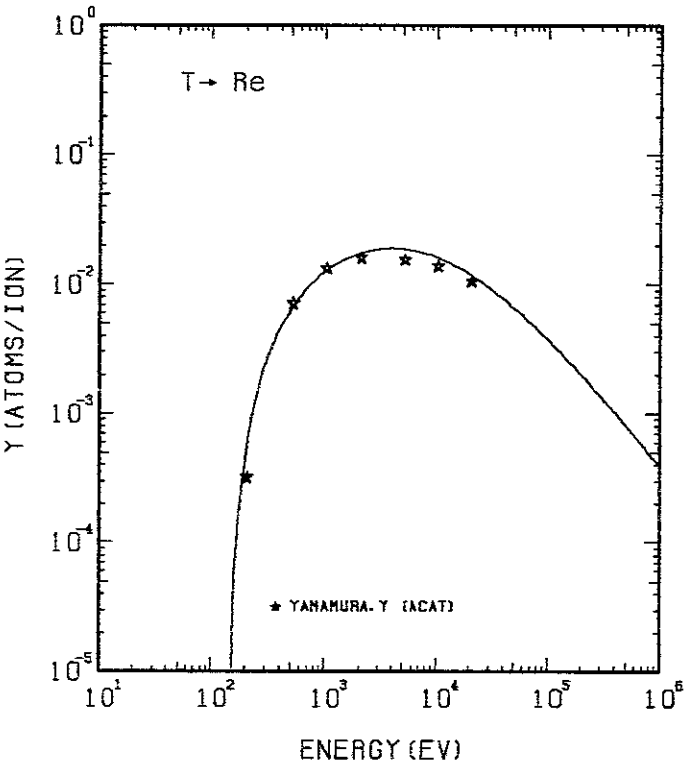

FIG. 111 ENERGY DEPENDENCE OF THE SPUTTERING YIELD OF RE WITH T^+.
A= 61.72, Q= 1.03, Us= 8.03EV, s= 2.50,
W= 0.35Us.

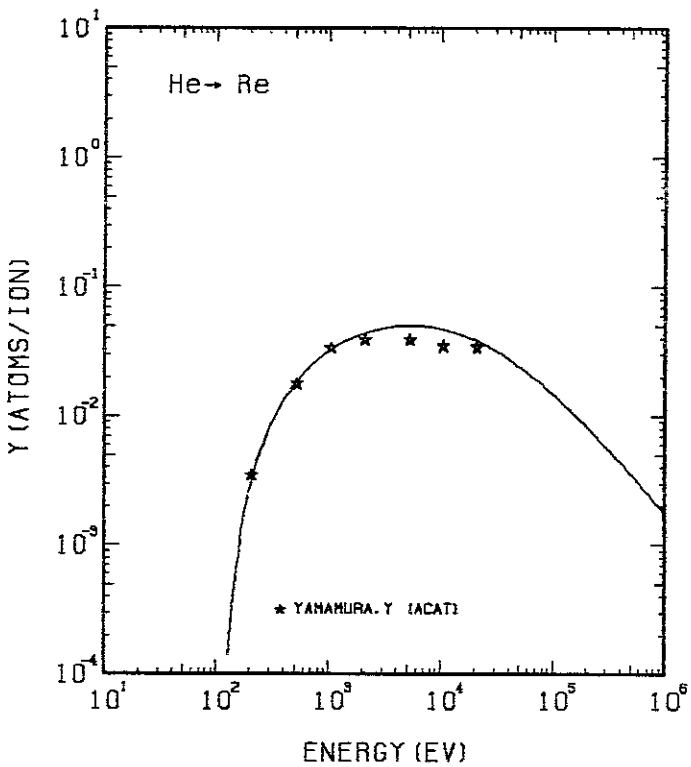

FIG. 112 ENERGY DEPENDENCE OF THE SPUTTERING YIELD OF RE WITH HE^+.
A= 46.52, Q= 1.03, Us= 8.03EV, s= 2.50,
W= 0.35Us.

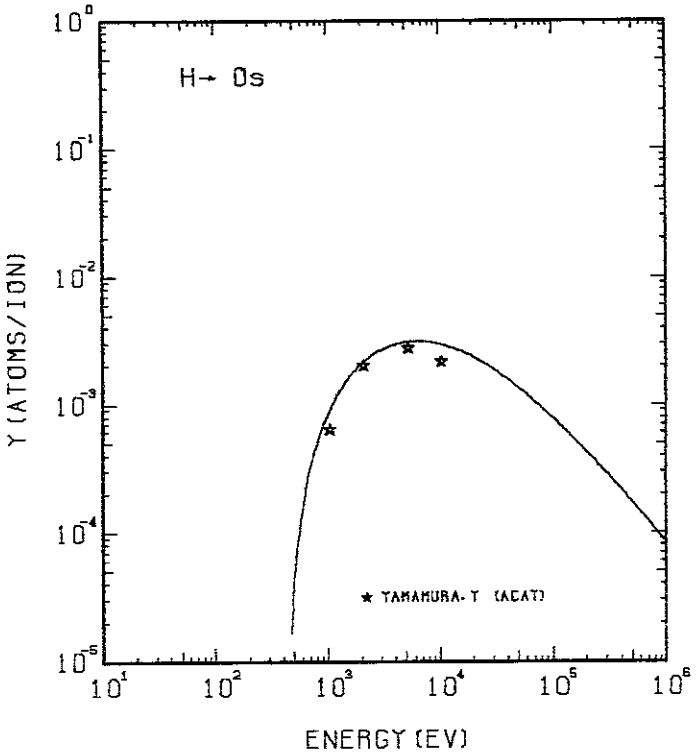

FIG. 113 ENERGY DEPENDENCE OF THE SPUTTERING YIELD OF OS WITH H^+.
A= 188.69, Q= 1.11, Us= 8.17EV, s= 2.50,
W= 0.35Us.

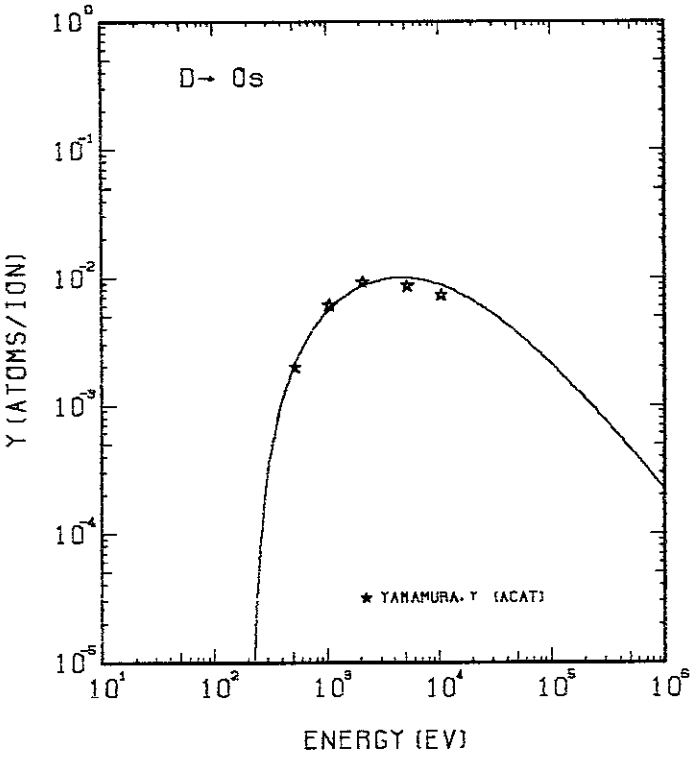

FIG. 114 ENERGY DEPENDENCE OF THE SPUTTERING YIELD OF OS WITH D^+.
A= 94.44, Q= 1.11, Us= 8.17EV, s= 2.50,
W= 0.35Us.

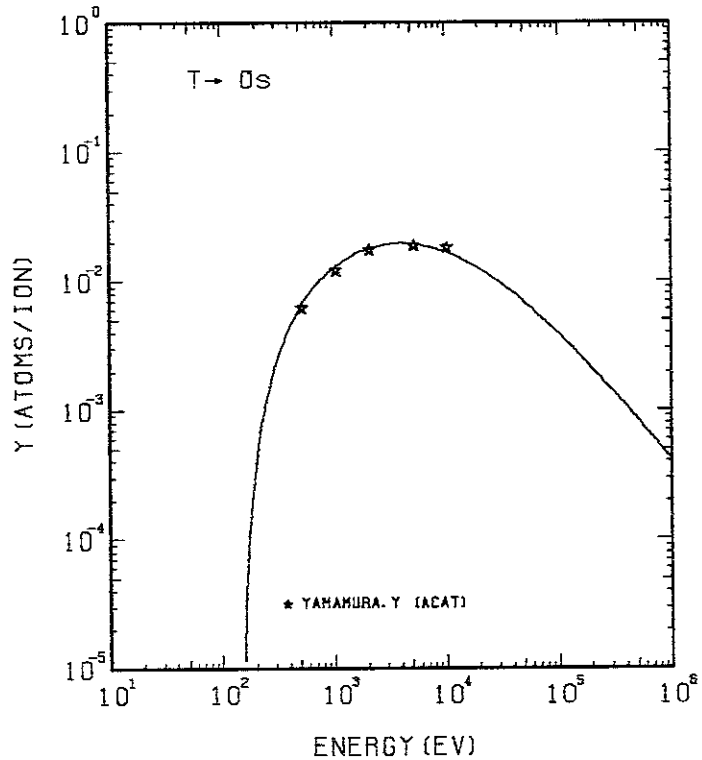

FIG. 115 ENERGY DEPENDENCE OF THE SPUTTERING YIELD OF OS WITH T^+.
A= 63.04, Q= 1.11, Us= 8.17EV, s= 2.50,
W= 0.35Us.

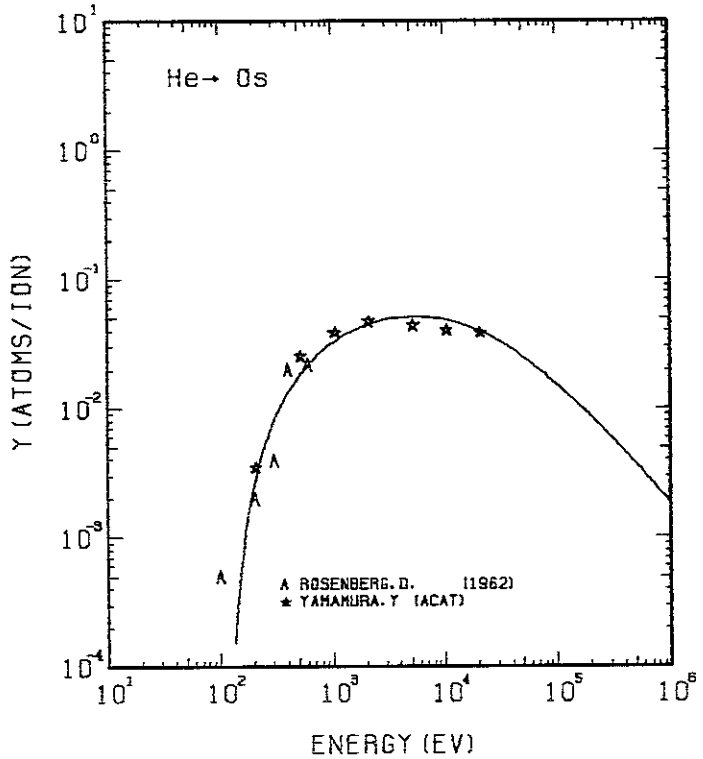

FIG. 116 ENERGY DEPENDENCE OF THE SPUTTERING YIELD OF OS WITH HE^+.
A= 47.51, Q= 1.11, Us= 8.17EV, s= 2.50,
W= 0.35Us.

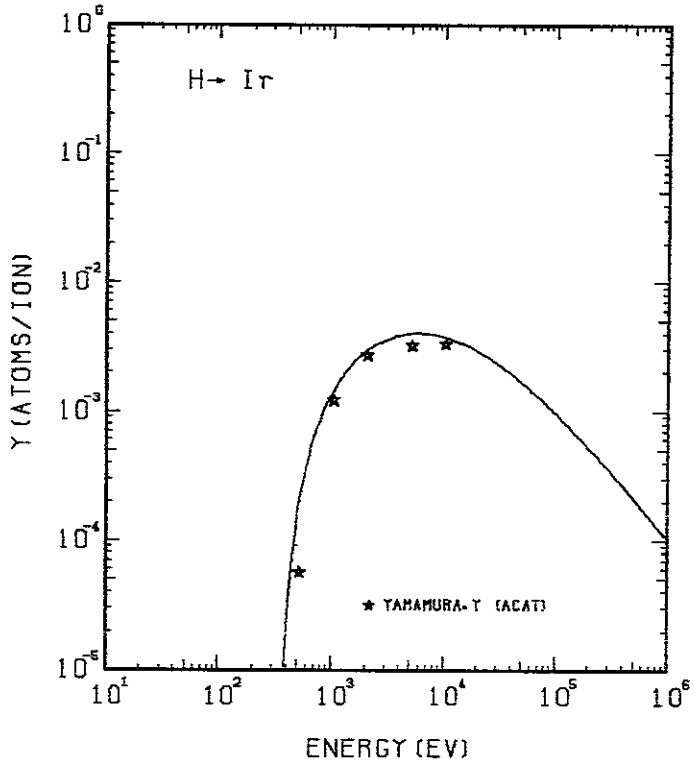

FIG. 117 ENERGY DEPENDENCE OF THE SPUTTERING YIELD OF IR WITH H^+.
A= 190.67, Q= 0.96, Us= 6.94EV, S= 2.50,
W= 0.35Us.

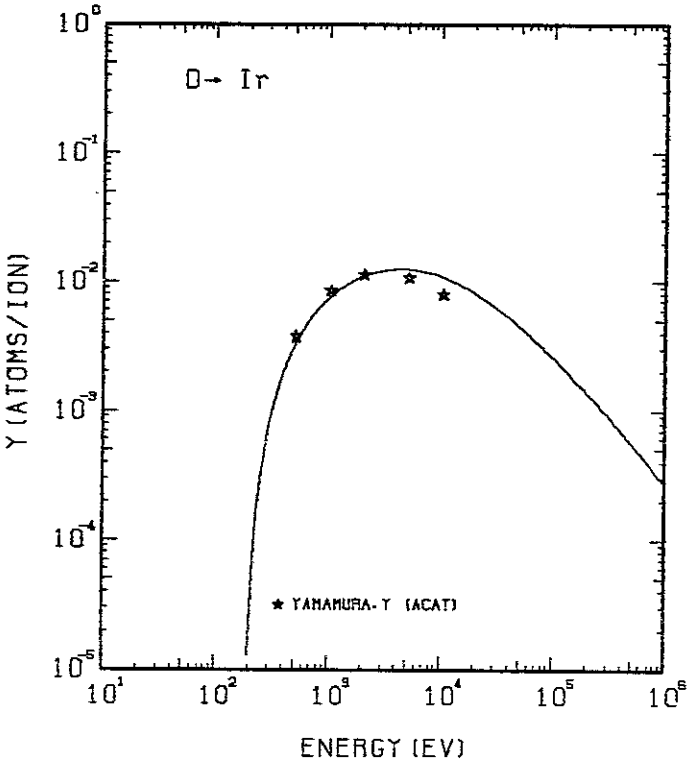

FIG. 118 ENERGY DEPENDENCE OF THE SPUTTERING YIELD OF IR WITH D^+.
A= 95.43, Q= 0.96, Us= 6.94EV, S= 2.50,
W= 0.35Us.

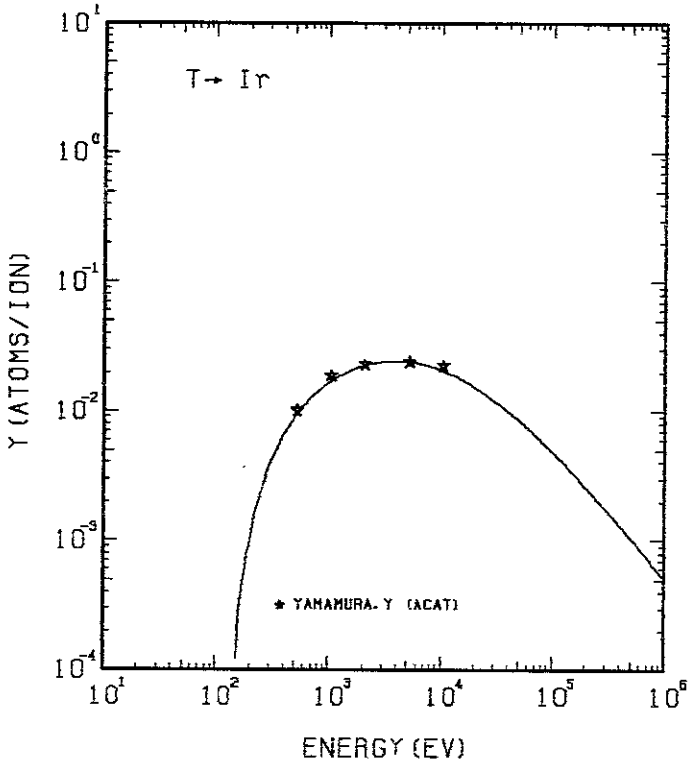

FIG. 119 ENERGY DEPENDENCE OF THE SPUTTERING YIELD OF IR WITH T^+.
A= 63.71, Q= 0.96, Us= 6.94EV, S= 2.50,
W= 0.35Us.

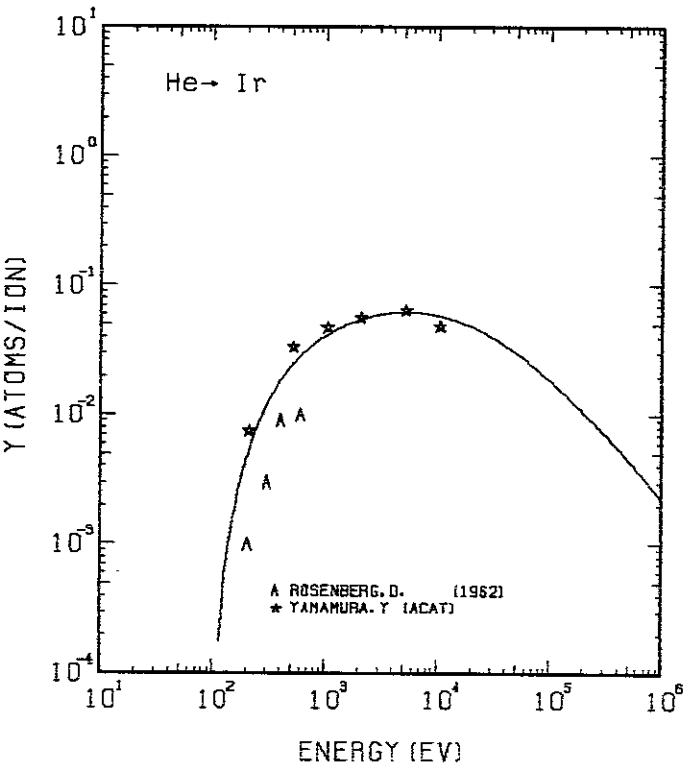

FIG. 120 ENERGY DEPENDENCE OF THE SPUTTERING YIELD OF IR WITH HE^+.
A= 48.01, Q= 0.96, Us= 6.94EV, S= 2.50,
W= 0.35Us.

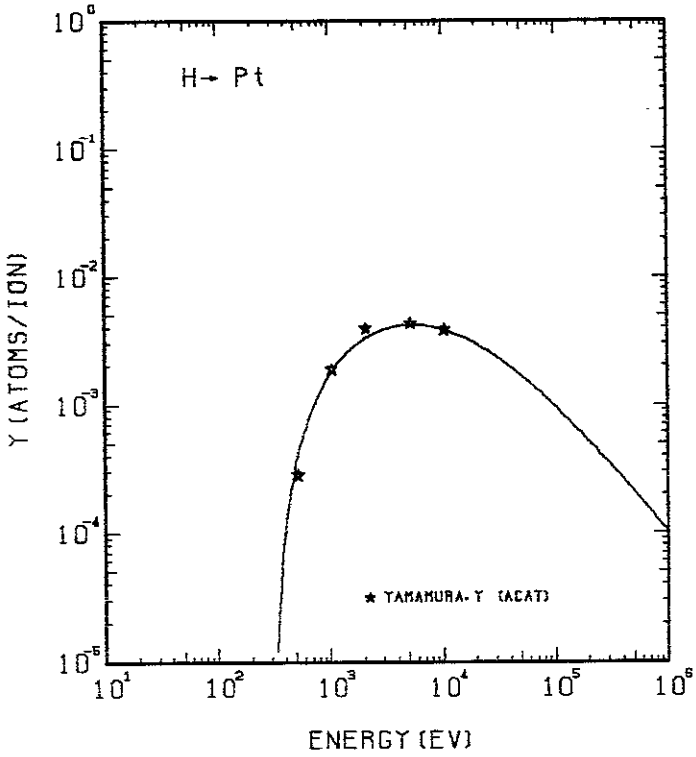

FIG. 121 ENERGY DEPENDENCE OF THE SPUTTERING YIELD OF PT WITH H^+.
A= 193.45, Q= 1.03, Us= 5.84EV, s= 2.50, W= 0.55Us.

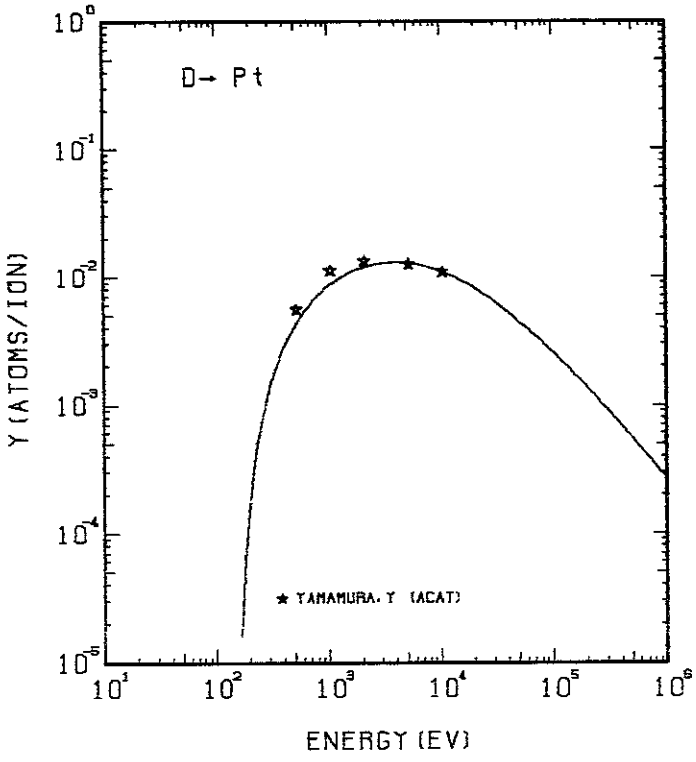

FIG. 122 ENERGY DEPENDENCE OF THE SPUTTERING YIELD OF PT WITH D^+.
A= 96.82, Q= 1.03, Us= 5.84EV, s= 2.50, W= 0.55Us.

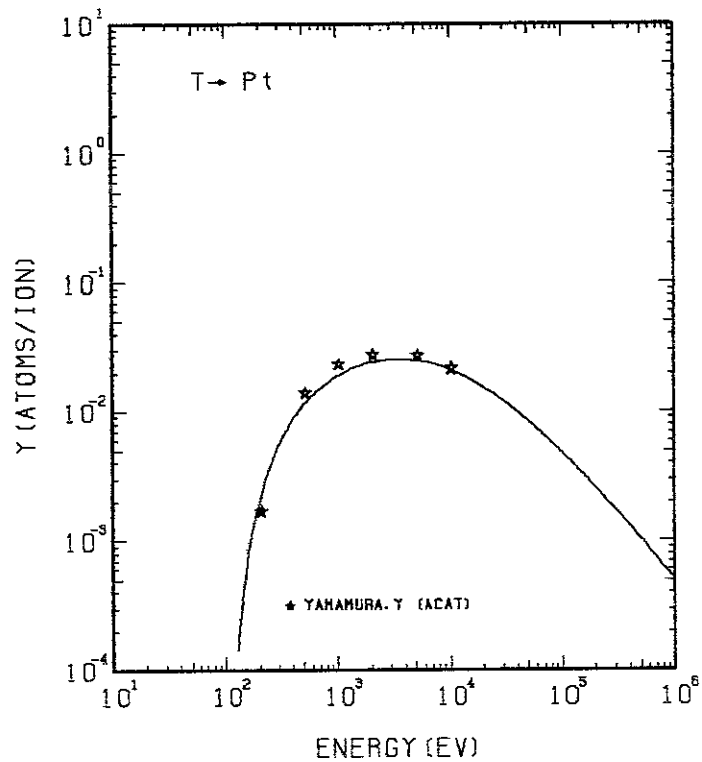

FIG. 123 ENERGY DEPENDENCE OF THE SPUTTERING YIELD OF PT WITH T^+.
A= 64.63, Q= 1.03, Us= 5.84EV, s= 2.50, W= 0.55Us.

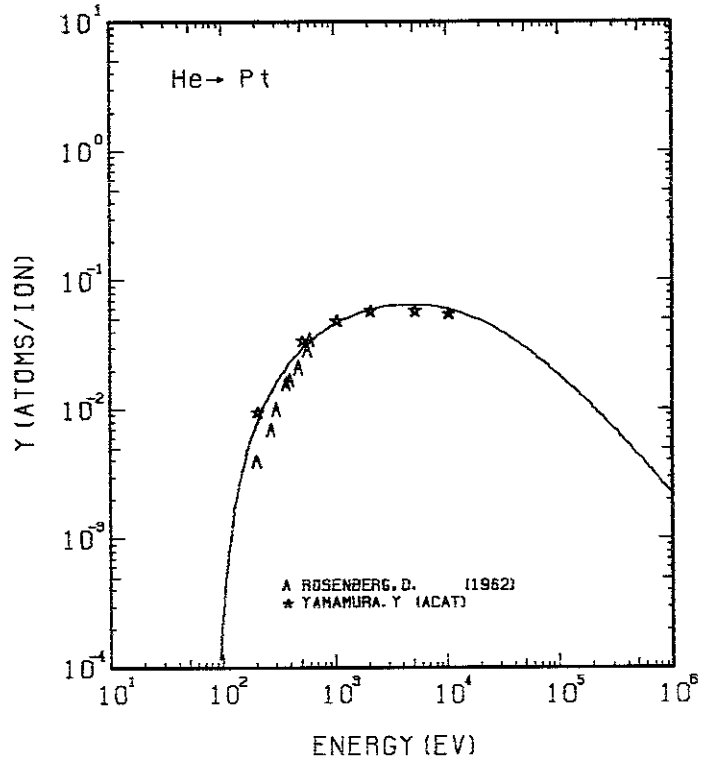

FIG. 124 ENERGY DEPENDENCE OF THE SPUTTERING YIELD OF PT WITH HE^+.
A= 48.71, Q= 1.03, Us= 5.84EV, s= 2.50, W= 0.55Us.

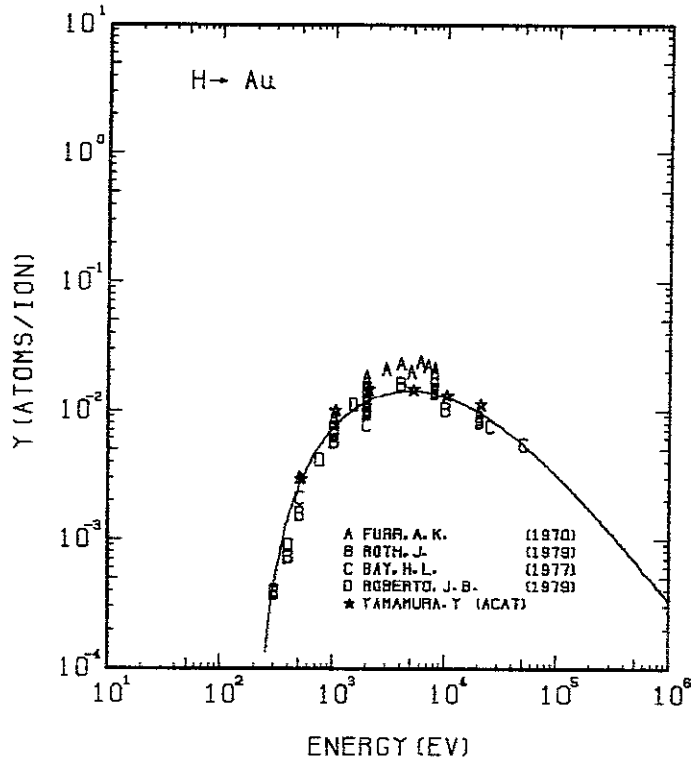

FIG. 125 ENERGY DEPENDENCE OF THE SPUTTERING YIELD OF AU WITH H^+.
A= 195.34, Q= 1.08, Us= 3.81EV, S= 2.80,
W= 0.43Us.

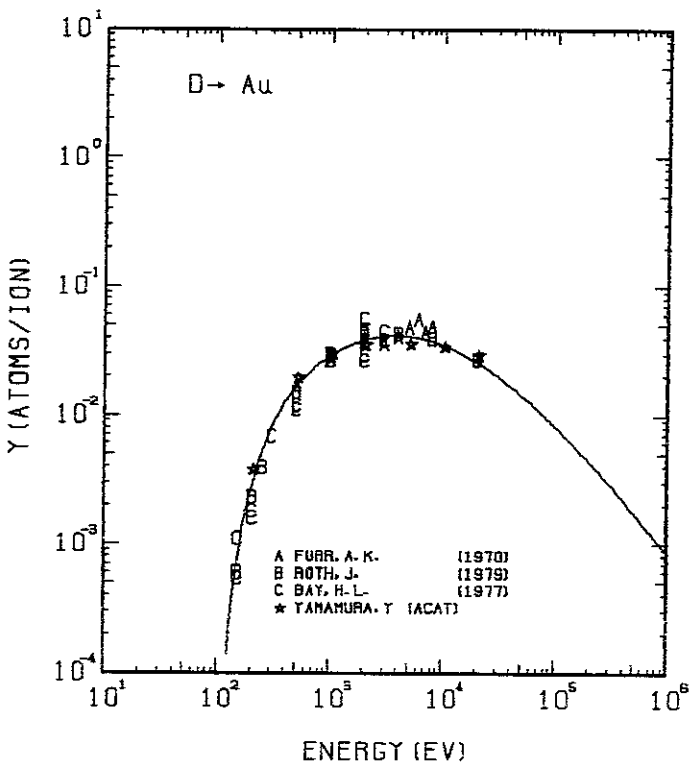

FIG. 126 ENERGY DEPENDENCE OF THE SPUTTERING YIELD OF AU WITH D^+.
A= 97.77, Q= 1.08, Us= 3.81EV, S= 2.80,
W= 0.43Us.

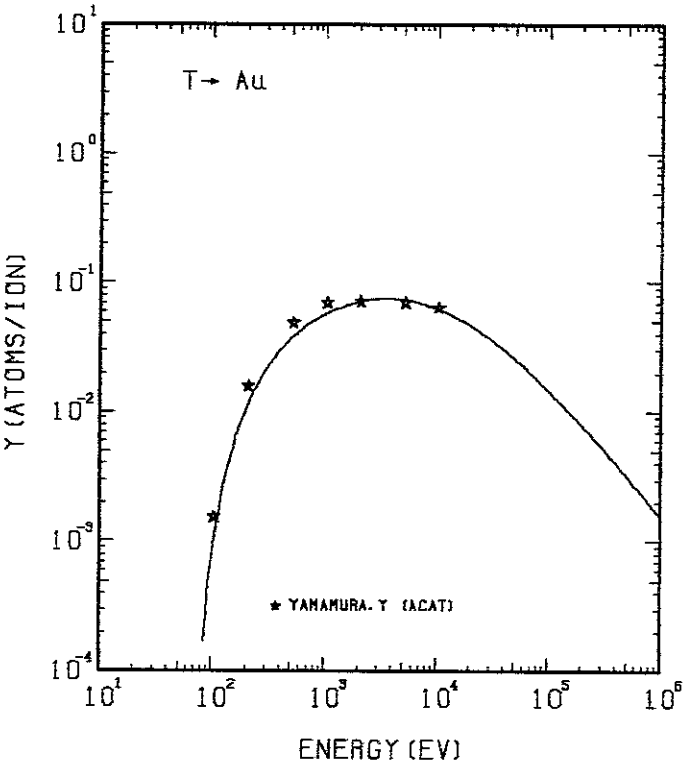

FIG. 127 ENERGY DEPENDENCE OF THE SPUTTERING YIELD OF AU WITH T^+.
A= 65.26, Q= 1.08, Us= 3.81EV, S= 2.80,
W= 0.43Us.

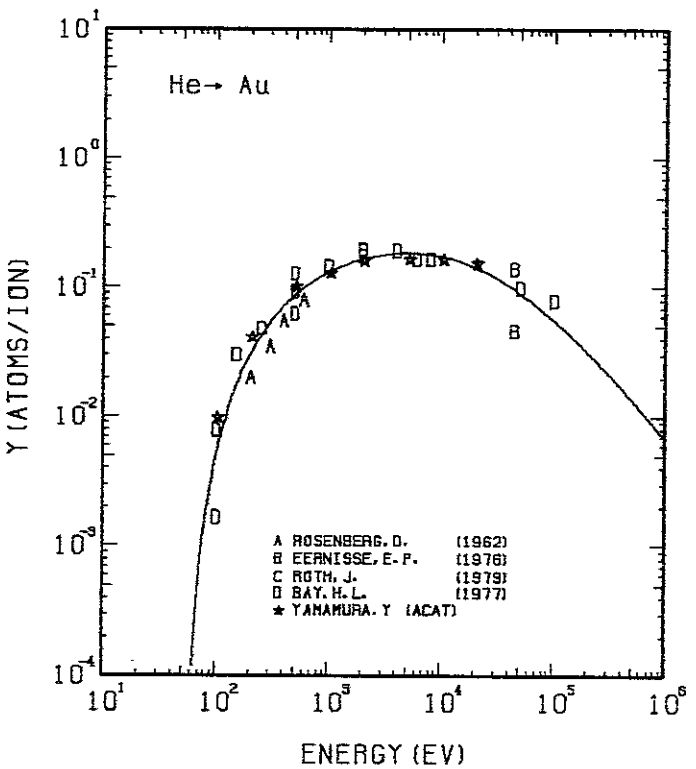

FIG. 128 ENERGY DEPENDENCE OF THE SPUTTERING YIELD OF AU WITH HE^+.
A= 49.19, Q= 1.08, Us= 3.81EV, S= 2.80,
W= 0.43Us.

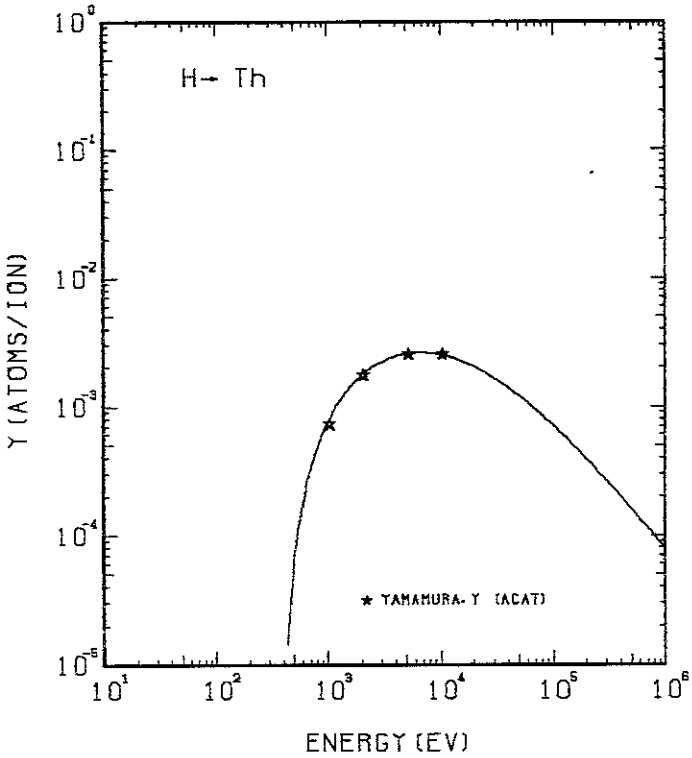

FIG. 129 ENERGY DEPENDENCE OF THE SPUTTERING YIELD OF TH WITH H^+.
A= 230.16, Q= 0.63, Us= 6.20EV, s= 2.50,
W= 0.45Us.

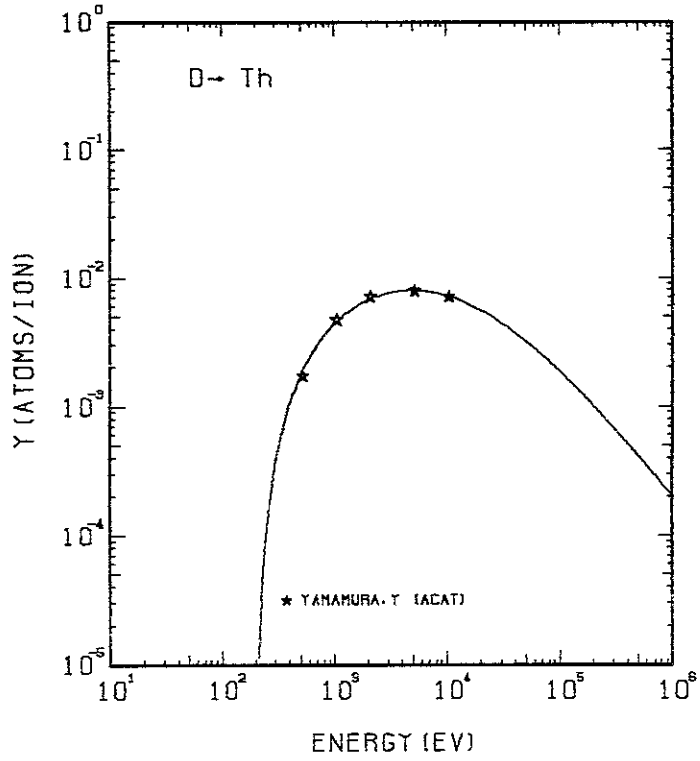

FIG. 130 ENERGY DEPENDENCE OF THE SPUTTERING YIELD OF TH WITH D^+.
A= 115.19, Q= 0.63, Us= 6.20EV, s= 2.50,
W= 0.45Us.

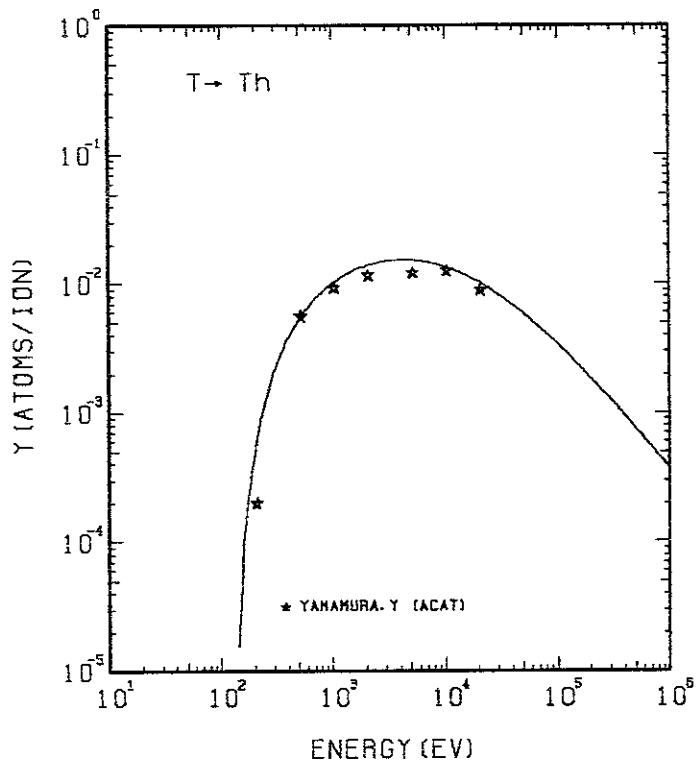

FIG. 131 ENERGY DEPENDENCE OF THE SPUTTERING YIELD OF TH WITH T^+.
A= 76.90, Q= 0.63, Us= 6.20EV, s= 2.50,
W= 0.45Us.

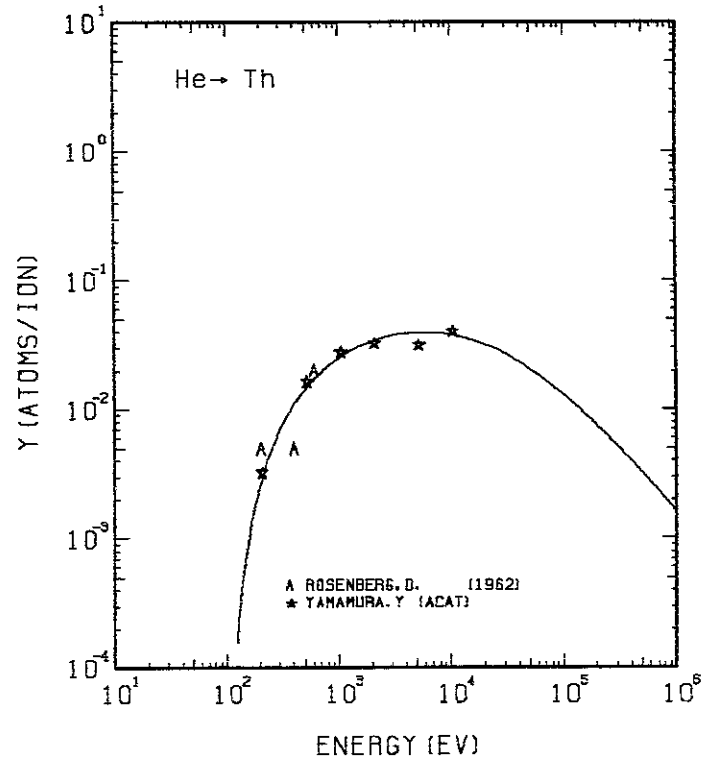

FIG. 132 ENERGY DEPENDENCE OF THE SPUTTERING YIELD OF TH WITH HE^+.
A= 57.96, Q= 0.63, Us= 6.20EV, s= 2.50,
W= 0.45Us.

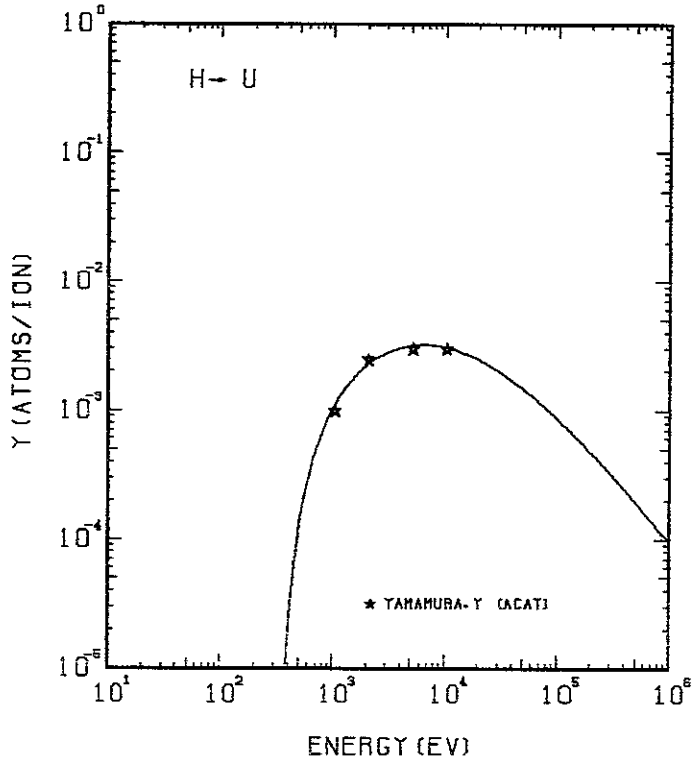

FIG. 133 ENERGY DEPENDENCE OF THE SPUTTERING YIELD OF U WITH H^+.
A= 236.11, Q= 0.66, Us= 5.55EV, s= 2.50,
W= 0.50Us.

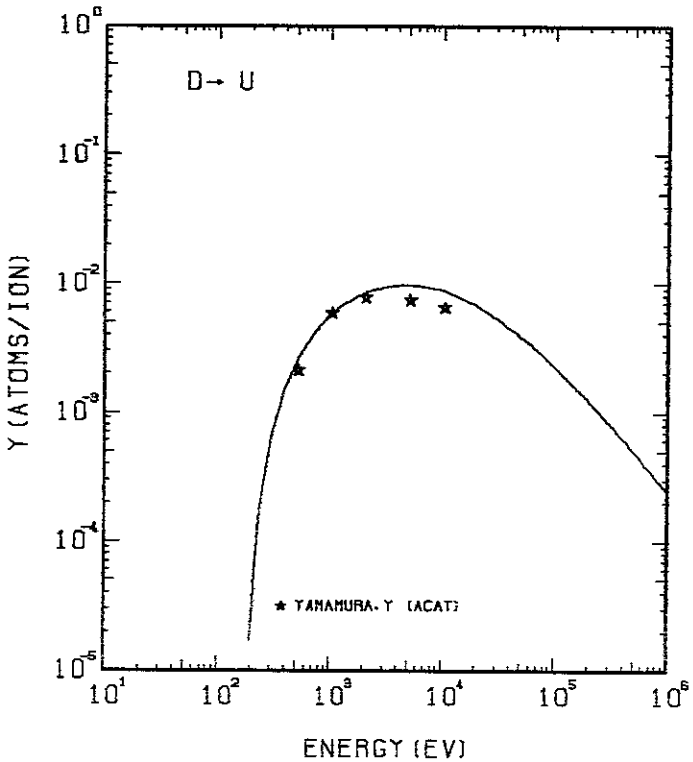

FIG. 134 ENERGY DEPENDENCE OF THE SPUTTERING YIELD OF U WITH D^+.
A= 118.17, Q= 0.66, Us= 5.55EV, s= 2.50,
W= 0.50Us.

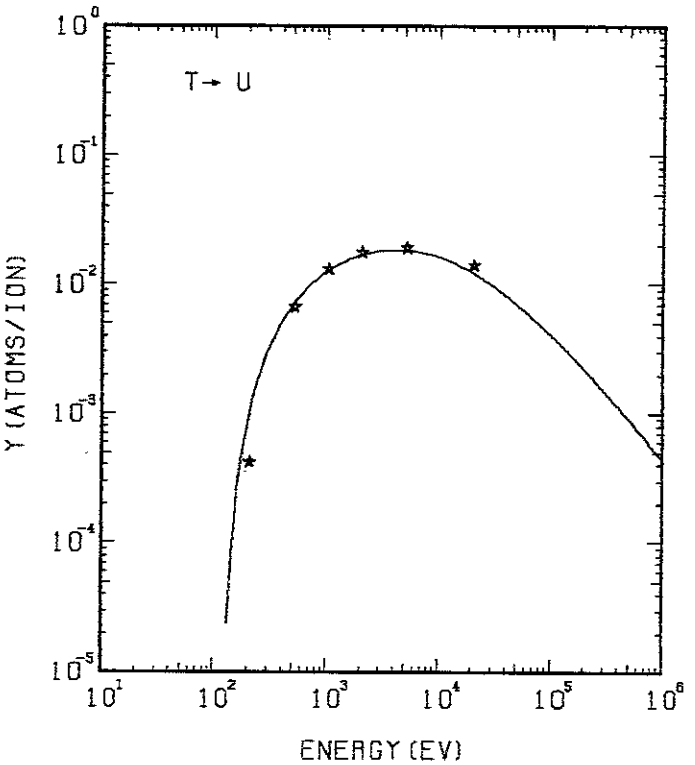

FIG. 135 ENERGY DEPENDENCE OF THE SPUTTERING YIELD OF U WITH T^+.
A= 78.89, Q= 0.66, Us= 5.55EV, s= 2.50,
W= 0.50Us.

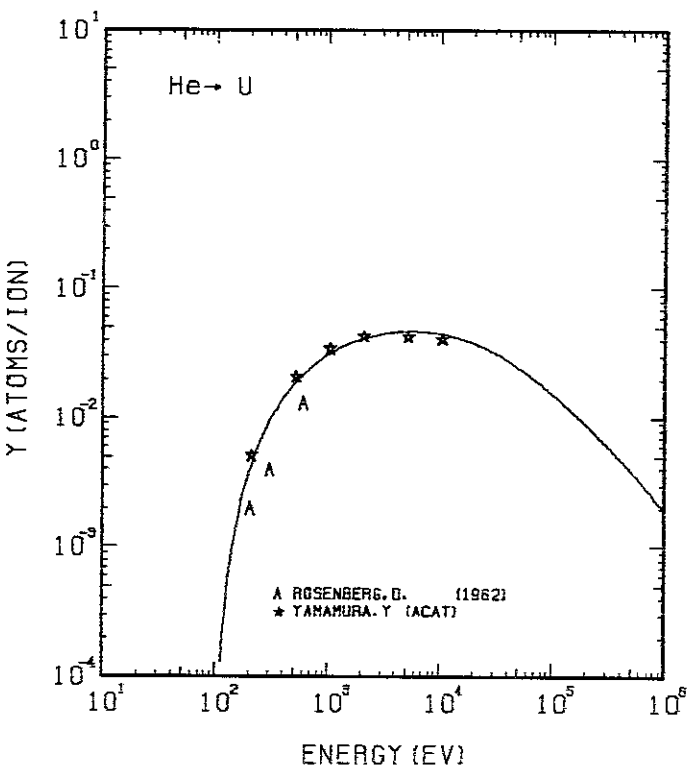

FIG. 136 ENERGY DEPENDENCE OF THE SPUTTERING YIELD OF U WITH HE^+.
A= 59.46, Q= 0.66, Us= 5.55EV, s= 2.50,
W= 0.50Us.

References for Graphs

Bay, H.L., J. Bohdansky and J. Roth ; J. Appl. Phys. **48**, 4722 (1977A)

Bay, H.L., J. Bohdansky and J. Roth ; Vacuum Congress and Solid Surface, Vienna (1977B)

Bay, H.L., J. Bohdansky and E. Hechtl ; Radiat. Eff. **41**, 77 (1979)

Benninghoven, A. ; Angew. Phys. **51**, 27 (1969)

Bohdansky, J., J. Roth and M.K. Sinha ;

Pro. 9th Symposium Fusion Technology, Pergamon (1976) p541.

Bohdansky, J. ; J. Nucl. Mater. **93&94**, 44 (1980)

Bohdansky, J., G.L. Chen, W. Eckstein, B.M.U. Scherzer and R. Behrisch ;

J. Nucl. Mater. **111&112**, 717 (1982)

Bohdansky, J., J. Roth and W. Ottenberger ;

Sputtering Measurements of Beryllium, Max-Plank-Institut für Plasmaphysik,

Report IPP-JET No.31 (1985)

Bohdansky, J., and J. Roth ; J. Nucl. Mater. **145**, 387 (1987)

Bohdansky, J., H. Linder, E. Hechtel, A.P. Martinelli and J. Roth ;

Nucl. Instr. Meth. **B18**, 509(1987)

Border, J.A., R.A. Langley and K.L. Wilson ; J. Nucl. Mater. **76&77**, 168 (1978)

Coburn, J.W., H.F. Winters and T.J. Chuang ; J. Appl. Phys. **48**, 3532 (1977)

Eckstein, W., C. Garcia-Rosales, J. Roth and W. Ottenberger, IPP 9/82

(Inst. Plasma Physics, Garching, Germany, 1993).

EerNisse, E.P. ; Appl. Phys. Lett. **29**, 14 (1976)

Fetz, H., and H. Oechsner ;

Proc. 6th Int. Conf. Ionization Phenomena in Gases, Paris, Vol. II (1963) p39

Finfgeld, C.R. ; Salem Va-Report Oro-3557-15 (1967)

Furr, A.K., and C.R. Finfgeld ; J. Appl. Phys . **41**, 1739 (1970)

Gronlund, F., and W.J. Moore ; J. Chem. Phys. **32**, 1540 (1960)

Guseva, M.I., and Y.V. Martynenko ; Fiz. Plaz. (USSR) Vol. **2**, No.4 593 (1976)

Haasz, A.A., and J.W. Davis ; J. Nucl. Mater. **162-164**, 915(1989)

Hechtl, E., A. Mazone W. Eckstein and J. Roth ; J. Nucl. Mater. **196-198**, 713 (1992).

Hintz, E., D. Rusbüldt, B. Schweer, J. Bohdansky and J. Roth ;
J. Nucl. Mater. **93/94**, 656 (1986).

Hofer, W.O., H.L. Bay and P.J. Martin ; J. Nucl. Mater. **76&77**, 156 (1978)

Kaminsky, M. ; private communication (1983)

Kenknight, C.E., and G.K. Wehner ; J. Appl. Phys. **35**, 322 (1964)

Keywell, F. ; Phys. Rev. **97**, 1611 (1955)

Lam, S.K., and M. Kaminsky ; J. Nucl. Mater. **89**, 205 (1980)

Merkle, K.L.,and W. Jäger ; Phil. Mag. **A44**, 741 (1981)

Miyagawa, S., Y. Ato and Y. Moriya ; J. Appl. Phys. **49**, 6194 (1978)

O'Brian, C.D., A. Linder and W.J. Moore ; J. Chem. Phys. **29**, 3 (1958)

O'Connor, J.P., L.M. Baumel, P.G. Blauner, K.M. Hubbard, M.R. Weller and R.A. Weller;
Nucl. Instr. Meth. **B13**, 365 (1986)

Oechsner, H. ; Z. Phys. **37**, 261 (1973)

Ohtsuka, H., R. Yamada, K. Sone, M. Saidoh, and T. Abe ;
J. Nucl. Mater. **76&77**, 188 (1978)

Ollerhead, R.W., F.M. Mann, D.W. Kneff, Z.E. Switkowskii and T.A. Tombrello ;
Phys. Rev. Lett. **36**, 439 (1976)

Poate, J. M., W.R. Brown, R. Homer, W.M. Augustyniak, J. W. Meyer, K.N. Tu
and W.F. Weg ; Nucl. Instr. Meth. **132**, 345 (1976)

Roberto, J.B., R.A. Zuhr, J.L. Moore and G.D. Alton ;
J. Nucl. Mater. **85&86**, 1073 (1979)

Rosenbarg, D., and G.K. Wehner ; J. Appl. Phys. **33**, 1842 (1962)

Roth, J., J. Bohdansky, W. Poschenrieder and M.K. Shinha ; J. Nucl. Mater. **63**, 229 (1976)

Roth, J., J. Bohdansky and W. Ottenberger ; IPP 9/26
(Inst. Plasma Physics, Garching, Germany, 1979)

Roth, J., J. Bohdansky and A.P. Martinelli ; Radiat. Eff. **48**, 213 (1980)

Roth, J., J. Bohdansky and K.L. Wilson ; J. Nucl. Mater. **111&112**, 775 (1982)

Saidoh, M., H. Gnaser and W.O. Hofer ; Appl. Phys. **A40**, 197 (1986)

Saiki, K., H. Tanaka, S. Tanaka and A. Koma ; J. Nucl. Mater. **97**, 173 (1981)

Santaniello, A., J. Appelt, J. Bohdansky and J. Roth ; J. Nucl. Mater. **162-164**, 951 (1989)

Smith, J.N.Jr., C.H. Meyer and J.K. Layton ; Nucl. Technol. **29**, 318 (1976)

Sommerfeldt, H., E.S. Mashkova and V.A. Molchanov ; Phys. Lett. **38A**, 237 (1972)

Sone, K., H. Ohtsuka,T. Abe, R. Yamada, K. Obara, T. Narusawa, O. Tsukakoshi, T. Satake and S. Komizo ; J. Vac. Soc. Japan **20**, 136 (1977)

Summers, A.J., N.J. Freeman and N.R. Daly ; J. Appl. Phys. **42**, 4774 (1971)

Switkowski, Z.E., F.M. Mann, K.W. Kneff, R.W. Ollerhead and T.A. Tombrello ; Radiat. Eff. **29**, 65 (1976)

Tomita, M., T. Nate, S. Miyagi and M. Sakisaka ; J. Nucl. Mater. **138**, 248 (1986)

Yamashita, M., S. Baba, and A. Kinbar ; Poc. 4th Sym. Ion Source and Ion Application (1980) p311

Yonts, O.C., and D.E. Harrison, Jr. ; ORNL-2802 (1959)

Yonts, O.C, C.E. Normann and D.E. Harrison, Jr.; J. Appl. Phys. **31**, 447 (1960)

Ziegler, J.F., J.J. Cuomo and J. Roth ; Appl. Phys. Lett. **30**, 268 (1977)

Publication List of NIFS-DATA Series

NIFS-DATA-1 Y. Yamamura, T. Takiguchi and H. Tawara,
Data Compilation of Angular Distributions of Sputtered Atoms; Jan. 1990

NIFS-DATA-2 T. Kato, J. Lang and K. E. Berrington,
Intensity Ratios of Emission Lines from OV Ions for Temperature and Density Diagnostics ; Mar. 1990 [At Data and Nucl Data Tables 44(1990)133]

NIFS-DATA-3 T. Kaneko,
Partial Electronic Straggling Cross Sections of Atoms for Protons ;Mar. 1990

NIFS-DATA-4 T. Fujimoto, K. Sawada and K. Takahata,
Cross Section for Production of Excited Hydrogen Atoms Following Dissociative Excitation of Molecular Hydrogen by Electron Impact ; Mar. 1990

NIFS-DATA-5 H. Tawara,
Some Electron Detachment Data for H^- Ions in Collisions with Electrons, Ions, Atoms and Molecules –an Alternative Approach to High Energy Neutral Beam Production for Plasma Heating–; Apr. 1990

NIFS-DATA-6 H. Tawara, Y. Itikawa, H. Nishimura, H. Tanaka and Y. Nakamura,
Collision Data Involving Hydro-Carbon Molecules; July 1990 [Supplement to Nucl. Fusion 2(1992)25]

NIFS-DATA-7 H.Tawara,
Bibliography on Electron Transfer Processes in Ion-Ion/Atom/Molecule Collisions –Updated 1990–; Aug. 1990

NIFS-DATA-8 U.I.Safronova, T.Kato, K.Masai, L.A.Vainshtein and A.S.Shlyapzeva,
Excitation Collision Strengths, Cross Sections and Rate Coefficients for OV, SiXI, FeXXIII, MoXXXIX by Electron Impact ($1s^22s^2$-$1s^22s2p$-$1s^22p^2$ Transitions) Dec.1990

NIFS-DATA-9 T.Kaneko,
Partial and Total Electronic Stopping Cross Sections of Atoms and Solids for Protons; Dec. 1990

NIFS-DATA-10 K.Shima, N.Kuno, M.Yamanouchi and H.Tawara,
Equilibrium Charge Fraction of Ions of Z=4-92 (0.02-6 MeV/u) and Z=4-20 (Up to 40 MeV/u) Emerging from a Carbon Foil; Jan.1991 [AT.Data and Nucl. Data Tables 51(1992)173]

NIFS-DATA-11 T. Kaneko, T. Nishihara, T. Taguchi, K. Nakagawa, M. Murakami, M. Hosono, S. Matsushita, K. Hayase, M.Moriya, Y.Matsukuma, K.Miura and Hiro Tawara,
Partial and Total Electronic StoppingCross Sections of Atoms for a Singly Charged Helium Ion: Part 1;Mar. 1991

NIFS-DATA-12 Hiro Tawara,
Total and Partial Cross Sections of Electron Transfer Processes for Be^{q+} *and* B^{q+} *Ions in Collisions with H,* H_2 *and He Gas Targets - Status in 1991-*; June 1991

NIFS-DATA-13 T. Kaneko, M. Nishikori, N. Yamato, T. Fukushima, T. Fujikawa, S. Fujita, K. Miki, Y. Mitsunobu, K. Yasuhara, H. Yoshida and Hiro Tawara,
Partial and Total Electronic Stopping Cross Sections of Atoms for a Singly Charged Helium Ion : Part II; Aug. 1991

NIFS-DATA-14 T. Kato, K. Masai and M. Arnaud,
Comparison of Ionization Rate Coefficients of Ions from Hydrogen through Nickel ; Sep. 1991

NIFS-DATA-15 T. Kato, Y. Itikawa and K. Sakimoto,
Compilation of Excitation Cross Sections for He Atoms by Electron Impact; Mar. 1992

NIFS-DATA-16 T. Fujimoto, F. Koike, K. Sakimoto, R. Okasaka, K. Kawasaki, K. Takiyama, T. Oda and T. Kato,
Atomic Processes Relevant to Polarization Plasma Spectroscopy ; Apr. 1992

NIFS-DATA-17 H. Tawara,
Electron Stripping Cross Sections for Light Impurity Ions in Colliding with Atomic Hydrogens Relevant to Fusion Research; Apr. 1992

NIFS-DATA-18 T. Kato,
Electron Impact Excitation Cross Sections and Effective Collision Strengths of N Atom and N-Like Ions -A Review of Available Data and Recommendations- ; Sep. 1992

NIFS-DATA-19 Hiro Tawara,
Atomic and Molecular Data for H_2O, CO & CO_2 *Relevant to Edge Plasma Impurities*, Oct. 1992

NIFS-DATA-20 Hiro. Tawara,
Bibliography on Electron Transfer Processes in Ion-Ion/Atom/Molecule Collisions -Updated 1993-; Apr. 1993

NIFS-DATA-21 J. Dubau and T. Kato,
Dielectronic Recombination Rate Coefficients to the Excited States of C I from C II; Aug. 1994

NIFS-DATA-22 T. Kawamura, T. Ono, Y. Yamamura,
*Simulation Calculations of Physical Sputtering and Reflection Coefficient of Plasma-Irradiated Carbon Surface;*Aug. 1994

NIFS-DATA-23 Y. Yamamura and H. Tawara,
Energy Dependence of Ion-Induced Sputtering Yields from Monoatomic Solids at Normal Incidence; Mar. 1995

NIFS-DATA-24 T. Kato, U. Safronova, A. Shlyaptseva, M. Cornille, J. Dubau,
Comparison of the Satellite Lines of H-like and He-like Spectra; Apr. 1995

NIFS-DATA-25 H. Tawara,
Roles of Atomic and Molecular Processes in Fusion Plasma Researches - from the cradle (plasma production) to the grave (after-burning) -; May 1995

NIFS-DATA-26 N. Toshima and H. Tawara
Excitation, Ionization, and Electron Capture Cross Sections of Atomic Hydrogen in Collisions with Multiply Charged Ions; July 1995

NIFS-DATA-27 V.P. Shevelko, H. Tawara and E.Salzborn,
Multiple-Ionization Cross Sections of Atoms and Positive Ions by Electron Impact; July 1995

NIFS-DATA-28 V.P. Shevelko and H. Tawara,
Cross Sections for Electron-Impact Induced Transitions Between Excited States in He: n, n'=2,3 and 4; Aug. 1995

NIFS-DATA-29 U.I. Safronova, M.S. Safronova and T. Kato,
Cross Sections and Rate Coefficients for Excitation of $\Delta n = 1$ Transitions in Li-like Ions with $6<Z<42$; Sep. 1995

NIFS-DATA-30 T. Nishikawa, T. Kawachi, K. Nishihara and T. Fujimoto,
Recommended Atomic Data for Collisional-Radiative Model of Li-like Ions and Gain Calculation for Li-like Al Ions in the Recombining Plasma; Sep. 1995